The Pennsylvania State University

The Graduate School

Department of Electrical Engineering

NOISE MODULATED COVERT COMMUNICATIONS

A Thesis in

Electrical Engineering

by

Jack Chuang

Submitted in Partial Fulfillment
of the Requirements
for the Degree of

Doctor of Philosophy

August 2008

The dissertation of Jack Chuang was reviewed and approved* by the following:

Ram Narayanan
Professor of Electrical Engineering
Dissertation Advisor
Chair of Committee

Aylin Yener
Associate Professor of Electrical Engineering

Randy K. Young
Senior Research Associate of Applied Research Laboratory

Thomas F. Lin
Senior Research Associate of Applied Research Laboratory

W. Kenneth Jenkins
Professor of Electrical Engineering
Head of the Department of Electrical Engineering

*Signatures are on file in the Graduate School

ABSTRACT

In recent years, the Ultra-wideband (UWB) random noise waveforms have been getting increased attention in secure communications because they exhibit unpredictable behavior which can not be detected by conventional receivers and they are jam-resistance. This thesis describes a novel spread spectrum technique that can be used for covert communications. This noise modulated covert communication system (NMCC) is based on the use of heterodyne correlation techniques to inject coherence into a random noise signal. The BPSK-modulated signal to be transmitted containing the carrier is mixed with band-limited UWB random noise signal. The frequency range of the UWB noise signal is appropriately chosen so that the lower sideband of the mixing process falls over the same frequency range. Thus, the dispersive effects caused by the atmosphere and other factors are significantly reduced since both polarization channels operate over the same frequency band.

In military communications, the communication system will suffer interference from ambient noise, jamming from hostile force and multi-path. To fully understand this prototype system, the system behaviors in a Gaussian channel, various jamming environments and multi-path channels are properly modeled. The theoretical performance is compared with MATLAB simulation results and the results show the deviation between theory and simulation is smaller than 1 dB.

The system has also been built and tested in the open field. All the baseband processing is implemented in software defined radio architecture and allows processing of the real time audio and video experiment in the field. The audio and video can be

successfully retrieved and the result clearly validates that the system concept will work. The empirical mode decomposition (EMD) is applied into the baseband signal processing to alleviate the noise interference and allow the system to operate in a noisy or jamming channel. By using noise pilot and noise radar concept, the channel estimation in a multi-path channel can be accomplished while no code needs to be inserted in baseband signal processing and the system structure can be simple.

TABLE OF CONTENTS

LIST OF FIGURES vii

LIST OF TABLES xi

ACKNOWLEDGEMENTS xii

Chapter 1 Introduction 1

1.1 Introduction to spread spectrum communication system 1
1.2 Introduction to chaotic carrier spread spectrum system 7
1.3 Covert communication by using Gaussian noise 10
1.4 Thesis overview 12

Chapter 2 System overview of noise modulated covert communication system 14

2.1 Transmitter design 14
2.2 Receiver design 21
2.3 Transmitted signal analysis 23
2.4 System with software defined radio 26

Chapter 3 Performance of NMCC system in AWGN channel 29

3.1 Motivation 29
3.2 Single user performance in white Gaussian channel 30
3.2.1 Channel models 30
3.2.2 Modeling noise terms 33
3.2.3 Modeling signal term 41
3.2.4 Comparing simulation results and theoretical results 44
3.3 Multiuser performance in white Gaussian channel 50

Chapter 4 System implementation and comprehensive field experiment 54

4.1 Transmitter and receiver implementation 54
4.2 Baseband signal processing implementation 57
4.2.1 Board selection 57
4.2.2 Transmitter baseband signal processing design 57
4.2.3 Receiver baseband signal processing design 62
4.3 Comprehensive field experiment 66
4.4 Noise cancellation by EMD 73

Chapter 5 Performance of NMCC system subjected to interference 80

5.1 Partial-Band and Pulse-Noise jamming environment 80
5.2 Co-channel DS/SS interference 89

5.3 Multipath environment 98
5.3.1 Parameters 98
5.3.2 Cross-Multiple to alleviate multipath effect 99

Chapter 6 Conclusion and future work 111

6.1 Conclusion 111
6.2 Future work: Channel estimation 113
6.3 Future work: Carrier synchronization 119
6.4 Future work: Exact PDF of received noise 121

Bibliography 122

Appendix A Power of interference terms in jamming channel 126

Appendix B Power of interference terms in multipath channel 128

Appendix C Stage by stage measurement 130

Appendix D Matlab Code 140

LIST OF FIGURES

Figure **1-1**: A seven stages *m*-sequence PN sequence generator. 3

Figure **1-2**: Transmitter structure of DSSS system (top) Receiver structure of DSSS system (bottom). 4

Figure **1-3**: Time frequency comparison between DS-SS and FH-SS system. 6

Figure **1-4**: System structure of chaotic system [12]. 8

Figure **1-5**: (a) Transmitted bit sequence (b) Error between received signal and synchronized signal [12]. 10

Figure **2-1**: Channel diversity implementation possibilities 15

Figure **2-2**: Transmitter block diagram (AMP = amplifier, BPF = band-pass filter, DL = delay line, FPGA = field programmable gate array, H = horizontal, OSC = oscillator, PD = power divider, SSB = single sideband, V = vertical). 16

Figure **2-3**: Time domain plot of horizontally transmitted signal. 18

Figure **2-4**: Frequency domain plot of horizontally transmitted signal. 18

Figure **2-5**: Time domain plot of vertically transmitted signal. 20

Figure **2-6**: Frequency domain plot of vertically transmitted signal. 20

Figure **2-7**: Receiver block diagram Transmitter block diagram (AMP = amplifier, BPF = band-pass filter, DL = delay line, FPGA = field programmable gate array, H = horizontal, OSC = oscillator, V = vertical) 22

Figure **2-8**: Amplitude (top) and phase (bottom) plot of composite EM wave. 25

Figure **2-9**: Temporal variation of electric field vector of composite wave 25

Figure **2-10**: FPGA design overview. 28

Figure **3-1**: Power spectrum of received signal and noise 31

Figure **3-2**: Cumulative distribution function comparison between zero mean Gaussian and band-pass filtered noise term. 35

Figure **3-3**: Probability density function comparison between zero mean Gaussian and band-pass filtered noise term. 36

Figure **3-4**: Spectrum of $n_V(t-t_1)H(t)_{sum}$ 39

Figure **3-5**: Power spectrum of received baseband signal. 43

Figure **3-6**: Power spectrum of received baseband signal when Raised-Cosine filter added in the transmitter. 43

Figure **3-7**: Loss factor verse bandwidth of low-pass filter 45

Figure **3-8**: Comparison of SNR and BER characteristics between simulation and approximate model in a single user environment at different signal bandwidths (BW of low-pass filter is 20 MHz). 47

Figure **3-9**: Comparison of SNR and BER characteristics between simulation and approximate model in a single user environment at different signal bandwidths (BW of low-pass filter is 7 MHz) 48

Figure **3-10**: Comparison of SNR and BER characteristics between simulation and approximate model in a single user environment at different bit rates (BW of low-pass filter is 20 MHz) 49

Figure **3-11**: SNR at baseband verse different signal bandwidths. 50

Figure **3-12**: Comparison between approximate model and simulation in multi-user environment. 53

Figure **4-1**: Transmitter side implementation (BPF=band-pass filter). 55

Figure **4-2**: Receiver side implementation (BPF=band-pass filter, LPF=low-pass filter). 56

Figure **4-3**: The photo of Lyrtech SignalWAVe FPGA board. 59

Figure **4-4**: Transmitter side FPGA design. 60

Figure **4-5**: Design of header generator. 61

Figure **4-6**: An example of incorrect capture (Top) and correct capture (bottom) of the serial to parallel block. 63

Figure **4-7**: Receiver FPGA design. 64

Figure **4-8**: Simulation results of FPGA design. 65

Figure **4-9**: Experiment setup overview. 66

Figure **4-10**: Experiment setup transmitter view 67

Figure **4-11**: Experiment setup receiver view. 67

Figure **4-12**: Time and frequency domain plots of recorded signal..... 68

Figure **4-13**: Original transmitted bit stream (Top), Bit stream received in ideal channel (Second from top), Bit stream received in additive white Gaussian noise channel (Third from top), Bit stream received in single-tone interference channel (Bottom). 70

Figure **4-14**: Experiment setup of NMCC system passing trees. 71

Figure **4-15**: The spectrum of received signal in vertical channel after passing trees. 72

Figure **4-16**: The received baseband signal when the transmission path contains trees. 72

Figure **4-17**: Simplified spectrum plot of received baseband signal. 77

Figure **4-18**: Recorded baseband signal in noisy channel. 77

Figure **4-19**: IMF signals of recorded baseband signal. 78

Figure **4-20**: Comparison between the signals before and after noise cancellation..... 79

Figure **5-1**: Power spectrum of sum frequency signal which is generated by mixing two band-limited uncorrelated Gaussian random variables. 85

Figure **5-2**: Comparison of SIR and BER characteristics between simulation and approximate model in Partial-Band jamming environment when jamming signal is concentrated around the center frequency (1.5GHz)..... 88

Figure **5-3**: Comparison of SIR and BER characteristics between simulation and approximate model in Partial-Band jamming environment when jamming signal is concentrated at a frequency (1.3GHz) different from the center frequency. For comparison, jamming signal concentrated at center frequency (1.5GHz) is also shown. 88

Figure **5-4**: Comparison of SIR and BER characteristics between simulation and approximate model in DS/SS interference environment..... 94

Figure **5-5**: BER comparison before and after adding the band-stop filter when the center frequency of interference is inside $f_n - 0.5B_L - T_c^{-1} \le f_J \le f_n + 0.5B_L + T_c^{-1}$. 97

Figure **5-6**: BER comparison before and after adding the band-stop filter in the AWGN channel. 98

Figure **5-8**: Block diagram of cross-product method by using more than one pair. 104

Figure **5-9**: BER comparison in multipath environment. 109

Figure **5-10**: BER comparison in multipath environment. 110

Figure **6-1**: Structure of channel estimator (DL=delay line). 115

Figure **6-2**: Simulation results of delay time estimation 116

Figure **6-3**: The time domain plots of V_L (L=1,2,3). 118

Figure **6-4**: Frequency domain plots of V_L (L=1,2,3). 118

Figure **6-5**: Square loop that is implemented in the NMCC system. 120

Figure **C-1**: Transmitter block diagram (top) and receiver block diagram (bottom)... 130

Figure **C-2**: Recorded time (top) and frequency (bottom) plot at output of noise generator in the transmitter side. 131

Figure **C-3**: Recorded time (top) and frequency (bottom) plot at output of band-pass filter in the transmitter side. 132

Figure **C-4**: Recorded time (top) and frequency (bottom) plot at output of FPGA board in the transmitter side 133

Figure **C-5**: Recorded time (top) and frequency (bottom) plot at output of mixer in the transmitter side. 134

Figure **C-6**: Recorded time (top) and frequency (bottom) plot for the signal that will send to horizontal polarization antenna. 135

Figure **C-7**: Recorded time (top) and frequency (bottom) plot for the signal that will send to vertical polarization antenna. 136

Figure **C-8**: Recorded time (top) and frequency (bottom) plot at output of the first mixer in the receiver side. 137

Figure **C-9**: Recorded time (top) and frequency (bottom) plot at output of the band-pass filter in the receiver side. 138

Figure **C-10**: Recorded time (top) and frequency (bottom) plot at output of the low-pass filter in the receiver side. 139

LIST OF TABLES

Table **5-1**: Channel-1 setup 108

Table **5-2**: Channel-2 setup 108

Table **6-1**: Measured fractional power..... 119

ACKNOWLEDGEMENTS

I would like to thank my advisor Dr. Ram Narayanan for all the help and support, all my labmates for fruitful discussion and help, and my committees Dr. Aylin Yener, Dr. Randy Young, and Dr. Thomas Lin for their support. I would also like to thank Dr. Sven Bilen of the Pennsylvania State University for supplying the two field programmable gate array boards for the experiment and Star-H Corporation providing the location for the field test. Most important, the covert communication team very appreciate the Office of Naval Research (ONR) support this project (under Contract #N00014-04-1-0640) and we appreciate fruitful discussion with Mr. John Moniz and Mr. Timothy Wasilition of ONR.

Chapter 1

Introduction

1.1 Introduction to spread spectrum communication system

In military communications, there exist numerous potential threats to message security. The communication system may operate in a hostile environment where third parties may attempt to intercept and jam communications. One of the major needs in this area is protection for the signals transmitted over the well-known frequency bands with standard modulation formats making them susceptible to interception and jamming [1]. The primary objectives of today's wireless secure communications systems are therefore to simultaneously and reliably provide communications that are robust to jamming and also achieve low probability of detection and low probability of intercept in hostile environments.

The spread spectrum technique was initially developed during World War II [2]. Most of the development of spread spectrum communications was performed in the 60's and 70's. Today, these techniques have been widely used in wireless military applications because of their capability to communicate in the presence of intentional interference and also because they permit transmission with a very low power spectral density by spreading the signal energy over a large bandwidth [3],[4]. Hence, the spread spectrum techniques offer both security and low probability of detection features.

Spread spectrum is a means of using bandwidth in excess of the minimum required bandwidth that is necessary to transmit data. Its multipath rejection characteristics are useful for ground-based mobile communication systems and its multiple-access characteristics allow many users to use the same bandwidth at the same time. The two common spread spectrum modulations are direct sequence spread spectrum (DS-SS) and frequency hopping spread spectrum (FH-SS) [3]. Both of these use pseudo-noise (PN) sequences for the spreading spectrum or frequency hopping. The PN sequence can be generated by a cascaded feedback shift register and the code length is controlled by the number of shift registers. Figure **1-1** shows an example of a seven stage *m*-sequence PN code generator that is implemented using the Lyrtech field programmable gate arrays (FPGA) designing software. The length of this m-sequence is $2^7 - 1$. Each shift register contains its own binary initial value. When circuit is enabled by a free running counter, each shift register sends its value to next shift register while the feed back circuit, with modulo-2 sum, sends its output value to first shift register. The design is not unique. Different initial values and different feedback circuit will generate different m-sequence sequence with the same length.

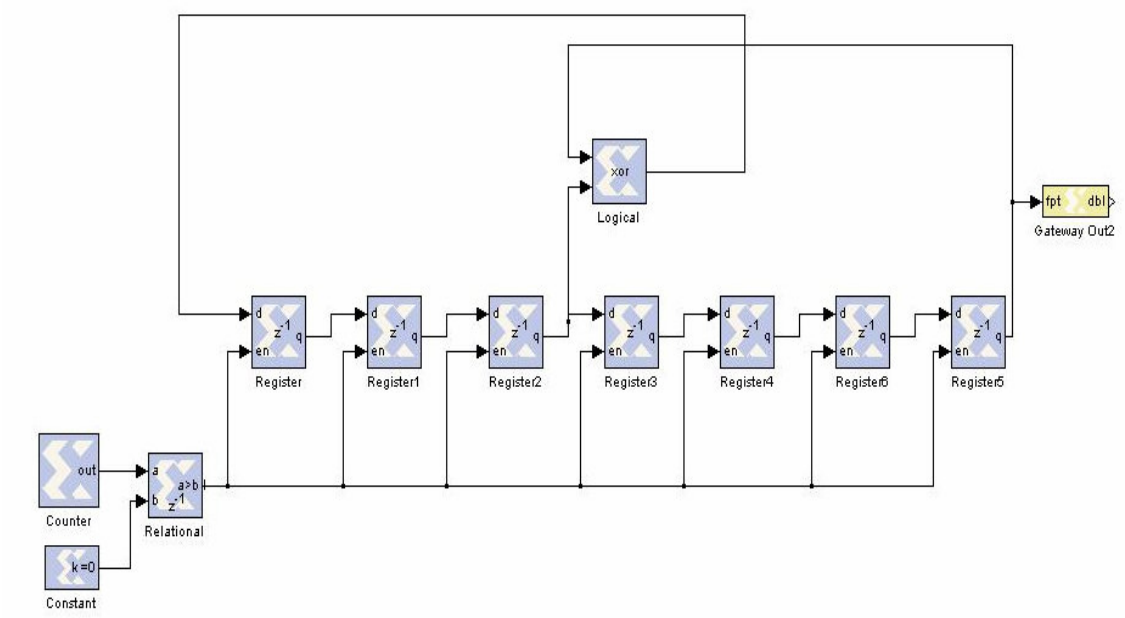

Figure **1-1**: A seven stages *m*-sequence PN sequence generator.

The full periodic autocorrelation function of a *m*-sequence with *m*-stages is shown in Eq. **1.1.** When m increases, the ratio of $\phi_m(j)/\phi_m(0)$ decreases. From a practical viewpoint, it can be seen as inconsequential and has similar characteristic as the delta function when m is increasing. The *m*-sequence is not the only PN sequence used in spread spectrum communications. Other sequences, such as Gold sequence and Kasami sequence are also widely used in spread spectrum communications. The non fully periodic autocorrelation functions of different sequences are also different but they all serve the same purpose to increase the peak-to-sidelobe ratio.

$$\phi_m(j) = \begin{cases} m & (j=0) \\ -1 & (1 \le j \le m-1) \end{cases} \qquad \textbf{1.1}$$

The code correlation property causes multipath to be almost uncorrelated with the desired received signal when the multipath delay exceeds the code duration time. Thus, multipath resistance can be achieved. By applying RAKE receiver to combine several resolvable multipath signals to form a stronger signal, the performance can be improved. The system structure of direct sequence spread spectrum system employs binary phase-shift keying is also shown in Figure **1-2.**

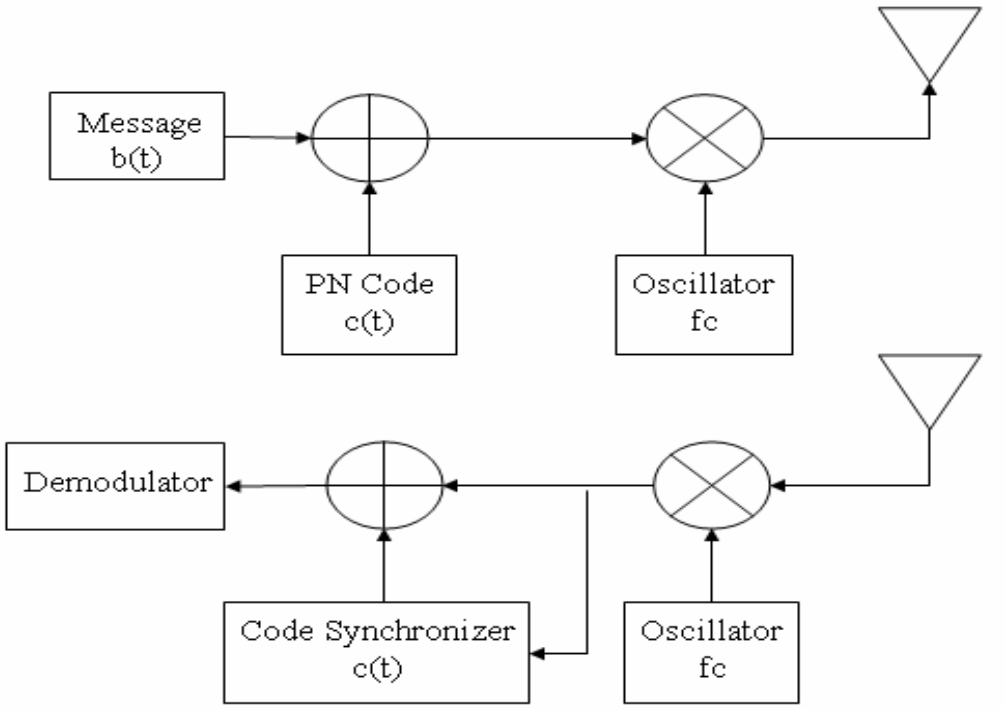

Figure **1-2**: Transmitter structure of DSSS system (top) Receiver structure of DSSS system (bottom).

The message $b(t)$ with bit duration time T_b is modulo-2 sum with PN sequence $c(t)$ with code duration time T_c. This procedure is called spreading and the message's spectrum will spread into large frequency range after modulo-2 sum procedure. The

spread signal is sent to the channel with carrier frequency f_c. The signal received by receiver's antenna can be expressed as

$$r(t) = \sqrt{2P}b(t)c(t)\cos\left(2\pi f_c t\right) + J(t) \qquad \textbf{1.2}$$

where P is power of transmitted signal. $J(t)$ is the tone jamming signal with power P_J. Assuming perfect carrier synchronization, the received baseband signal can be mathematically expressed in Eq. **1.3** where $J_b(t)$ is $J(t)$ after down conversion. Since the conversion loss for both signal and jamming source are the same, the signal to interference ratio (SIR) at baseband is maintained the same and is P/P_J [5].

$$r_b(t) = \sqrt{2P}b(t)c(t) + J_b(t) \qquad \textbf{1.3}$$

$$r_b^{'}(t) = \sqrt{2P}b(t) + J_b(t)c(t) \qquad \textbf{1.4}$$

Code synchronization methods have been already presented in [6][7]. We assume perfect code synchronization and the $r_b(t)$ is mixed or modulo-2 summed with the PN sequence $c(t)$ which is used in the transmitter. This procedure is called despreading and the signal after code synchronizer is expressed in Eq. **1.4**. The data can be successfully retrieved and the noise floor level is decreased since the power of the jamming signal is spread by $c(t)$. By implementing a proper filter with bandwidth T_b^{-1} to capture the desired signal, the SIR at the output of filter is improved compared to the SIR at the RF front, and is equal to $PT_c/P_J T_b$. T_c/T_b is defined as processing gain. A higher code rate implies a higher processing gain and better immunity to the jamming signal.

Unlike the DS-SS system, the FH-SS system uses the PN sequences to randomly hop carrier frequencies from one to another. Figure **1-3** shows how the DS-SS system and the FH-SS system use the frequency band in different ways. The DS-SS system uses the same frequency band all the time while the FH-SS system uses different frequency bands in different time intervals.

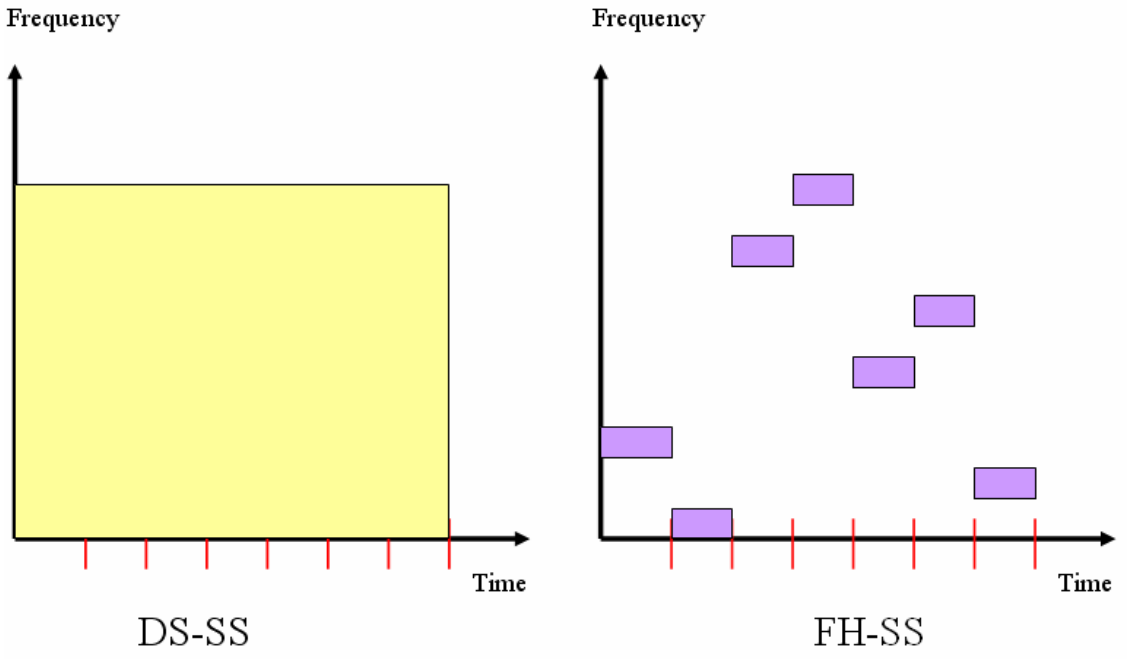

Figure **1-3**: Time frequency comparison between DS-SS and FH-SS system.

In multiuser environments, the users in the DS-SS system are simultaneously using the same frequency band. Each user is assigned his or her own PN code to minimize the co-channel interference. The FH-SS system operates in a different way. Ideally, all the users are simultaneously using different frequency bands. This feature provides the FH-SS system an advantage over the DS-SS system because it does not

suffer from the near-far problem. However, it cannot avoid more than one user simultaneously using the same frequency band in reality and collisions will occur. Even if the clocks of each user are synchronized, collisions still may occur because the various propagation delays will cause the signals to arrive at different times. For a fast-hopping scenario, i.e. more than one frequency hop within each symbol, the collision will not cause serous performance degradation. However, there will be a problem in a slow-hopping scenario and error correction coding can be used to improve performance. On the other hand, for a single user, the DS-SS system uses larger instantaneous bandwidth than FH-SS system and it provides better noise immunity than FH-SS systems.

1.2 Introduction to chaotic carrier spread spectrum system

Since the transmitting signal is hidden under the ambient noise, the spread spectrum techniques offer both low probability of interception and low probability of detection features. However, by exploiting the statistical properties of the pseudo-noise sequences used in direct-sequence spread-spectrum systems and the pseudorandom frequency-hopping sequences used in frequency-hopping spread-spectrum systems, statistical processing techniques such as triple correlation [8], [9], fluctuations of autocorrelation estimators [10], and multi-hop maximum likelihood detection [11] have been developed. These methods permit a third party to detect the spread spectrum signal even if it is hiding under the ambient noise.

Because the communications involve data exchange between transmitter and receiver, the strategy to interfere with an enemy's communication system in the battle

field is to locate the source and then disturb the communication link by broadcasting higher power jamming signals in the environment. During the past twenty years, several researches made great efforts to design a covert communication system which can transmit unpredictable signals. The random behavior of the transmitted signal enhances the security of data transmission and also prevents the hostile forces from detecting data transmission. The most well-known system is the Lorenz-Based Chaotic system and the system structure is shown in Figure **1-4.** $u(t)$ and $u_m(t)$ are output signals generated by transmitter's and receiver's Lorenz systems. $e(t)$ is error between $u(t)$ and $u_m(t)$ and $n(t)$ is channel noise.

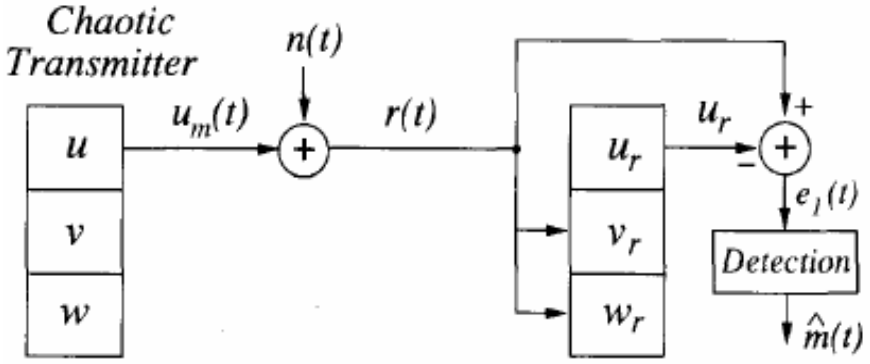

Figure **1-4**: System structure of chaotic system [12].

If the Jacobian functions of the Lorenz systems at transmitter side and receiver side have the same parameters σ and r, the Jacobian function of Lorenz system at transmitter side is shown in Eq. **1.5** and the Jacobian function of Lorenz system at receiver side is shown in Eq. **1.6.** $m(t)$ is binary bit sequence that system intends to transmit and v and w are driven signals.

$$\begin{aligned} u' &= \sigma(v-u) \\ v' &= ru - v - uw \\ w' &= uv - m(t)w \end{aligned} \qquad \textbf{1.5}$$

$$\begin{aligned} u' &= \sigma(v-u) \\ v' &= ru - v - uw \\ w' &= uv \end{aligned} \qquad \textbf{1.6}$$

The chaotic system uses the fact that any two identical Lorenz systems can be synchronized with the same parameter and the system recovers the bit sequence by comparing the error between the received signal and synchronized signal. When a bit-0 is sent, the value of $m(t)$ is zero and the Eq. **1.5** and Eq. **1.6** are exactly the same. The error signal $e_l(t)$ in the Figure **1-4** is relatively small comparing with the period that the bit-1 is sent [12]. An example comparing the error signal and send data is shown in Figure **1-5.** If the error is greater than a specified threshold, the demodulator will recognize that the bit-1 is sent. Otherwise, the demodulator will recognize that the bit-0 is sent.

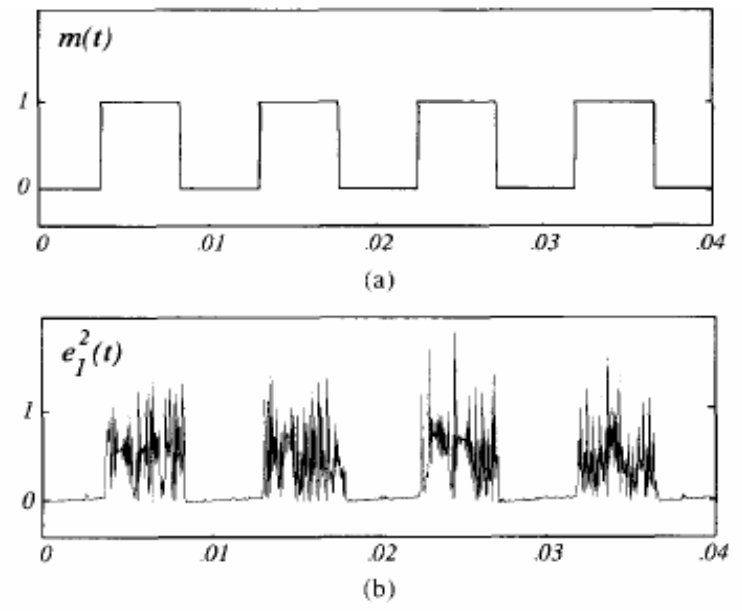

Figure **1-5**: (a) Transmitted bit sequence (b) Error between received signal and synchronized signal [12].

Most theory of chaotic systems has been completely developed in 90's and the commercial product is available. The transmitted waveform of chaotic systems present unpredictable behavior but one major problem restricts the application. The self-synchronization properties of Lorenz system will be lost in a noisy channel. Thus, this system can not operate in the channel with low signal to noise (SNR) ratio and will not suitable for wireless military communication since the SNR in the battle field is relatively low compared with the commercial environment.

1.3 Covert communication by using Gaussian noise

In order to maintain both covertness and performance during the data transmission, researchers started to use pure white Gaussian noise for data transmission

in the early 1980's. The most well-known method uses different delays to accomplish the modulation. For example, the modulation can be accomplished by assigning different delays to different messages and the modulated signal is summed with original noise before transmitting through the channel. To increase the security for the data transmission, the transmitted signal is summed with more than one delayed signals and only one of them is controlled by the message [13]. By using this modulation technique, the transmitted signal can be expressed as

$$s(t) = n(t) + n(t - T_i) + \sum_{g=1}^{n} n(t - T_g) \qquad \textbf{1.7}$$

where $n(t)$ is a zero mean band-limited white Gaussian noise. T_i is specific delay that assign to the corresponding message. T_g is fixed during the whole data transmission. For binary modulation, T_1 is assigned to bit-0 and T_2 is assigned to bit-1. The demodulator receives $s(t)$ and than find its autocorrelation $R_{s,s}(\tau)$. If the peak is showing up at τ equal to T_1, the demodulator makes a decision that the bit-0 is sent. Using the same concept, the demodulator makes decision that the bit-1 is sent when the peak appears at τ equal to T_2. The modulation technique shows random behavior in the time domain and the system has better noise immunity compared to the chaotic system. The major disadvantage of this system is that the third party may be aware there is a signal transmitting in the channel since the autocorrelation function of intercepted signal shows multiple peaks.

1.4 Thesis overview

By combining heterodyne correlation receiver and using band-limited Gaussian noise as spreading source, the Radar and Communications Laboratory at The Pennsylvania State University has developed a prototype UWB covert communication system. The main contribution is that the system provides excellent covertness. In the time domain, the transmitted waveform has characteristics similar to white Gaussian noise and this feature prevents the transmitted signal from being detected by the higher autocorrelation method. On the other hand, the flat spectrum of transmitted signal provides good immunity to the "average spectrum" detecting method when the transmitted signal is hidden under noise floor. The preliminary field test results successfully validate our concept. By assuming filtered noise can be approximated by a white Gaussian, validated by numerical result, we obtained the approximate bit error rate (BER) models in white Gaussian channel, partial-Band jamming channel, and channel contains DS/SS interference.

The thesis contains five subsequent chapters. Chapter-2 provides the block diagram and theoretical analysis of noise modulated covert communication (NMCC) system. Chapter-3 analyzes and models the system performance in the white Gaussian noise channel (AWGN) in single user and multi-user environment. Chapter-4 shows the system implementation and real-time field test results which clearly validate this concept can be realized. The FPGA implementation is also included in Chapter-4. Chapter-5 analyzes the system performance in the Partial-band jamming channel, the channel with DS-SS signal interference, and multipath channel. A new algorithm is also presented in

this chapter to improve the BER performance in the multipath channel. Finally, Chapter-6 gives conclusions and future work that need to be done to achieve push to talk.

Chapter 2

System overview of noise modulated covert communication system

2.1 Transmitter design

The motivation for designing NMCC system is to be able to conceal a message from an adversary and to avoid jamming countermeasures while maintaining an acceptable performance level. Instead of using a pseudo-noise sequence, a band-limited Gaussian noise waveform is used to spread the signal's power over a large bandwidth. Thus, a large processing gain is achieved and the system can operate in a noisy or jammed channel. Since non-periodic random waveform is using for the NMCC system, the reference signal and message signal should both be sent to the receiver in order to implement the heterodyne correlation receiver. There are three possibilities for transmitting the two signals through the channel as shown in Figure **2-1** .

In the delay diversity approach, one of the two signals is delayed by τ , summed with the other, and the composite signal transmitted using a single antenna. At the receiver, an identical delay is used to separate the signals prior to correlation in the mixer [14]. The hardware implementation in this scheme is slightly complicated, but it conserves bandwidth as the signals occupy the same frequency band. In the band stacking approach, the two transmit signals are arranged so as to occupy contiguous frequency bands, thereby increasing bandwidth, but sharing a single antenna. The receiver structure is quite simple, however. This is similar to the frequency-offset noise modulation

technique [15]. To conserve bandwidth, maintain a simple receiver structure, and eliminate self-interference due to the receiver mixing process in the time and frequency diversity schemes, the NMCC system injects polarization diversity into the system and transmits the reference signal and message via orthogonally-polarized antennas. The block diagram of the transmitter section of our secure communications system is shown in Figure **2-2.**

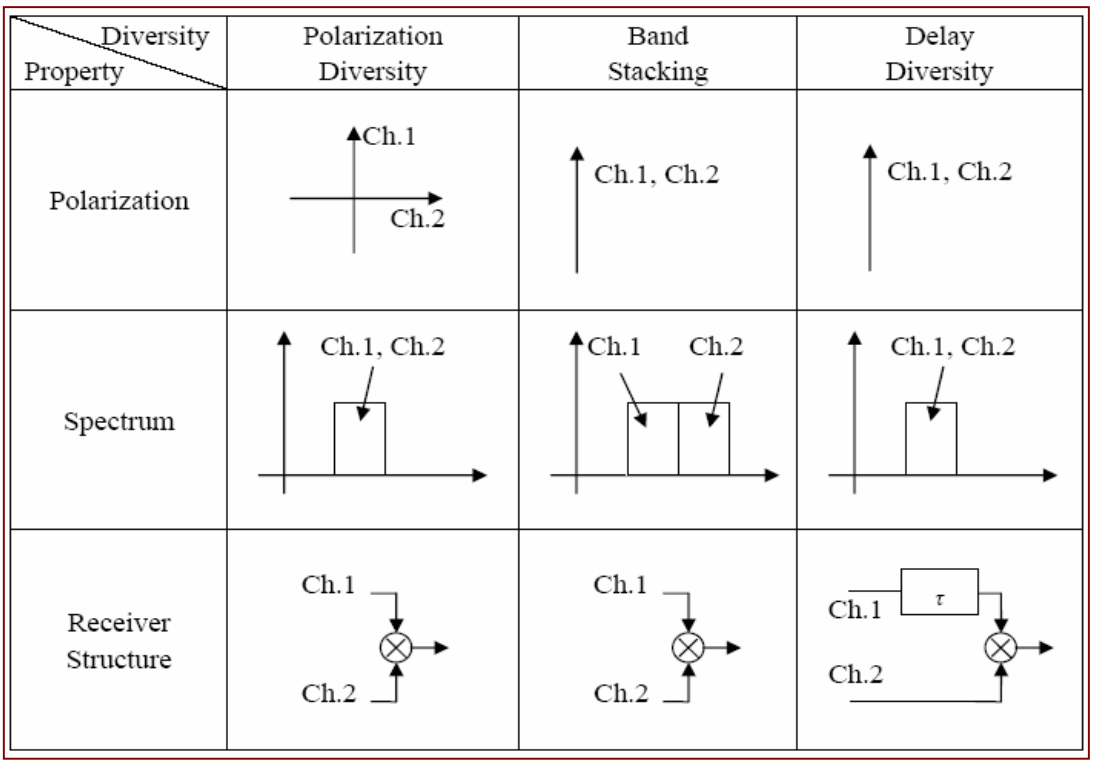

Figure **2-1**: Channel diversity implementation possibilities.

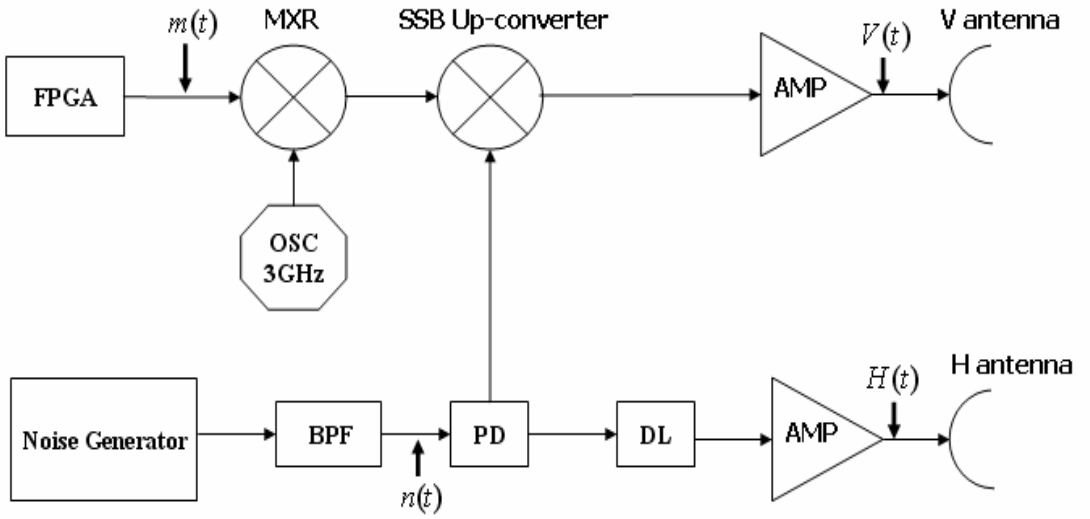

Figure **2-2**: Transmitter block diagram (AMP = amplifier, BPF = band-pass filter, DL = delay line, FPGA = field programmable gate array, H = horizontal, OSC = oscillator, PD = power divider, SSB = single sideband, V = vertical).

The noise generator generates a zero-mean band-limited Gaussian noise waveform with center frequency f_n (1.5-GHz). This Gaussian noise is passed through a band-pass filter. The band-pass filter ensures that the signal is confined within the antenna operation frequency range (1–2-GHz) and the mathematic expression of this filtered band-limited noise is shown in Eq. **2.1** . The $s_I(t)$ and $s_Q(t)$ are independent Gaussian random processes. The Eq. **2.1** can be also written in an alternative expression and is shown in Eq. **2.2** [16].

$$n(t) = s_I(t)\cos\left(2\pi f_n t\right) - s_Q(t)\sin\left(2\pi f_n t\right) \qquad \textbf{2.1}$$

$$n(t) = a(t)\cos\left(2\pi f_n t + \phi(t)\right) \qquad \textbf{2.2}$$

where $a(t)$ is a Rayleigh distributed random variable and $\phi(t)$ is an uniformly distributed random variable in the range $[-\pi, \pi]$. Further descriptions of these two random variables are given in Eq. **2.3** and Eq. **2.4** .

$$a(t) = \sqrt{s_I^2(t) + s_Q^2(t)} \qquad \textbf{2.3}$$

$$\phi(t) = \tan^{-1}\left[\frac{s_Q(t)}{s_I(t)}\right] \qquad \textbf{2.4}$$

This filtered noise $n(t)$ is then fed to a power divider. One output of the power divider connects to a delay line with delay t_1. The delayed band-limited noise is amplified and transmitted through a horizontally polarized antenna as the reference. The reference signal can be mathematically expressed in Eq. **2.5** and the time and frequency domain plots of reference signal are shown in Figure **2-3** and Figure **2-4**.

$$H(t) = a(t - t_1)\cos\left(2\pi f_n (t - t_1) + \theta(t - t_1)\right) \qquad \textbf{2.5}$$

This specific delay time assigned to each user increases the security of the system. Without knowledge of this delay time, a third party cannot recover the transmitted data even if they know that the reference and message are being transmitted and know the frequency range and polarization of the transmitted signal. On the other hand, assigning different delay times to different users allow more than one user to share the same channel at the same time. The detailed discussion of multiuser communication for NMCC systems will presented in the Chapter-3.

.

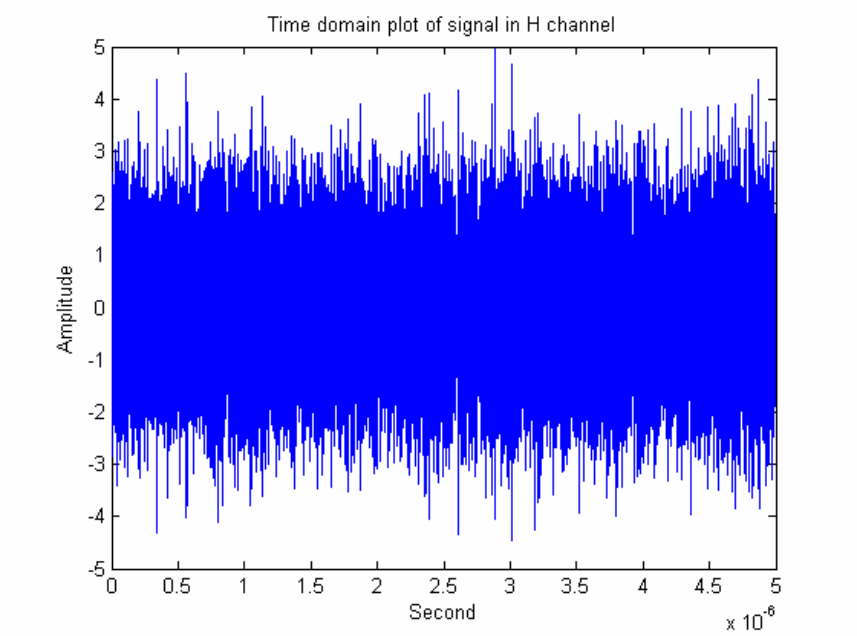

Figure **2-3**: Time domain plot of horizontally transmitted signal.

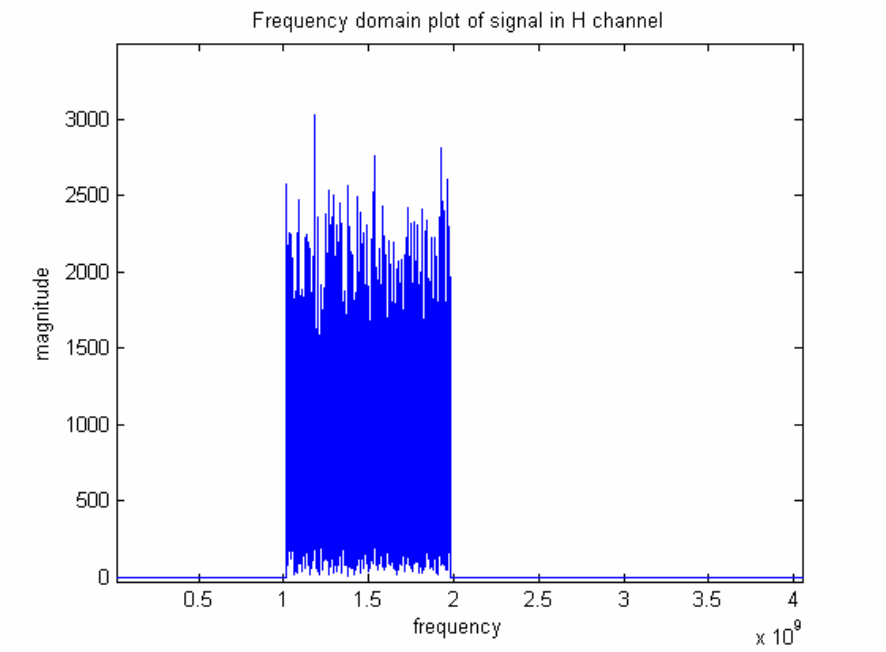

Figure **2-4**: Frequency domain plot of horizontally transmitted signal.

A binary bit sequence $m(t)$ is sent from the digital to analog converter to the mixer and is mixed with the 3-GHz (= f_c) carrier that is generated by a phase-locked oscillator. This narrow-band (3-GHz) modulated RF message signal is used as the local oscillator of the single sideband up-converter and mixed with the 1–2-GHz band-limited noise which is from the other output of the power divider. The single sideband up-converter is a device which can exactly select the upper sideband (centered at $f_c + f_n$) or the lower sideband (centered at $f_c - f_n$) of the mixing process. In our system, the lower sideband is selected. This noise-like signal is amplified and transmitted through a vertically polarized antenna which we denote as $V(t)$. The amplifier gains are adjusted to equalize the transmit power levels at the two antennas. The time and frequency domain plots of $V(t)$ is shown in Figure **2-5** and Figure **2-6** and $V(t)$ can be expressed as

$$V(t) = m(t)a(t)\cos\left(2\pi(f_c - f_n)t - \theta(t)\right) \qquad \textbf{2.6}$$

By judiciously choosing $f_c = 2f_n$, the system can ensure that the lower sideband is located in the same frequency range as $H(t)$. Thus, the dispersive effects caused by the atmosphere and other factors are significantly reduced since both polarization channels operate over the same frequency band**.** It is evident that the spread spectrum process is accomplished within the single sideband up-converter and this noise-like signal contains the message that we wish to transmit covertly.

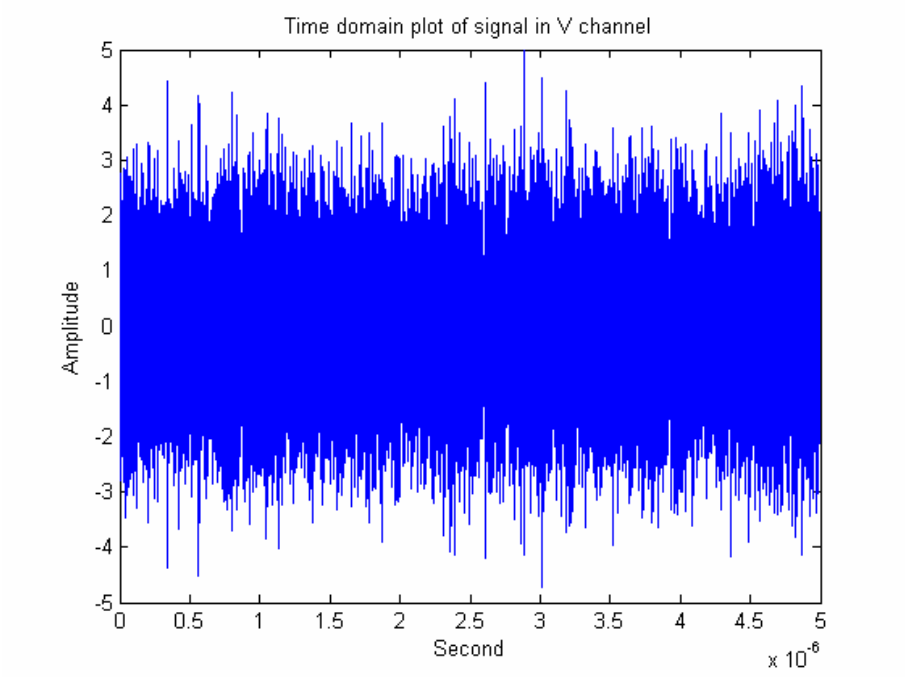

Figure **2-5**: Time domain plot of vertically transmitted signal.

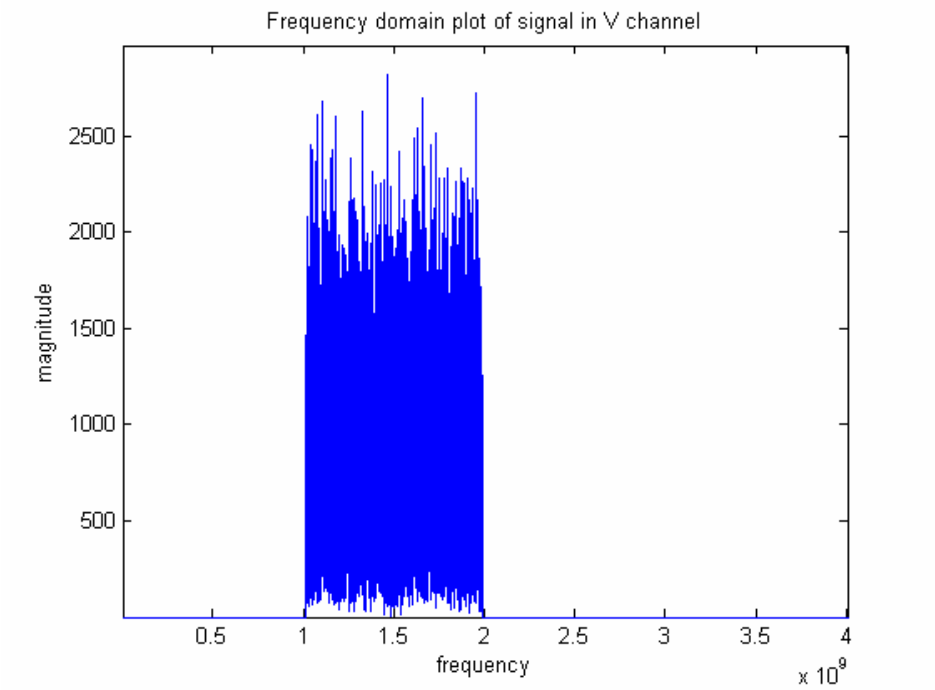

Figure **2-6**: Frequency domain plot of vertically transmitted signal.

From Figure **2-3** to Figure **2-6**, the transmitted signals in both channels show the random behavior and the spectrum is flat similar to white Gaussian noise. These characteristics increase the difficulty for third party to recognize that there is message transmitting in the channel.

2.2 Receiver design

The receiver block diagram is shown in Figure **2-7**. For short-range (less than 5 km) and low frequency (less than 20 GHz) applications, we can assume that the amplitude and phase factors are the same for both polarization channels, since they are specifically designed so as to operate over the same frequency band. The received signals $\bar{V}(t)$ and $\bar{H}(t)$ for the vertically and horizontally polarized channels, respectively, are given by

$$\bar{V}(t) = Am(t)a(t)\cos\left(2\pi(f_c - f_n)t - \theta(t)\right) \qquad \textbf{2.7}$$

And

$$\bar{H}(t) = Aa(t - t_1)\cos\left(2\pi f_n(t - t_1) + \theta(t - t_1)\right) \qquad \textbf{2.8}$$

where A is the amplitude factor caused during propagation and under the assumption that the channel is noiseless. Without loss of generality, we can assume that $A = 1$. These signals are received simultaneously by a dual linear polarization antenna.

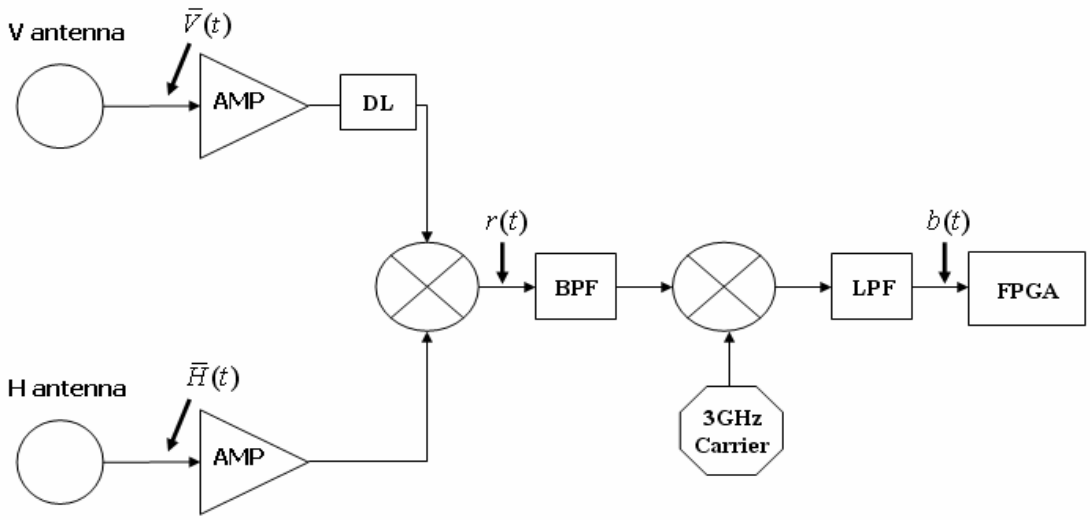

Figure **2-7**: Receiver block diagram Transmitter block diagram (AMP = amplifier, BPF = band-pass filter, DL = delay line, FPGA = field programmable gate array, H = horizontal, OSC = oscillator, V = vertical).

The $\bar{V}(t)$ is passed through a delay line with the same delay time t_1 and is then mixed with $\bar{H}(t)$ in the mixer. This brings the two channels in synchronization. If this delay does not exactly match the corresponding transmit delay, no message can be extracted from the mixed signal. Only a friendly receiver knows the exact value of this delay. Thus, an unfriendly receiver will not be able to perform the proper correlation to decode the hidden message.

The mixed signal contains both sum frequency signal $s(t)$ and a difference frequency signal $d(t)$. It can be expressed in Eq. **2.9**:

$$\begin{aligned} r(t) &= 0.5a^2(t-t_1)m(t-t_1)\cos\left(2\pi f_c(t-t_1)\right) + 0.5a^2(t-t_1)m(t-t_1)\cos\left(2\theta(t-t_1)\right) \\ &= s(t) + d(t). \end{aligned} \qquad \textbf{2.9}$$

Because the difference frequency signal contains the random phase $2\theta(t-t_1)$ and can be discarded as interference, a band-pass filter with center at f_c only catches the sum frequency signal which always has a center located at f_c (3-GHz). The filtered RF signal is than mixed with a 3-GHz carrier in order to strip off the carrier. The received baseband signal $b(t)$ at the output of the low-pass filter is expressed as

$$b(t) = 0.25a^2(t-t_1)m(t-t_1) \otimes h(t) \qquad \textbf{2.10}$$

where $h(t)$ is filter impulse response. Since binary modulation is used and the $a^2(t-t_1)$ term is always positive, the transmitted bit sequence can be successfully retrieved from $b(t)$.

2.3 Transmitted signal analysis

From above discussion, the transmitted signals in both channels demonstrate random behavior and the stochastic characteristic is similar to white Gaussian noise. To ensure the third party cannot recognize there is a message transmitting in the channel, we also need to ensure the amplitude and phase of composite electronic magnetic (EM) wave has random behavior. If $V(t_k)$ and $H(t_k)$ are the instantaneous magnitudes of the electric fields in the vertical and horizontal polarization channel at time 't_k' respectively, the instantaneous amplitude and the instantaneous polarization angle (with respect to the horizontal) of the composite transmitted wave are given by Eq. **2.11** and Eq. **2.12.**

$$E(t_k) = \sqrt{V^2(t_k) + H^2(t_k)} \qquad \textbf{2.11}$$

And

$$\phi(t_k) = \tan^{-1}\left(V(t_k)/H(t_k)\right) \qquad \textbf{2.12}$$

Applying Eq. **2.6** and Eq. **2.5** into Eq. **2.11** and Eq. **2.12**, the instantaneous amplitude and angle of the transmitted composite EM wave can be plotted in the Figure **2-8** and the temporal variation of the composite EM wave is shown in Figure **2-9**. Six sequential samples with time interval 0.333 ns are used to plot Figure **2-9.** Unlike single carrier communication systems, the samples of the RF signals have aperiodic behavior. The simulation results demonstrate that the composite transmitted signal appears totally unpolarized to any outside observer. It is therefore very difficult for a third party to recognize that there is a message propagating in the air since the waveform appears as unpolarized noise, thereby providing the covertness feature.

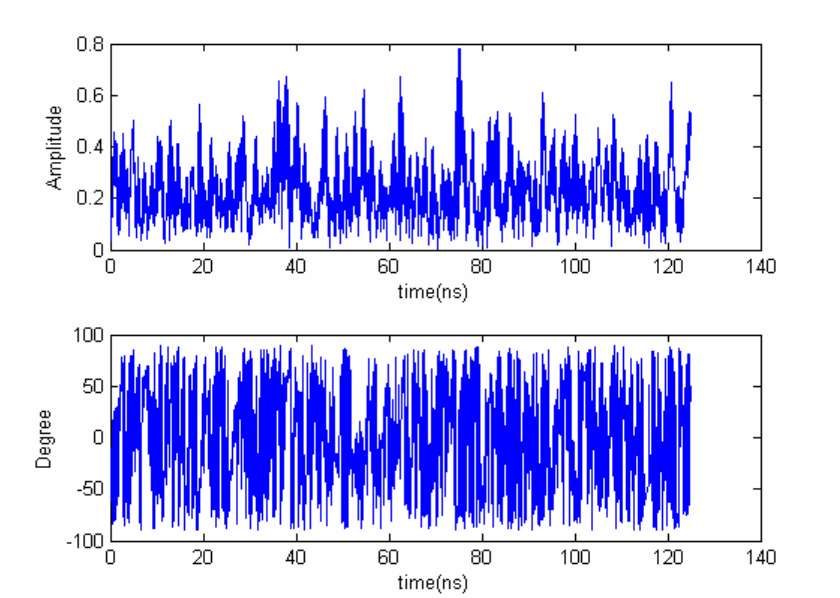

Figure **2-8**: Amplitude (top) and phase (bottom) plot of composite EM wave.

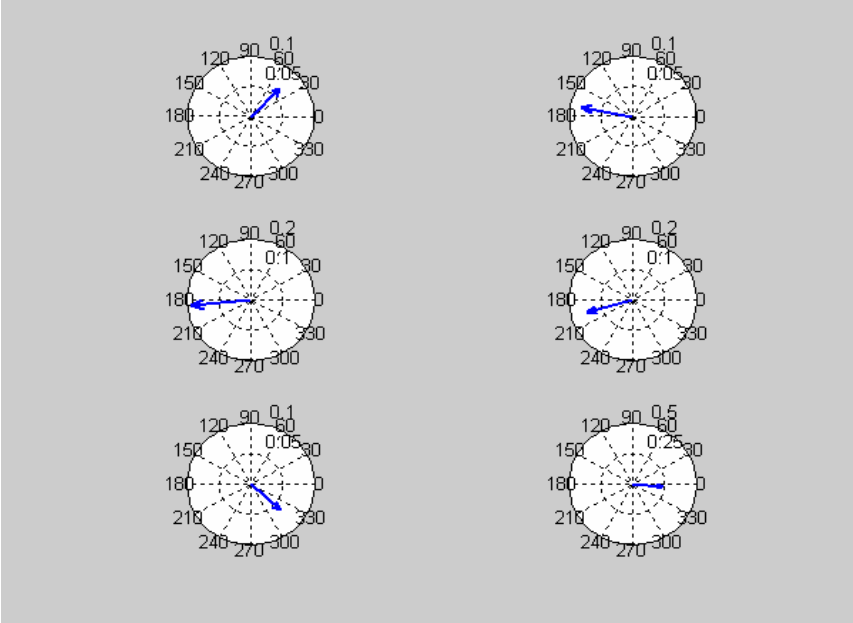

Figure **2-9**: Temporal variation of electric field vector of composite wave.

2.4 System with software defined radio

The software-defined radio (SDR) is defined as a radio system that uses software to control a variety of modulation techniques, communications security functions, and other IF and baseband signal processing [17]. This concept was proposed at the end of the 1980's and is broadly used by the armed forces as well as in wireless communications such as global positioning systems (GPS), Bluetooth, Wideband Code Division Multiple Access (WCDMA), and through-wall radar systems. The SDR technique provides more flexibility for engineers to design a novel communication system. By programming IF or baseband signal processing on the FPGA board, the prototype system with low size and weight and controllable by software is possible to be realized.

In our prototype system, all the baseband signal processing is implemented in the high speed FPGA board and a portable system has been built for real time audio and video field test. The SDR based covert communication system has several advantages compared to the conventional communication systems. By using hardware description languages to program the FPGA board, the numbers of RF components can be reduced. This feature minimizes the difference between simulation results and the experiment results because analog type RF components usually will generate extra noise. Other advantages of FPGA are listed below.

(1) The FPGA board is programmable. It allows the designer to change the system block diagram without buying extra components.

(2) Powerful DSP functionality, applying the digital filter, and channel coding on the board is possible.

(3) Fast computation of FPGA board makes real time processing possible.

(4) The cost can be reduced.

Figure **2-10** shows the FPGA design overview of the NMCC system. At transmitter side, the voice or music input is sampled by an analog-to-digital converter (ADC). The ADC translates each sample value to a frame and each frame contains a fixed number of binary bits. The bit sequence is sent to modulator. In our design, the binary modulation is chosen and the modulated antipodal bit sequence is sent to channel encoder. The channel coding maintains the system performance against the distortion that caused by a non-ideal channel. The coded data sends to digital-to-analog covert (DAC) where the bit-1 translates to positive voltage signal and bit-0 translates to negative voltage signal. The DAC connect to a mixer and up-convert the message to RF frequency range.

At receiver side, the output of low-pass filter is connected with the ADC. The sampled bit sequence sends to the threshold detector and then to the channel decoder. The original frame can be retrieved after the channel decoder and the DAC translates these frames back to analog voice format and broadcast with a speaker. The detailed real-time audio FPGA design will be shown in the Chapter-4 while the real-time video FPGA design is shown in [18].

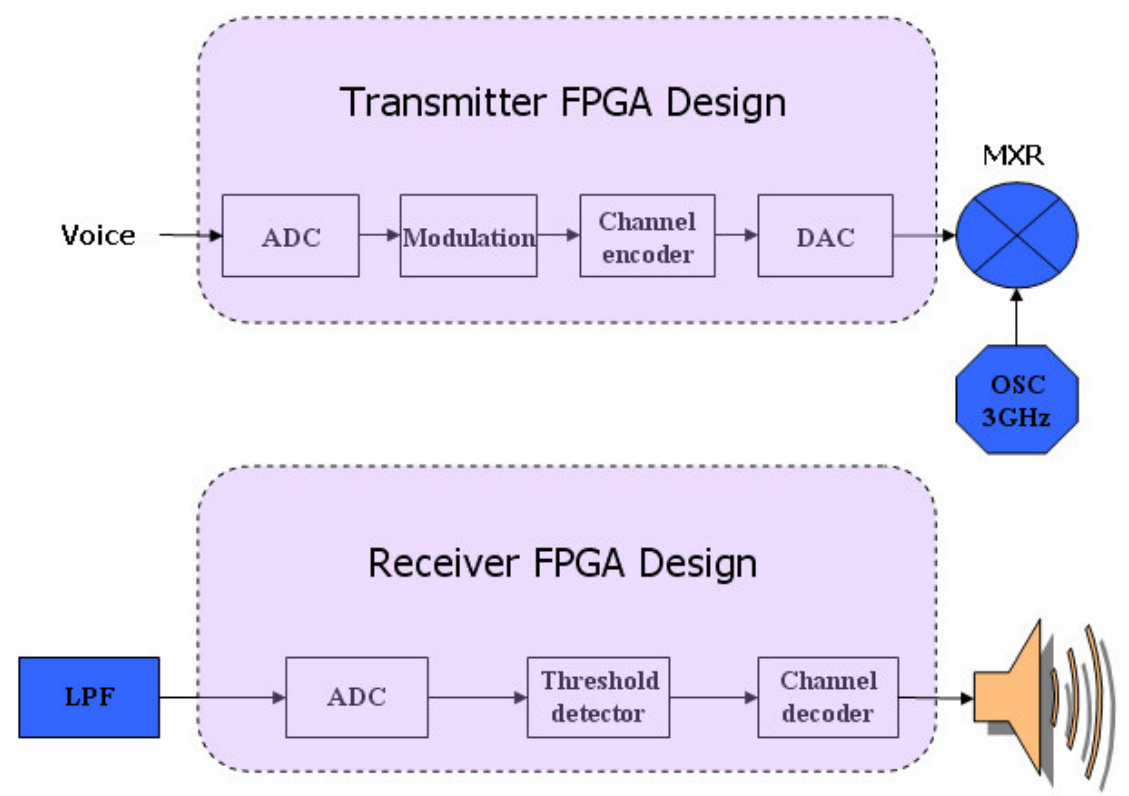

Figure **2-10**: FPGA design overview.

Chapter 3

Performance of NMCC system in AWGN channel

3.1 Motivation

In wireless communications, the bit error rate (BER) is an indicator used to gauge and compare the system performance. Since the NMCC system is a new architecture, the theoretical BER performance in additive white Gaussian noise (AWGN) channel is derived and is compared with simulation results in this chapter. Unlike other single-channel spread spectrum systems, the low-pass equivalent model can directly be used to model the system behavior in the Gaussian channel. The spreading and despreading process of our system is accomplished at the RF front-end. The noise floor at the antenna output is not the same as that at the output of the first mixer and the noise terms within the system are generated by the mixing of two zero mean independent Gaussian random variables. Thus, the system behavior needs to be modeled based upon the relationship between the SNR at the output of receiver antenna and the probability of bit error. In this chapter, we will demonstrate that the mixed noise can be approximated as white Gaussian after passing through a narrow band filter and the BER equation can be approximated by the Q-function. The bandwidths of the signal, antenna, low-pass filter and the SNR at the output of receiver's antenna are the parameters which dominate the BER when the bit rate is fixed.

3.2 Single user performance in white Gaussian channel

3.2.1 Channel models

In the system implementation, the antenna's bandwidth will slightly greater than the bandwidth of $V(t)$ and $H(t)$. Thus, the power spectrum of received signals in both channels will not be truncated by the antenna and they have rectangular spectrum shapes. Since the channel noise is a zero mean white Gaussian noise, the power spectrum density function of channel noise at antenna's output also has a rectangular shape. Figure **3-1** shows an example of the power spectrum density function of received signal and received channel noise at the output of vertical polarization antenna. The received signal has spectrum magnitude S_s and bandwidth B_s while the noise has spectrum magnitude S_n and bandwidth B_n. Under this condition, the SNR at the output of antenna can be found using Eq. **3.1**. In this chapter, the SNR at the output of vertical and horizontal polarized antennas are denoted as SNR_V and SNR_H respectively.

$$SNR_v = \frac{S_s B_s}{S_n B_n} \qquad \textbf{3.1}$$

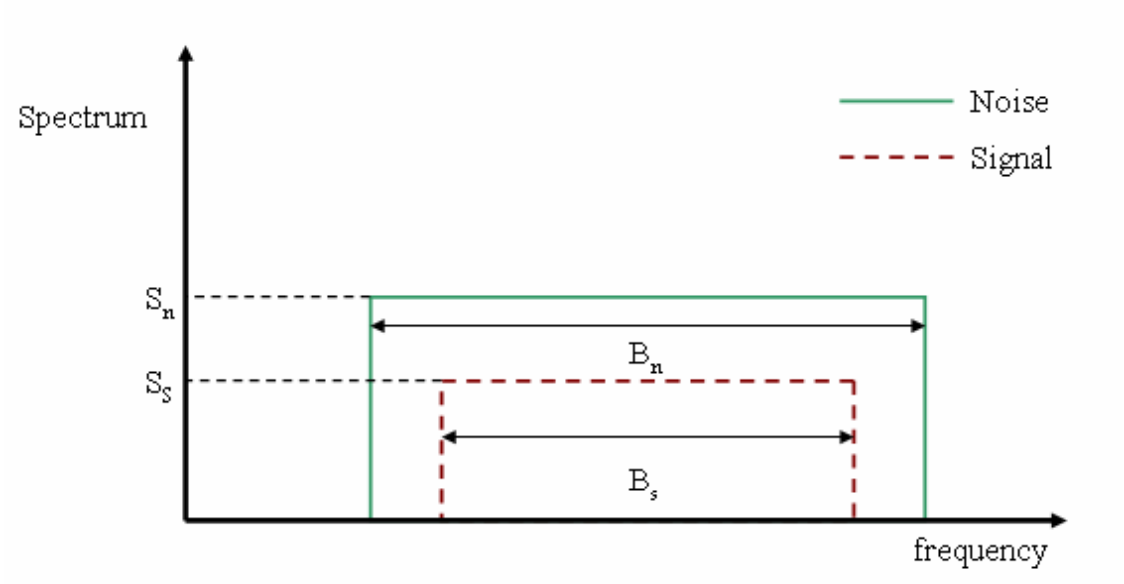

Figure **3-1**: Power spectrum of received signal and noise.

In AWGN channel, the actual received signal from the vertically polarized antenna $\tilde{V}(t)$ and the horizontally polarized antenna $\tilde{H}(t)$ can be written as, respectively,

$$\tilde{V}(t) = \bar{V}(t) + n_v(t) \quad \textbf{3.2}$$

$$\tilde{H}(t) = \bar{H}(t) + n_H(t) \quad \textbf{3.3}$$

where $\bar{V}(t)$ and $\bar{H}(t)$ are received message and reference. $n_V(t)$ and $n_H(t)$ terms are zero mean band-limited white Gaussian noise and these two terms are assumed uncorrelated since they are received on different channels. These two noise terms are independent of $\bar{V}(t)$ and $\bar{H}(t)$. The analytical forms of these two noise terms are shown in Eq. **3.4** and Eq. **3.5**.

$$n_V(t) = a_V(t)\cos(2\pi f_n + \theta_V(t)) \quad \textbf{3.4}$$

$$n_H(t) = a_H(t)\cos(2\pi f_n + \theta_H(t)) \quad \textbf{3.5}$$

$a_V(t)$ and $a_H(t)$ are independent Rayleigh distribution random variables and $\theta_V(t)$ and $\theta_H(t)$ are independent uniform distribution random variables within the range $[\pi, -\pi]$. The power of $n_V(t)$ and $n_H(t)$ are equal to their variance since they are zero mean random variables and these are denoted as σ_V^2 and σ_H^2, respectively. We further assume that the power of $\bar{V}(t)$ and $\bar{H}(t)$, both of which are zero-mean band-limited Gaussian processes, are the same and these are denoted as σ_S^2 . From Eq. **3.1**, the SNR_V and SNR_H values at the output of vertical and horizontal polarized antennas are σ_S^2/σ_V^2 and σ_S^2/σ_H^2 respectively. In reality, the bandwidth of $V(t)$ is slightly greater than that of $H(t)$ due to the modulation $m(t)$ induced on it. To hide the signal under the ambient noise and maintain system performance, the bandwidth of $m(t)$ should be very small compared with $H(t)$. Thus, we can assume that the signal bandwidth of $V(t)$ and $H(t)$ (hence the bandwidth of $\bar{V}(t)$ and $\bar{H}(t)$) is B_S, and that the bandwidth of $n_V(t)$ and $n_H(t)$ is B_n (equal to the receive antenna bandwidth). In real system implementation, the B_n is not exactly the same as B_S but will very close to B_S in order to avoid receiving extra interference.

From the discussion in Chapter-2, $\tilde{V}(t)$ will pass through a delay lines, the delay time being the same as the delay line that is implemented in the transmitter. The output of delay line is expressed in Eq. **3.6**.

$$\tilde{V}'(t) = \bar{V}(t - t_1) + n_v(t - t_1) \qquad \textbf{3.6}$$

where t_1 is the delay time of the delay line. The receiver mixes Eq. **3.6** with Eq. **3.3**. The mixed signal $S(t)$ contains the desired signal term $\bar{H}(t-t_1)\bar{V}(t)$ (first term below) and three interference cross terms given by

$$S(t) = \bar{V}(t-t_1)\,\bar{H}(t) + n_V(t-t_1)\,\bar{H}(t) + n_H(t)\,\bar{V}(t-t_1) + n_V(t-t_1)n_H(t) \qquad \textbf{3.7}$$

All the terms in Eq. **3.7** contain the sum frequency components signal and the difference frequency components signal. In the real system implementation, the band-pass filter is used to capture just the sum frequency signal centered at f_c (3 GHz) containing the information message, while discarding all difference frequency signals contained in $S(t)$ are discarded as noise. The sum frequency components signal of each noise term in $S(t)$ is given by

$$\begin{aligned} n_V(t-t_1)\bar{H}(t)_{sum} &= 0.5a(t-t_1)a_V(t-t_1)\cos(2\pi f_c t + \theta(t-t_1) + \theta_V(t-t_1) + 2\delta) \\ n_H(t)\bar{V}(t-t_1)_{sum} &= 0.5a_H(t)a(t-t_1)m(t-t_1)\cos(2\pi f_c t - \theta(t-t_1) + \theta_H(t) + \delta) \\ n_H(t)n_v(t-t_1)_{sum} &= 0.5a_H(t)a_V(t-t_1)\cos(2\pi f_c t + \theta_H(t) + \theta_V(t-t_1) + \delta) \end{aligned} \qquad \textbf{3.8}$$

where $\delta = -2\pi f_n t_1$.

3.2.2 Modeling noise terms

Let $\mathrm{BPF}\big(x(t)\big)$ denote the band-pass filtered output of the signal $x(t)$. The band-pass filtered noise signals are denoted as $n_1(t)$, $n_2(t)$, and $n_3(t)$, where $n_1(t) = \mathrm{BPF}\big(n_V(t-t_1)\bar{H}(t)_{sum}\big)$, $n_2(t) = \mathrm{BPF}\big(n_H(t)\bar{V}(t-t_1)_{sum}\big)$, and $n_3(t) = \mathrm{BPF}\big(n_H(t)n_V(t-t_1)_{sum}\big)$. In order to calculate the BER, the probability density function (PDF) of filtered noise needs to be found. Because the PDF of multiple two independent zero mean Gaussian

variable is approximated by a modified Bessel function of the second kind as shown in Eq. **3.9**, the closed form probability density function for the sum $n_1(t)+n_2(t)+n_3(t)$ is extremely difficult to derive. σ_x and σ_y in Eq. **3.9** are square root of the variance of the random variable x and y respectively.

$$f(n)=\frac{1}{\pi\sigma_x\sigma_y}K_0\left(\frac{|n|}{\sigma_x\sigma_y}\right) \qquad \textbf{3.9}$$

Because the bandwidth of filtered noise is much smaller than before filtering, the noise spectrum following the filter is relatively flat compared to the sum frequency noise. Thus, we assume the filtered noise to be a white Gaussian random variable. For convenience, we assume that the bandwidth of the band-pass filter is twice that of the low-pass filter following the second down-conversion, since the low-pass filter is the key component dominating the received noise spectrum before the decision circuit. Later in this chapter, we will compare the approximate model with simulation results to show that our derivation by applying this assumption also works when the bandwidth of band-pass filter is much greater than bandwidth of low-pass filter.

Based on our simulation analysis, a cumulative distribution function (CDF) and probability density function comparison between $n_1(t)$ (a representative interference term) and a zero mean band-limited Gaussian with the same power and frequency range are shown in Figure **3-2** and Figure **3-3**. In the simulation, the bandwidth of band-pass filter is 40 MHz (B_L =20 MHz), the bandwidth of signal B_S is 970 MHz, and the bandwidth of the channel noise B_n is 980 MHz. From results shown in Figure **3-2** and

Figure **3-3**, both CDF and PDF plots are very close. Thus, these results validate our assumption that the filtered sum frequency noise terms can be approximated as Gaussian

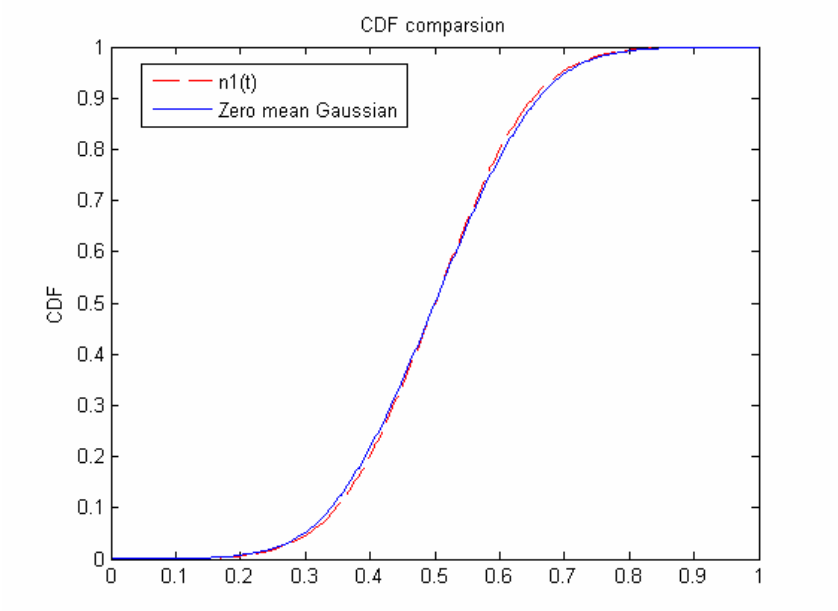

Figure **3-2**: Cumulative distribution function comparison between zero mean Gaussian and band-pass filtered noise term.

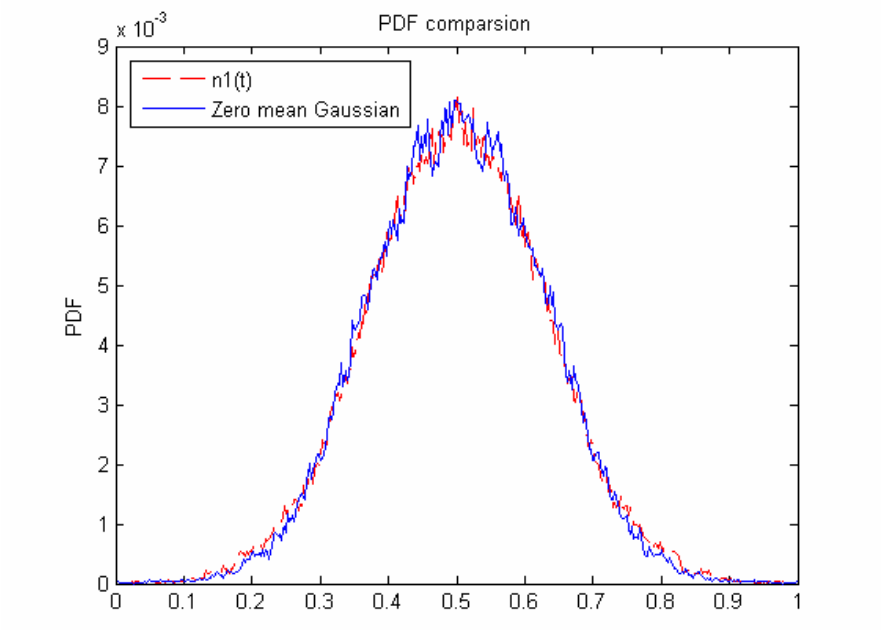

Figure **3-3**: Probability density function comparison between zero mean Gaussian and band-pass filtered noise term.

After recognizing that the filtered noise can be approximated as a Gaussian, the means and variances of the filtered noise terms need to be found for calculating the BER. Since the ideal filter is considered as a linear component, the mean of $n_1(t)$ can be found by

$$\begin{aligned} E\left[n_1(t)\right] &= E\left[\int_{-\infty}^{\infty} h(\tau) n_V(t-t_1-\tau)\bar{H}(t-\tau)d\tau\right] \\ &= \int_{-\infty}^{\infty} h(\tau) E\left[n_V(t-t_1-\tau)\right] E\left[\bar{H}(t-\tau)\right] d\tau \\ &= 0 \end{aligned} \qquad \textbf{3.10}$$

where the $h(\tau)$ is impulse response of band-pass filter [19]. Similarly, the mean of signals of $n_2(t)$ and $n_3(t)$ are both zero. The next step is to calculate the variance of filtered noise and the variance of filtered noise which is equal to its power. Clearly, the

power of $n_1(t)$, $n_2(t)$, and $n_3(t)$ can be obtained by integrating the power spectrum of the sum frequency noise of $n_V(t-t_1)\bar{H}(t)$, $n_H(t)\bar{V}(t-t_1)$, and $n_V(t-t_1)n_H(t)$ within the band-pass filter frequency range.

Again, we try to find the variance of $n_1(t)$ first and then use the same concept to find the variance of the $n_2(t)$ and $n_3(t)$. It is clear to show that the power of $n_1(t)$ is equivalent to integrating the power spectrum of $n_V(t-t_1)\bar{H}(t)_{sum}$ within the band-pass filter frequency range. The power spectrum of $n_V(t-t_1)\bar{H}(t)_{sum}$ is denoted as $S_{n_V,\bar{H}}(f)$. The average power of this sum frequency component noise needs to be found first in order to find the mathematical expression of $S_{n_V,\bar{H}}(f)$. We know that for a given ergodic random process $x(t)$, its autocorrelation function $R_{xx}(\tau)$ and its power spectral density $S_x(f)$ form a Fourier Transform pair, i.e. $R_{xx}(\tau) \leftrightarrow S_x(f)$. Furthermore, the average power of such a random process is the value of the autocorrelation function at zero lag, i.e. equal to $R_{xx}(0)$. From the above discussion and Eq. **3.8**, the average power of $n_V(t-t_1)\bar{H}(t)_{sum}$ can be found by

$$\begin{aligned} P_S &= E[(0.5a(t-t_1)a_V(t-t_1)\cos(2\pi f_c t+\theta(t-t_1)+\theta_V(t-t_1)+2\delta))^2] \\ &= 0.125E\left[a^2(t-t_1)a_V^2(t)\cos(4\pi f_c t+2\theta(t-t_1)+2\theta_V(t-t_1)+4\delta)\right]+0.125E[a^2(t-t_1)a_V^2(t-t_1)] \\ &= 0.125E\left[a^2(t-t_1)\right]E\left[a_V^2(t-t_1)\right]. \end{aligned} \quad \textbf{3.11}$$

Recognizing that $a(t-t_1)$ and $a_V(t-t_1)$ are independent Rayleigh distributed random variables. Furthermore, the k^{th} moment of a Rayleigh distributed random variable x is noted as

$$E[x^k] = \begin{cases} 1 \cdot 3 \cdots k\sigma^k \sqrt{\pi/2} & k = 2n+1 \\ 2^n n! \sigma^{2n} & k = 2n \end{cases} \quad \textbf{3.12}$$

where $\sqrt{\pi\sigma^2/2}$ is the mean. Appling $k = 2$ and $n = 1$ into Eq. **3.12**, the $E\left[a^2(t-t_1)\right]$ and $E\left[a_V^2(t-t_1)\right]$ can be calculated as $2\sigma_s^2$ and $2\sigma_V^2$ respectively. Therefore, we have

$$P_S = 0.5\sigma_S^2\sigma_V^2 \quad \textbf{3.13}$$

$S_{n_V,\bar{H}}(f)$ has a trapezoidal shape with center at f_c and the bandwidth is B_n plus B_S because $S_{n_V,\bar{H}}(f)$ is generated by convolution of two rectangular spectra. The center frequency of these two spectra is $0.5f_c$ and the bandwidth of these two spectra are B_n and B_S respectively. Since B_n will be very close to B_S in the system implementation, the $S_{n_V,\bar{H}}(f)$ can be considered as an isosceles triangle shape with the center at f_c and the bandwidth $B_n + B_S$. By using the known fact that the integration of $S_{n_V,\bar{H}}(f)$ is $0.5\sigma_S^2\sigma_V^2$ and knowing the bandwidth, shape, and center of $S_{n_V,\bar{H}}(f)$, the mathematical forms of the $S_{n_V,\bar{H}}(f)$ can be found as

$$S_{n_V,\hat{H}}(f) = \begin{cases} \dfrac{-2\sigma_V^2\sigma_S^2|f-f_c|}{(B_n+B_S)^2} + \dfrac{\sigma_V^2\sigma_S^2}{B_n+B_S}, & f_c - 0.5(B_n+B_S) \le f \le f_c + 0.5(B_n+B_S) \\ 0, & \text{otherwise.} \end{cases} \quad \textbf{3.14}$$

A simulation result of $S_{n_V,\bar{H}}(f)$ is shown in Figure **3-4** and which proves that $S_{n_V,\bar{H}}(f)$ has an isosceles triangle shape. In the simulation, B_n is 980 MHz while B_S is 960 MHz. Because the finite length data are used to plot the spectrum and finite length data cannot exactly describe the behavior of a random variable, the magnitude fluctuation

appears in Figure **3-4** .That is the same reason to explain why the spectrum plots of $V(t)$ and $H(t)$ in Chapter-2 also have magnitude fluctuation.

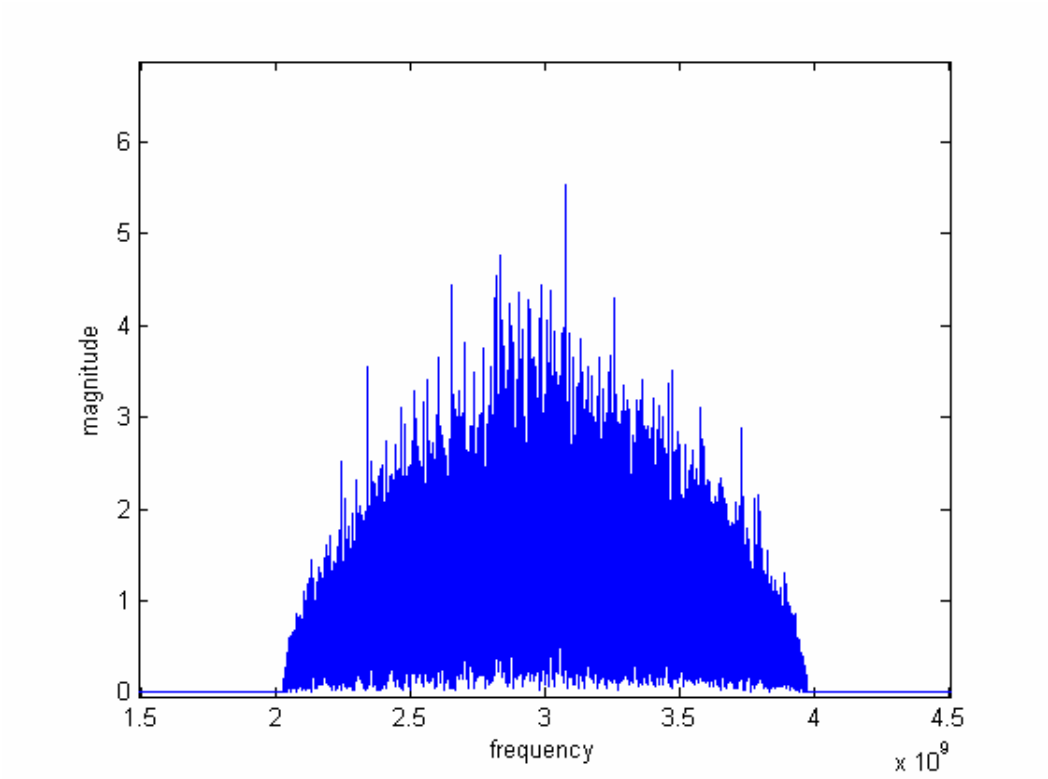

Figure **3-4**: Spectrum of $n_V(t-t_1)H(t)_{sum}$.

Using Eq. **3.14**, the average power (variance) of filtered noise $n_1(t)$ can be found by

$$P_{n1} = \int_{f_c - B_L}^{f_c + B_L} S_{n_V,\hat{H}}(f)df = 0.5G_1\sigma_S^2\sigma_V^2 \qquad \textbf{3.15}$$

where G_1 is given by

$$G_1 = \left(1 - \left(1 - \frac{2B_L}{B_n + B_S}\right)^2\right) \qquad \textbf{3.16}$$

In a similar manner, $n_2(t)$ and $n_3(t)$ can be derived as $0.5G_1\sigma_S^2\sigma_H^2$ and $0.5G_2\sigma_V^2\sigma_H^2$, respectively, where G_2 is given by

$$G_2 = \left(1 - \left(1 - \frac{B_L}{B_n}\right)^2\right) \qquad \textbf{3.17}$$

From above derivation, the $n_1(t)$, $n_2(t)$, and $n_3(t)$ terms can be considered as zero mean band-limited Gaussian with variances $0.5G_1\sigma_S^2\sigma_V^2$, $0.5G_1\sigma_S^2\sigma_H^2$, and $0.5G_2\sigma_V^2\sigma_H^2$. The summation of $n_1(t)$, $n_2(t)$, and $n_3(t)$, representing the total interference component, is also a zero mean band-limited Gaussian random variable and we denote it as $n(t)$. The variance of $n(t)$ is equal to its average power and is given by

$$\begin{aligned}\text{var}(n) = \text{var}(n_1) + \text{var}(n_2) + \text{var}(n_3) + \text{cov}(n_1, n_2) \\ + \text{cov}(n_1, n_3) + \text{cov}(n_2, n_3)\end{aligned} \qquad \textbf{3.18}$$

where $\text{cov}(x, y)$ is the covariance between x and y defined as

$$\text{cov}(x, y) = E[xy] - E[x]E[y] \qquad \textbf{3.19}$$

It can be readily shown that $\text{cov}(n_1, n_2)$, $\text{cov}(n_1, n_3)$, and $\text{cov}(n_2, n_3)$ are zero because $n_1(t)$, $n_2(t)$, and $n_3(t)$ are uncorrelated to each other. Applying this result to the Eq. **3.18**, the Eq. **3.18** can be reduced as

$$\text{var}(n) = 0.5(G_1\sigma_S^2\sigma_V^2 + G_1\sigma_S^2\sigma_H^2 + G_2\sigma_V^2\sigma_H^2) \qquad \textbf{3.20}$$

$n(t)$ can be expressed as $N(0, 0.5(G_1\sigma_S^2\sigma_V^2 + G_1\sigma_S^2\sigma_H^2 + G_2\sigma_V^2\sigma_H^2))$. This RF band-limited Gaussian noise is mixed with the 3-GHz carrier and then down conversion to the baseband. The power of the baseband noise is 25% of $n(t)$ due to the mixing process.

The baseband noise is also zero mean Gaussian random variable with power $0.125(G_1\sigma_S^2\sigma_V^2 + G_1\sigma_S^2\sigma_H^2 + G_2\sigma_V^2\sigma_H^2)$.

3.2.3 Modeling signal term

From Eq. **2.10**, when the low-pass filter does not truncate the spectrum of received baseband signal, the average power of received baseband signal can be calculated by finding the fourth moment of $a(t-t_1)$ and can be shown as

$$P_b \approx E\left[(0.25a^2(t-t_1))^2\right] = 0.5\sigma_S^4 \qquad \textbf{3.21}$$

Because the $a^2(t-t_1)$ term in Eq. **2.10** will spread the baseband signal power into large frequency range and is much wider than the bandwidth of low-pass filter, the low-pass filter adding in the receiver will truncate the signal spectrum and the received baseband signal power will smaller than $0.5\sigma_S^4$. The power loss factor ρ should be included in Eq. **3.21** to properly reflect the effect of adding a low-pass filter. ρ is defined as the ratio between the truncated baseband signal power after the low-pass filter to the untruncated baseband signal. Clearly, the loss factor satisfies $0 \le \rho \le 1$ and the power of the received baseband signal at the output of low-pass filter is represented as $0.5\rho\sigma_S^4$. Figure **3-5** shows MATLAB simulation results of the spectrum plots of the received baseband signal. In the simulation, the bandwidth of transmitted signal is 970-MHz and the bit rate is 5 Mbps. The plots demonstrate that the signal power disperses into large frequency range and this spectrum leakage will decrease the power efficiency and contaminate the adjacent channel. In digital communication, the pulse shaping is

commonly used to solve this problem but our research shows that $a^2(t-t_1)$ term still disperses the received baseband signal power into a large frequency range even if the pulse shaping filter is implemented in the transmitter [20]. An example of adding Raised-Cosine filter with roll-off factor of 0.25 in the system is shown in Figure **3-6.** From Figure **3-6**, we can observe that the pulse shaping technique does not solve this problem. Thus, increasing the power efficiency for NMCC system is still an open problem.

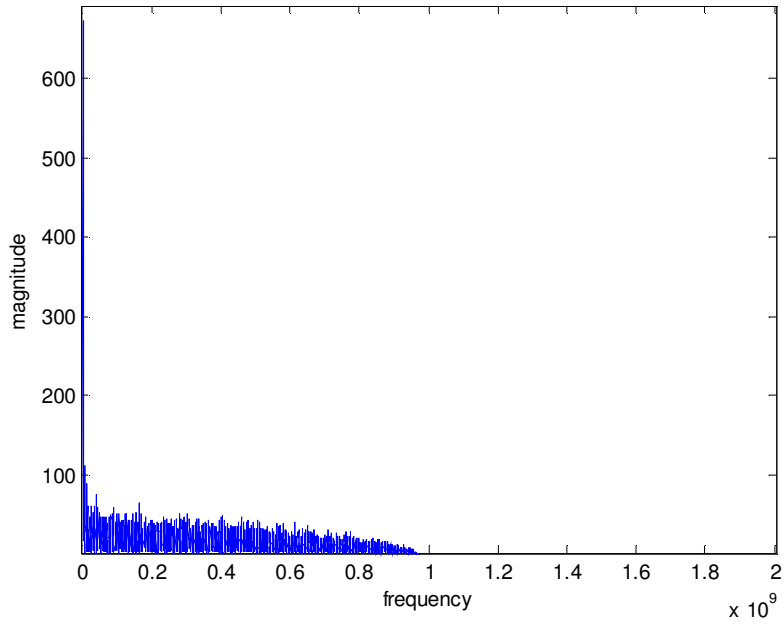

Figure **3-5**: Power spectrum of received baseband signal.

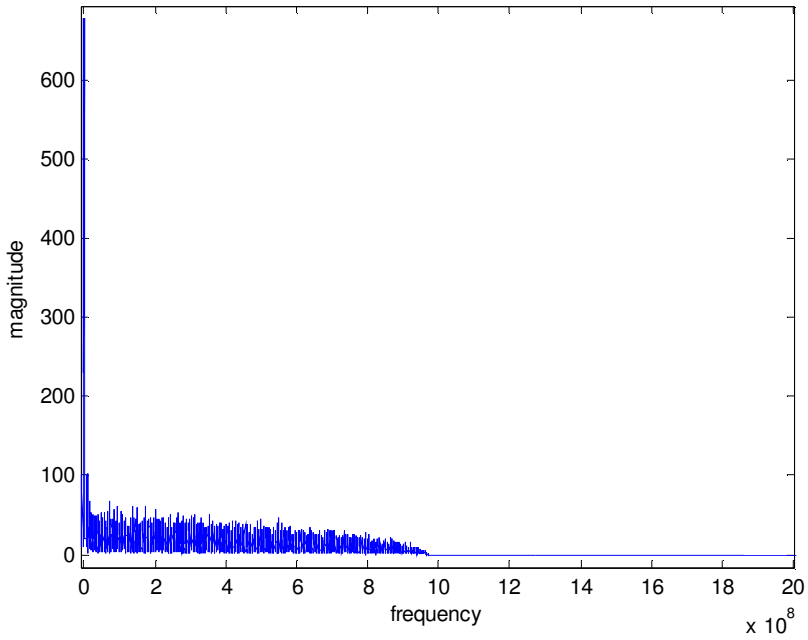

Figure **3-6**: Power spectrum of received baseband signal when Raised-Cosine filter added in the transmitter.

3.2.4 Comparing simulation results and theoretical results

Since the baseband noise can be approximated to a zero mean Gaussian noise and the binary modulation is used, the BER equation of the NMCC system can be expressed by the Q-function with two parameters. One is the spectrum magnitude of the noise (N_0) and the other is bit energy (E_b) [21]. The spectrum magnitude of the baseband noise can be found by dividing its power with its bandwidth and the bit energy can be found by times the power of the received baseband signal with the bit duration time T_b. The power of the baseband noise is found in Section-3.2.2 and is $0.125(G_1\sigma_S^2\sigma_V^2 + G_1\sigma_S^2\sigma_H^2 + G_2\sigma_V^2\sigma_H^2)$. The power of received baseband signal is found in Section-3.2.3 and is $0.5\rho\sigma_S^4$. With these information, the BER of the NMCC system with a two sided spectrum can be modeled as

$$P_e = Q\left(\sqrt{\frac{E_b}{N_0}}\right) = Q\left(\sqrt{\frac{8\rho\sigma_S^4 T_b B_L}{G_1\sigma_S^2\sigma_V^2 + G_1\sigma_S^2\sigma_H^2 + G_2\sigma_V^2\sigma_H^2}}\right) \qquad \textbf{3.22}$$

The well-known $Q(x)$ function is shown below for reference as

$$Q(A) = \frac{1}{\sqrt{2\pi}}\int_A^\infty e^{-x^2/2}dx \qquad \textbf{3.23}$$

Eq. **3.22** can be also expressed using $\mathrm{SNR_V}$ and $\mathrm{SNR_H}$ as follows

$$P_e = Q\left(\sqrt{\frac{8\rho T_b B_L}{G_1\mathrm{SNR_V^{-1}} + G_1\mathrm{SNR_H^{-1}} + G_2\mathrm{SNR_V^{-1}SNR_H^{-1}}}}\right) \qquad \textbf{3.24}$$

Because the PDF of baseband signal after passing through a low-pass filter does not have a closed form, the loss factor ρ is numerically found by Matlab simulation. In order to

find the loss factor properly, the bandwidth of the band-pass filter in the simulation must be wide enough (2-4 GHz) to ensure that the filter will not truncate the spectrum of the sum frequency components signal while successfully discarding the difference frequency components signal. An example shown in Figure **3-7** reveals that the spectrum of received baseband signal is more concentrated near 0-Hz when the bandwidth of $V(t)$ and $H(t)$ is decreases.

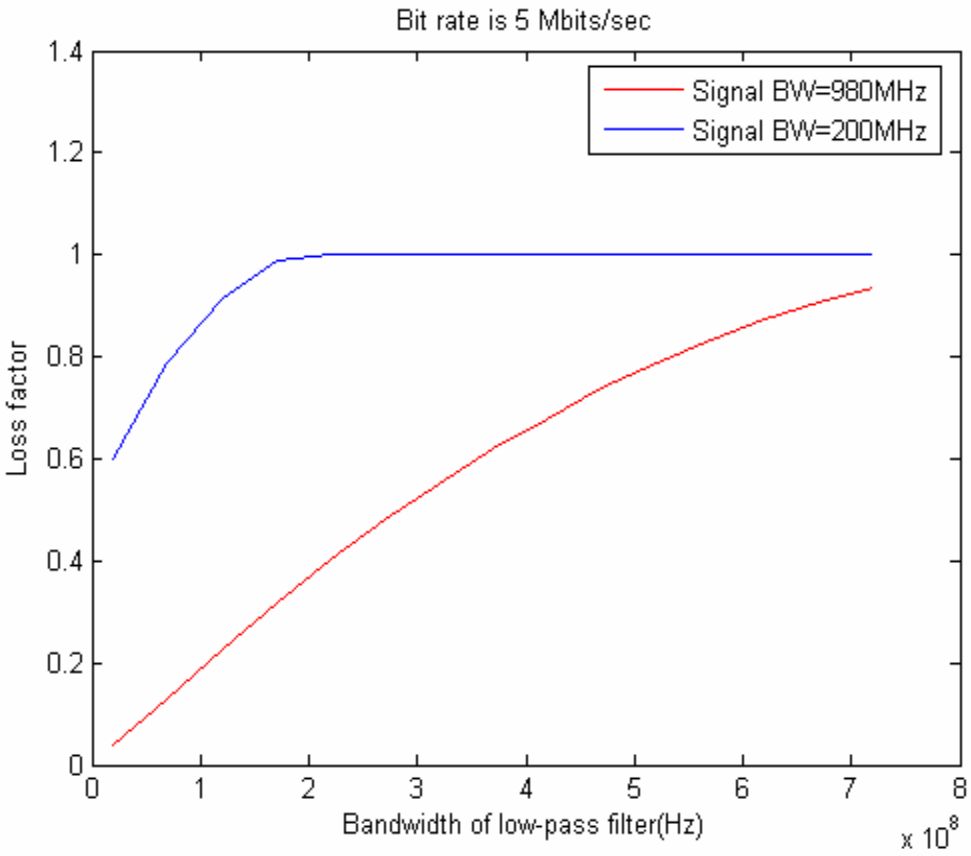

Figure **3-7**: Loss factor verse bandwidth of low-pass filter

As finding the loss factor, a whole system simulation is performed to compare simulation results with Eq. **3.24** and the results are plotted in Figure **3-8**, Figure **3-9**, and Figure **3-10**. Since the NMCC system is an UWB communication system, we only discuss the cases when the bandwidth of transmitted signals is greater than 500 MHz. In the simulation setup, the SNR_V and SNR_H are equal. The bandwidth of the antenna is equal to the bandwidth of transmitted signal ($B_S = B_n$). The band-pass filter has a bandwidth of 100 MHz and is centered at 3 GHz while the low-pass filter bandwidth is 20 MHz or 7 MHz. From our independent simulation results, bit rate is 5 Mbps, the value of ρ is 0.5 and 0.487 when the bandwidth of low-pass filter is 20 MHz and 7 MHz, respectively, and the bandwidth of antenna is 980 MHz. ρ is approximately 0.52 and 0.5 when the bandwidth of low-pass filter is 20 MHz and 7 MHz ,respectively, and the bandwidth of antenna is 500 MHz. The value of ρ is 0.49 and 0.518 when the bit rate is 10 Mbps and 2 Mbps respectively for a antenna bandwidth of 980 MHz and low-pass filter bandwidth of 20 MHz.

From Figure **3-8**, Figure **3-9**, and Figure **3-10**, we observe that the system performance is improved when the bandwidth of $V(t)$ and $H(t)$ increases. That is because the noise power will be dispersed into larger frequency ranges after the mixing process and the processing gain will increase.

We also note that the maximum deviation between the simulation results and approximate model is 1 dB. As the bandwidth of $V(t)$ and $H(t)$ decreases, the deviation between simulation results and approximate model increases. In our derivation, we assume that the filtered noise is white Gaussian. As the ratio between the bandwidth of

filtered noise and the bandwidth of the sum frequency components noise decrease, the spectrum of filtered noise losses the flat spectrum characteristic and the filtered noise loss the white Gaussian noise characteristics. Thus, the deviation increases. Comparing with the results in Figure **3-8** and Figure **3-9**, the deviation decreases when the ratio between the bandwidth of low-pass filter and the bandwidth of the sum frequency components noise decrease and this phenomenon proves our above discussion.

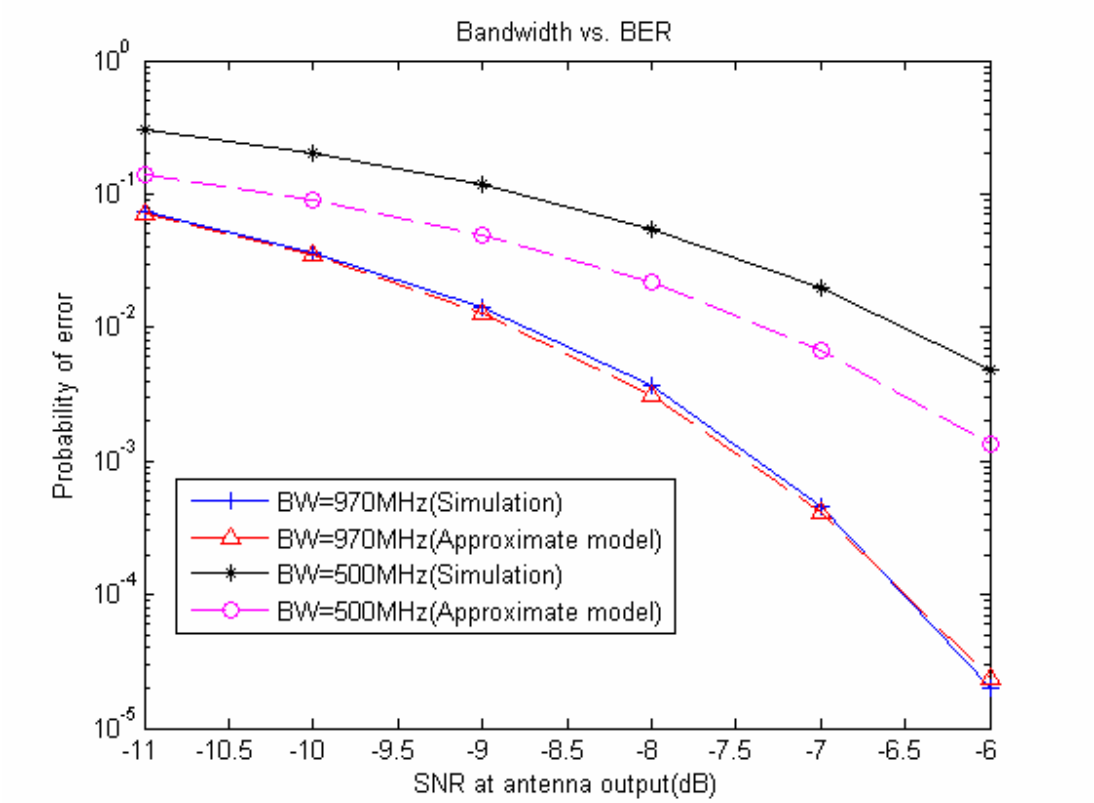

Figure **3-8**: Comparison of SNR and BER characteristics between simulation and approximate model in a single user environment at different signal bandwidths (BW of low-pass filter is 20 MHz).

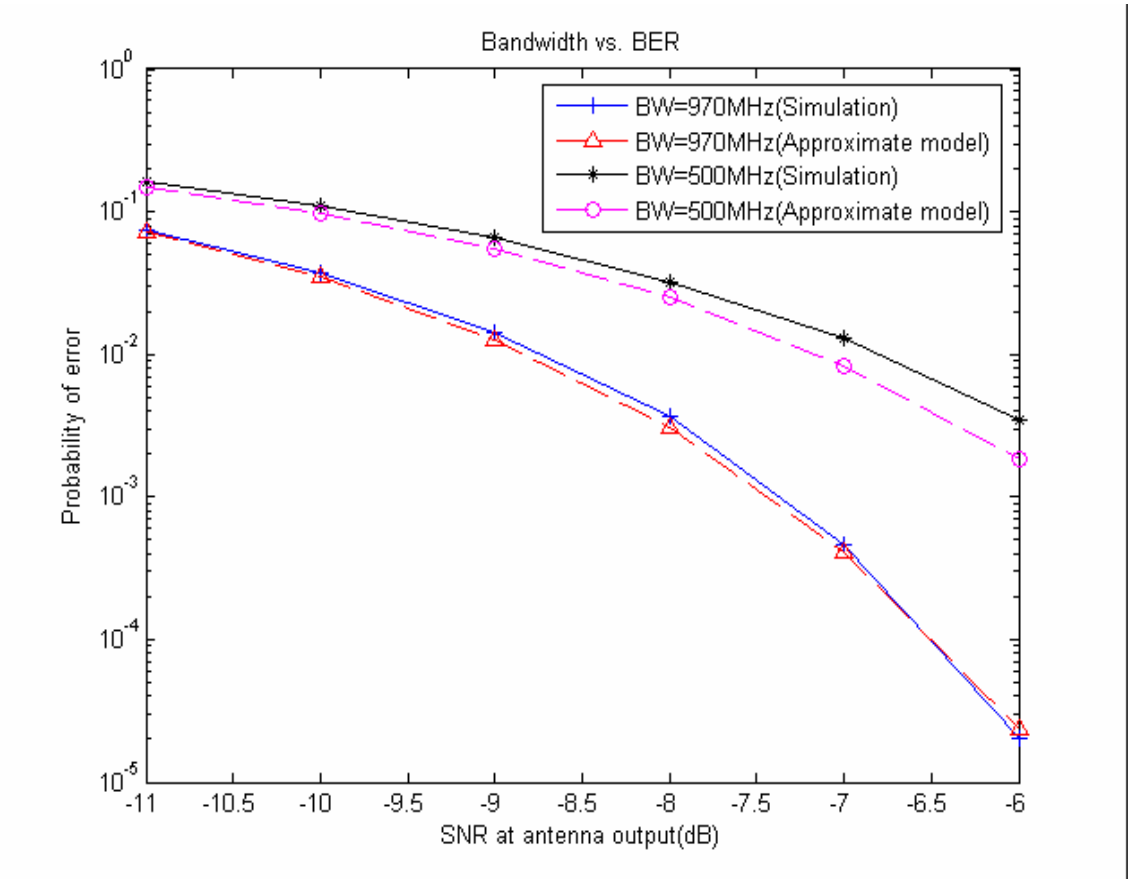

Figure **3-9**: Comparison of SNR and BER characteristics between simulation and approximate model in a single user environment at different signal bandwidths (BW of low-pass filter is 7 MHz).

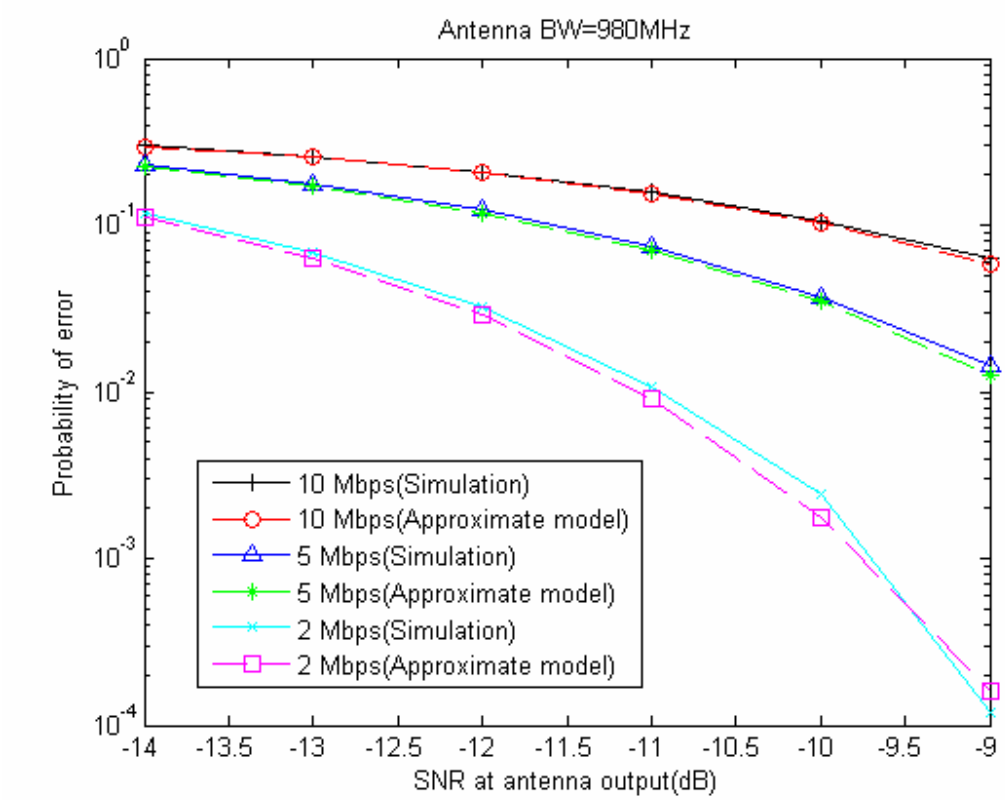

Figure **3-10**: Comparison of SNR and BER characteristics between simulation and approximate model in a single user environment at different bit rates (BW of low-pass filter is 20 MHz).

The relation between the SNR at output of the low-pass filter and the SNR at receiver antenna's output is shown in Eq. **3.25** .The plot of Eq. **3.25** is shown in Figure **3-11**.

$$\mathrm{SNR}_{\mathrm{base}} = \frac{4\rho}{(G_1\mathrm{SNR}_{\mathrm{V}}^{-1} + G_1\mathrm{SNR}_{\mathrm{H}}^{-1} + G_2\mathrm{SNR}_{\mathrm{V}}^{-1}\mathrm{SNR}_{\mathrm{H}}^{-1})} \qquad \textbf{3.25}$$

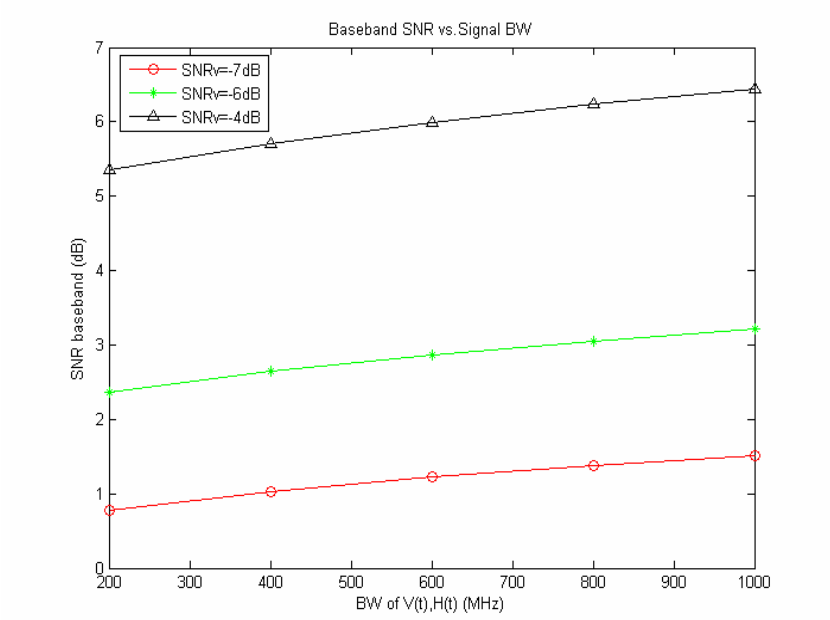

Figure **3-11**: SNR at baseband verse different signal bandwidths.

3.3 Multiuser performance in white Gaussian channel

In a multiuser environment, each user uses the same channel but is assigned a different delay. The receiver contains a switchable delay bank between the vertical polarization antenna and the first mixer to select a particular user. If σ_i^2 is the signal

power corresponding to the i^{th} user, the received signals in the vertically and horizontally polarized antennas in an additive white Gaussian noise channel are given by

$$\tilde{V}_N(t) = \sum_{i=1}^{N} \bar{V}_i(t) + n_V(t) \qquad \textbf{3.26}$$

$$\tilde{H}_N(t) = \sum_{i=1}^{N} \bar{H}_i(t - t_i) + n_H(t) \qquad \textbf{3.27}$$

when there are N users in the channel. The t_i term in Eq. **3.27** is the specific delay time assigned to the i^{th} user, and the receiver already knows this information. $\bar{V}_i(t)$ and $\bar{H}_i(t)$ are message and reference signals corresponding to i^{th} user. Since the output signals of different noise generators are independent of each other, the $\bar{V}_i(t)$ terms are independent to each other and so are the $\bar{H}_i(t)$ terms.

For any user who wants to receive the message from the i^{th} user, the delay line with the delay t_i between vertical polarization antenna and the first mixer in the receiver is activated. Then, the signal at the output of the first mixer can be written as

$$\begin{aligned} S_N(t) = {} & \bar{V}_i(t - t_i)\bar{H}_i(t - t_i) + \sum_{n=1}^{N}\sum_{m=1}^{N} \bar{V}_m(t - t_i)\bar{H}_n(t - t_n) \\ & + \sum_{m=1}^{N} (\bar{V}_m(t - t_i)n_H(t) + \bar{H}_m(t - t_m)n_V(t - t_i)) + n_V(t - t_i)n_H(t), \qquad (m,n) \neq (i,i). \end{aligned} \qquad \textbf{3.28}$$

The second term in Eq. **3.28** can be considered as interference and its characteristics are similar to the third and fourth terms when the difference between each t_i term is large enough. Thus, the sum frequency signal in Eq. **3.28** contains $N^2 - 1$ interference terms with bandwidth $2B_S$, $2N$ interference terms with bandwidth $B_S + B_n$, and one interference term with bandwidth $2B_n$. All the interference terms are centered at f_c.

Using the same method that was used to derive the BER for the single-user environment, the BER equation for N users in the additive white Gaussian noise channel can be modeled as

$$P_e = Q\left(\sqrt{\frac{8\rho\sigma_i^4 T_b B_L}{G_3\sum_{n=1}^{N}\sum_{m=1}^{N}\sigma_n^2\sigma_m^2 + G_1\sum_{m=1}^{N}(\sigma_m^2\sigma_H^2 + \sigma_m^2\sigma_V^2) + G_2\sigma_V^2\sigma_H^2}}\right), \qquad (m,n) \neq (i,i). \qquad \textbf{3.29}$$

The G_1 and G_2 terms are shown in Eq. **3.16** and Eq. **3.17** respectively, and G_3 is given by

$$G_3 = \left(1 - \left(1 - \frac{B_L}{B_S}\right)^2\right) \qquad \textbf{3.30}$$

In our simulation, we assume that each user has the same power, in which case, Eq. **3.29** reduces to

$$P_e = Q\left(\sqrt{\frac{8\rho\sigma_S^4 T_b B_L}{((N^2-1)G_3\sigma_S^4 + G_1 N(\sigma_S^2\sigma_H^2 + \sigma_S^2\sigma_V^2) + G_2\sigma_V^2\sigma_H^2)}}\right) \qquad \textbf{3.31}$$

The bit rate is 5 Mbps and the bandwidth of antenna and the signal are 980 MHz and 970 MHz respectively. The simulation results are shown in Figure. **3-12** from which we note that the deviation between the simulation results and theoretical results is less than 0.5 dB. As the number of users increases, the noise floor also increases and the BER degrades.

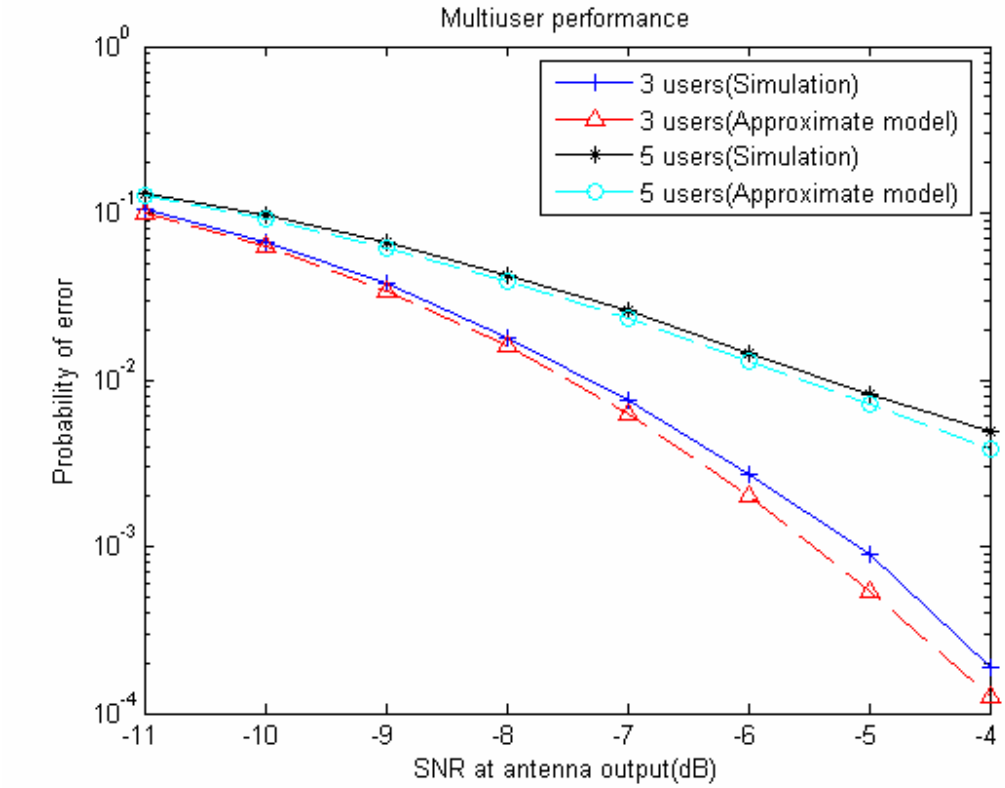

Figure **3-12**: Comparison between approximate model and simulation in multi-user environment.

Chapter 4

System implementation and comprehensive field experiment

4.1 Transmitter and receiver implementation

Since the characteristics of wideband noise propagation in the channel are an open problem, the prototype system is built and is tested in the field to verify this idea functionally. At transmitter side, a 1–2-GHz noise source at a power level of 0 dBm is used. The noise source is connected with a 1.2–1.8-GHz band-pass filter and then to an amplifier and a power divider. One output of power divider is connected with horizontal polarization antenna and the other output of the power divider is connected to the single sideband up-converter. The binary modulated bit sequence that generated by the FPGA board is mixed with a 3-GHz carrier as radio frequency modulated signal. This RF modulated signal is amplified and then mixes with filtered noise in the single sideband up-converter. The lower sideband is chosen, amplified, and sent to the vertical channel. The transmitted signals in both vertical and horizontal channels have a power level of 10-dBm.

At receiver side, the 40-dB gain limiting-amplifiers are connected after antennas to drive mixer in the square-low region. A 2.9–3.1-GHz band-pass filter and two 14-dB gain amplifiers are connected after the mixer at the receiver. The output of the amplifier is connected to the second mixer and then to a low-pass filter with 1.9-MHz bandwidth. The low-pass filter is connected to the second FPGA board where the bit sequence can be

retrieved by proper timing and framing synchronization. The transmitter side implementation and receiver side implementation are shown in Figure **4-1** and Figure **4-2**.

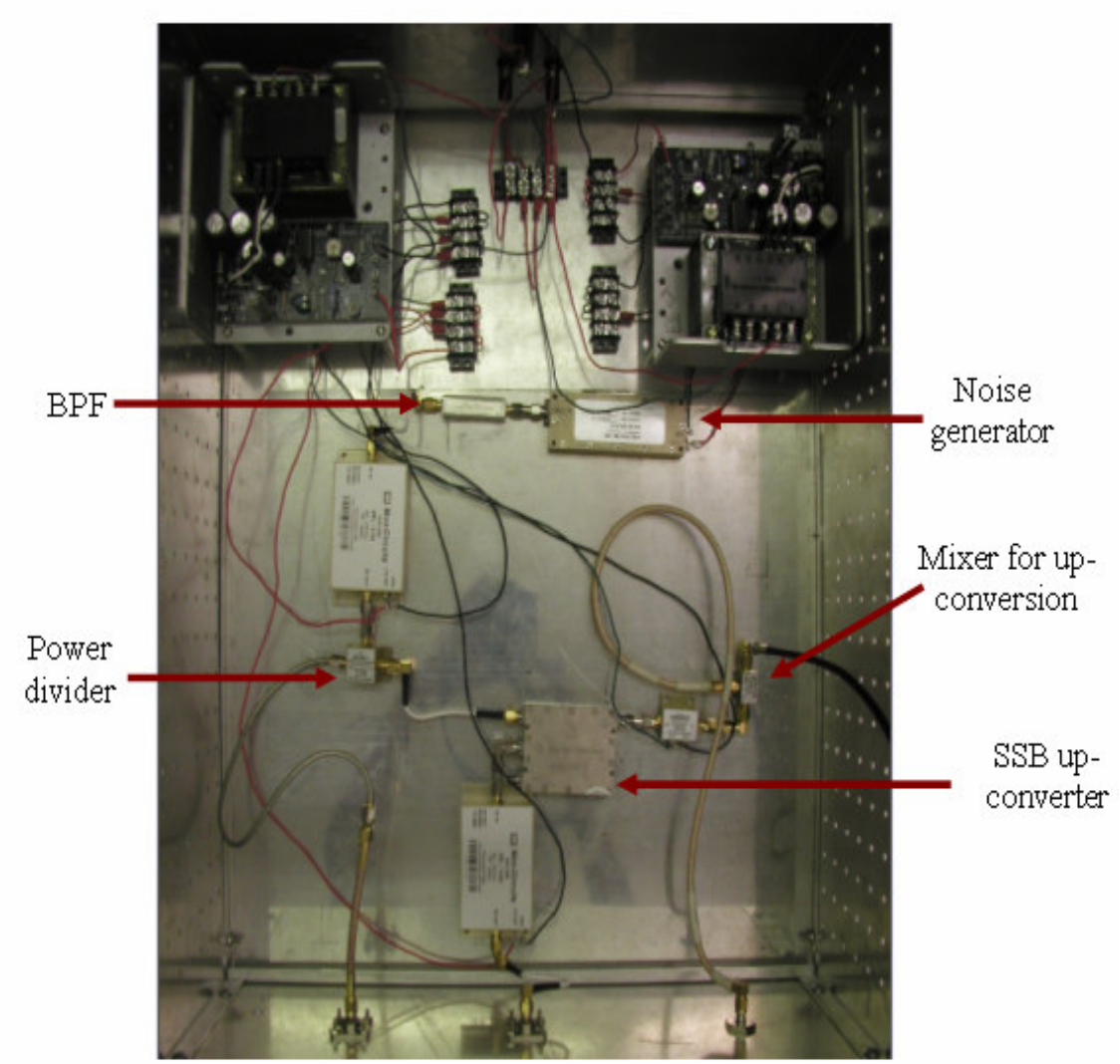

Figure **4-1**: Transmitter side implementation (BPF=band-pass filter).

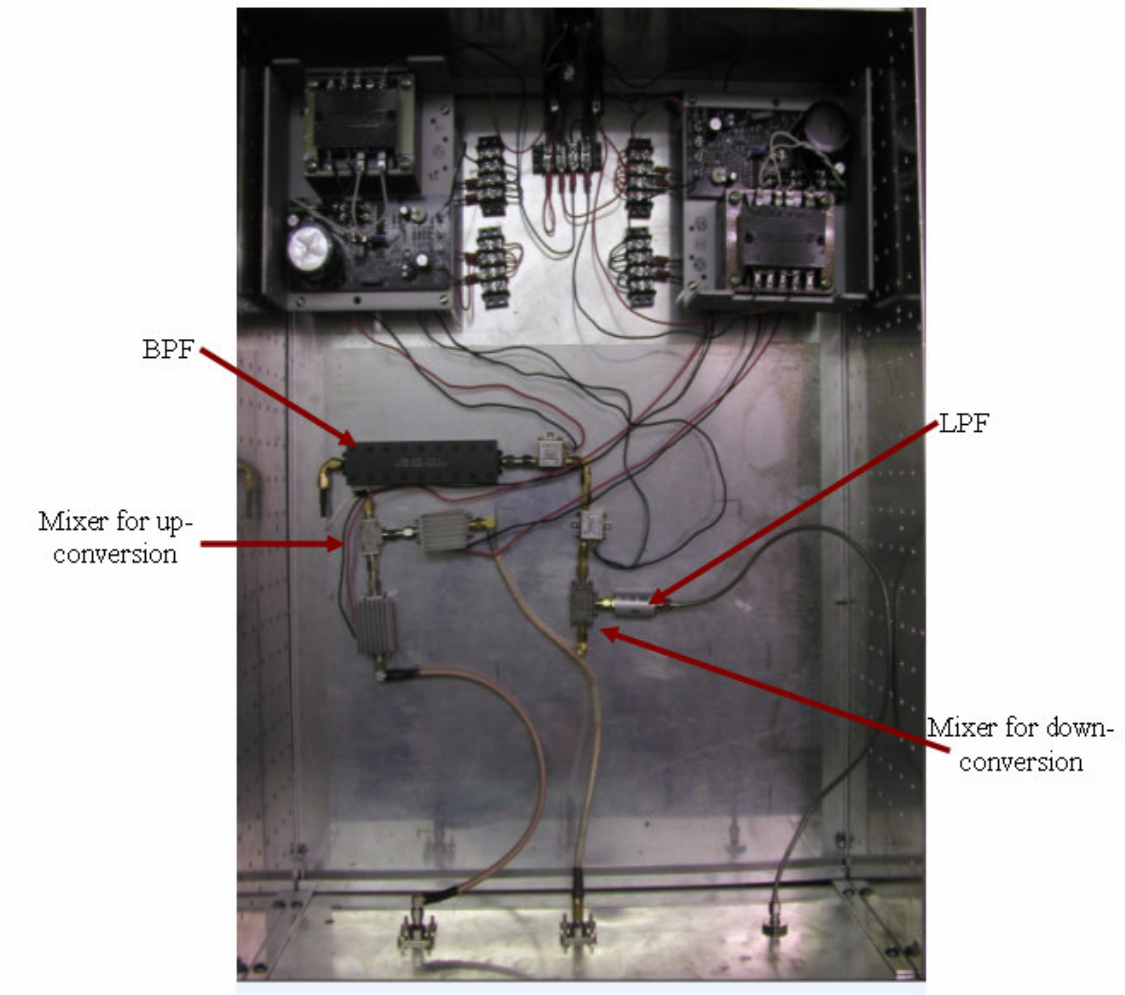

Figure **4-2**: Receiver side implementation (BPF=band-pass filter, LPF=low-pass filter).

4.2 Baseband signal processing implementation

4.2.1 Board selection

In order to accomplish the real time audio experiment, the baseband signal processing is implemented into the Lyrtech SignalWAVe FPGA board. The photo of this board is shown in Figure **4-3**. The SignalWAVe is an entry level DSP/FPGA design platform but provides all the functions that we need. It features include wireless video and audio signals capabilities. A complementary function of this FPGA architecture enables the user to design the system under Matlab/ Simulink environment. This FPGA board has one Xilinx Virtex-2 chip and one Texas Instruments 'TMS320C6713' DSP chip. The ADC in the board has a 65-MHz sample frequency and the DAC has a 125-MHz sample frequency with programmable gain [22].

4.2.2 Transmitter baseband signal processing design

At transmitter side, the "PCM 3008" block controls the "Audio in" port which has sample frequency 3.85-KHz. The sampled value is send to FPGA design portion by "DSP Bus" block and the FPGA design of the transmitter is shown in Figure **4-4**. Each sampled value translates to 14-bit frame and then sends to the multiplexer. The multiplexer will insert header between data frame and is controlled by the counter. When the value in the counter is smaller or equal to fourteen, the multiplexer enables the "d0" port and the system start to insert the header. Otherwise, the "d1" port is enabled and the multiplexer

selects the data which is from DSP bus. In our design the header is inserted between every seven thousand data frames.

The design of header generator is show in Figure **4-5**. The counters in the header generator should synchronize with the counter which controls the multiplexer. The header is composed by 15 registers with initial value set [1,0,1,1,1,0,1,0,1,0,0,0,0,0,0]. When counter value is smaller or equal to fourteen, the registers will be enabled and the header will start sending to the multiplexer. When the counter value is equal to seven thousands, all the registers will reset and the header generator will start to insert the header into the data frame again.

The bit sequence with header converts to analog value ±1 by "Convert-2" block. The bit-1 translates to 1 while the bit-0 translates to -1. Clearly, the binary modulation is accomplished in this step. To increase the Euclidean distance between bit-1 and bit-0, the translated value multiples a proper gain. The higher gain means the higher output power of the DAC (Larger Euclidean distance). By setting gain value is equal to 2^{14}, we can have the maximum output power since this FPGA board uses 14-bit frame to presents any analog value. The bits rate in our audio design is approximately 54 Kbps because the sample frequency for sampling the audio is 3.85-KHz and each sample value translates to 14-bit frame.

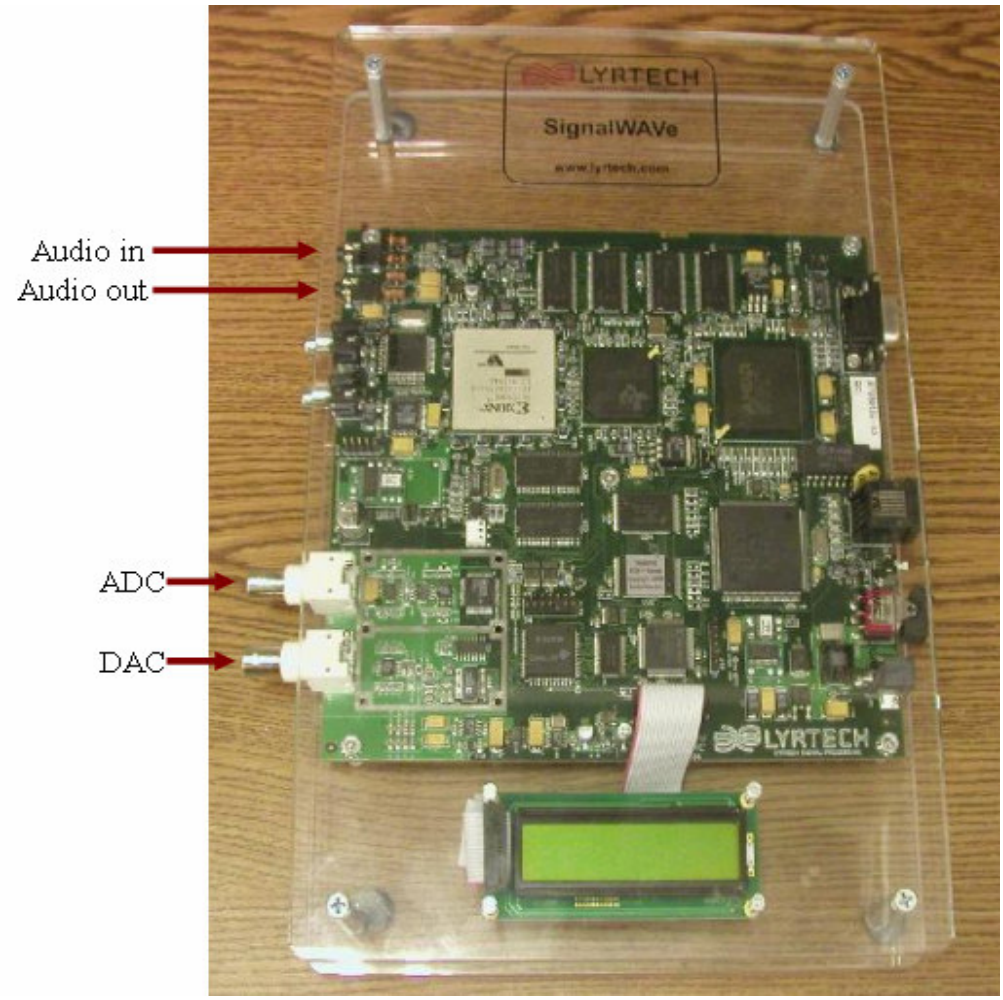

Figure **4-3**: The photo of Lyrtech SignalWAVe FPGA board.

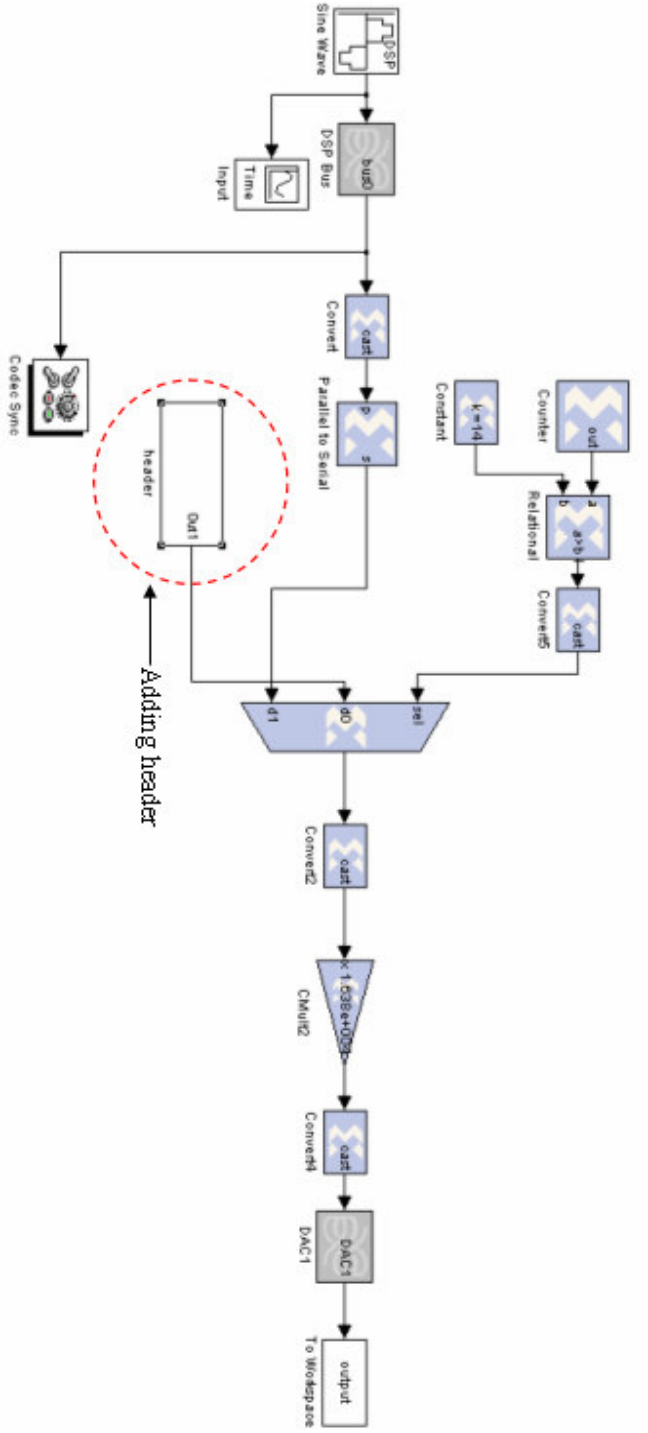

Figure **4-4**: Transmitter side FPGA design.

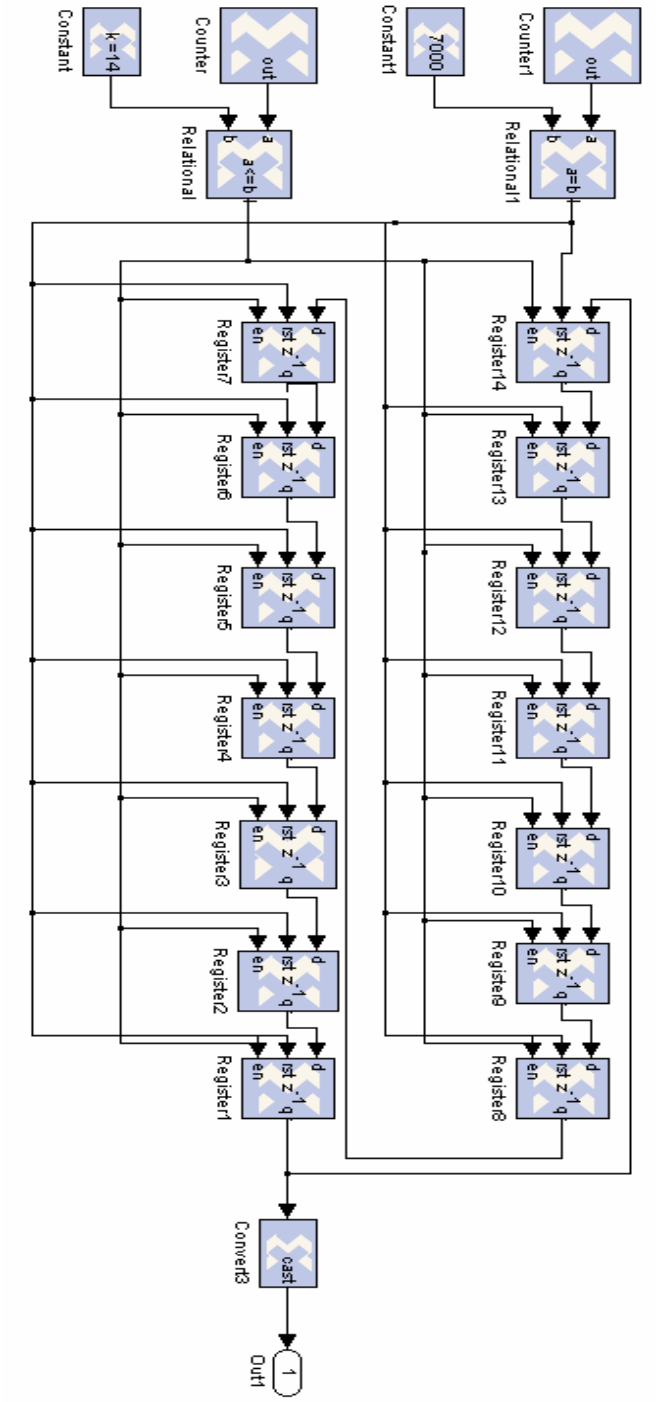

Figure **4-5**: Design of header generator.

4.2.3 Receiver baseband signal processing design

The receiver's FPGA design is shown in Figure **4-7**. The ADC samples the received signal with sample frequency 54-KHz. This implies that only one sample is taken from each bit for making decision. The sampled signal passes through a threshold detector where the negative voltage presents as -1 and the positive voltage presents as 1. Because the output of threshold detector is a signed fixed point integer with 2-bits long, the -1 is presented by bits [0,1] while the 1 is presented by bits [1,0]. The Xilinx "Shift" block , added after the threshold detector, is used to catch the first bit of each input value that is sending from the threshold detector. Thus, the output of "Shift" block is bit-0 when the input is -1. Otherwise, the output is bit-1. Clearly, the demodulation of binary modulated signal is accomplished by threshold detector and "Shift" block.

After demodulation, the next step is to reconstruct the original analog waveform from the demodulated bit stream. In order to retrieve the original waveform properly, we need to ensure the bits which are captured by "Serial-to-Parallel" block coming from the same frame. The "Serial-to-Parallel" block will continuously take every 14-bit and then translates back to an analog value when the receiver turns on. Due to the delay causing by propagation and wiring, the 14-bit that catch by this block may come from adjacent frames and the receiver can not correctly retrieve the original analog waveform. An example of correct capture and error capture is shown in Figure **4-6**.

By using header detector and address shift register, we can ensure the "Serial-to-Parallel" block catches the correct bits. The demodulated bit stream is sent to the header detector where the detector compares incoming bit stream with the known header

([1,0,1,1,1,0,1,0,1,0,0,0,0,0]) bit by bit. The output of header detector is connected with an address shift register with 14 bits length. As detecting the header, the counter, counting from 14 to 1 continuously, will export it's currently value to the address shift register. This value will indicate the "Serial-to-Parallel" block to catch correct bit in correct position and the original analog value can be retrieved. This value will not change until the header detector detects the next header.

A simulation is done to verify the design working properly and the results are shown in Figure **4-8**. In the simulation, the channel is ideal and the input signal is sinusoid wave. From Figure **4-8**, our design can successfully retrieve the sending waveform and the delay between input and output is caused by wiring.

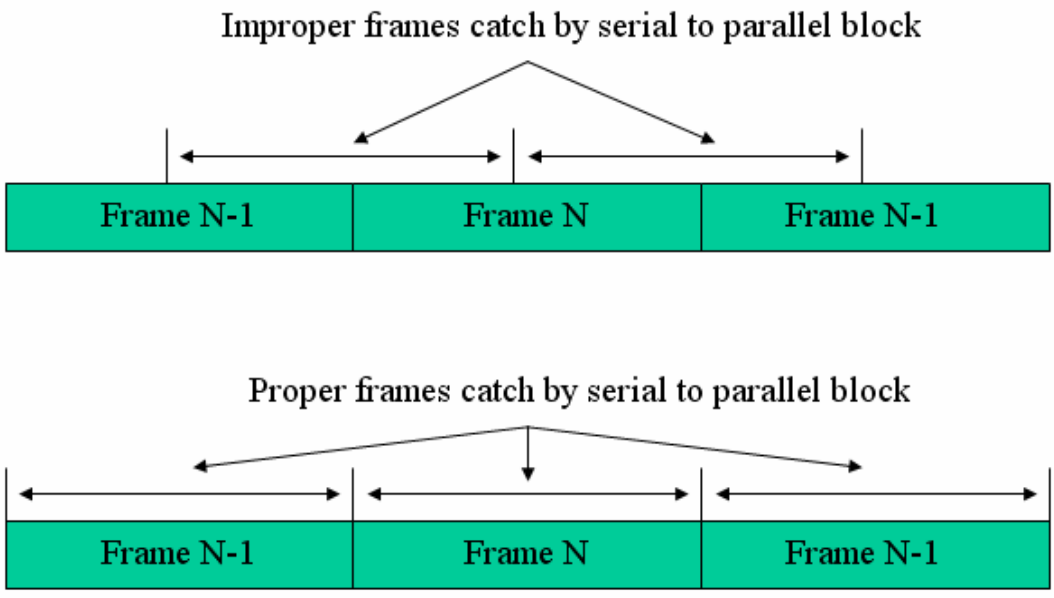

Figure **4-6**: An example of incorrect capture (Top) and correct capture (bottom) of the serial to parallel block.

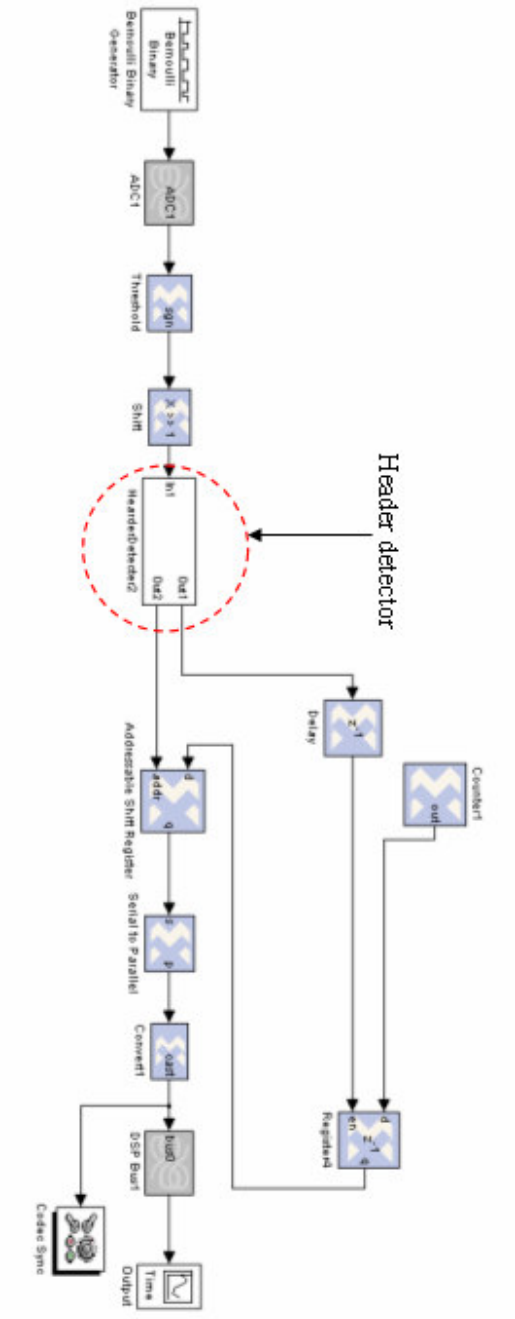

Figure **4-7**: Receiver FPGA design.

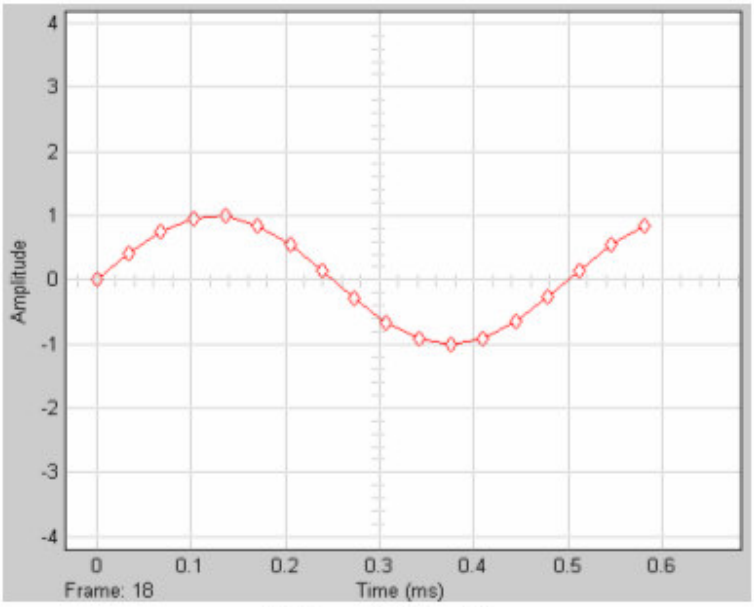

(a) Input Signal

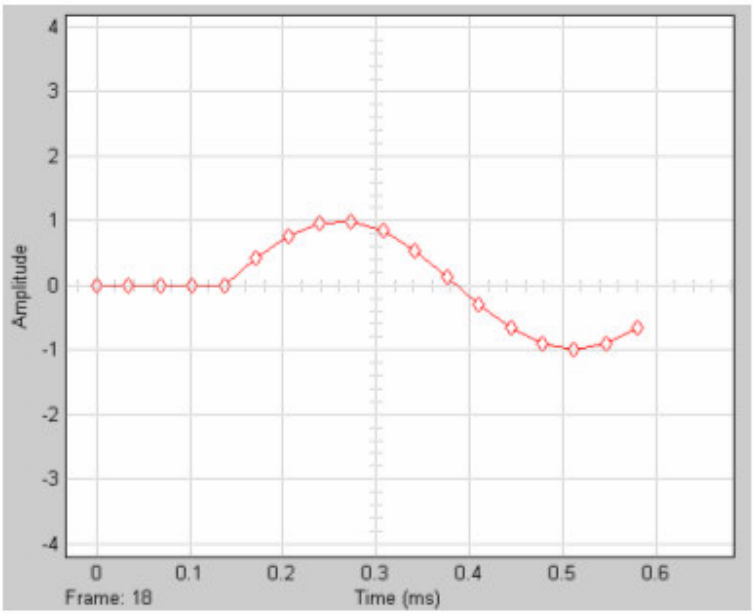

(b) Output Signal

Figure **4-8**: Simulation results of FPGA design.

4.3 Comprehensive field experiment

In the experiment, the system is placed in the open field with grass terrain and the distance between the transmitter and receiver is 30 meters. Based on the free space path loss equation, an additional 10-dB attenuator is added to imitate a distance of 94 meters [23]. Since the carrier synchronization circuit is not built in the receiver, an Agilent E4438C vector signal generator is used as a common frequency source. The experimental setup is shown in Figure **4-9** , Figure **4-10**, and Figure **4-11**.

At the receiver side, the power of received signals in the vertical channel and horizontal channel is -43 dBm and -45 dBm, respectively. The HP-8562E spectrum analyzer and Agilent DSO-80804B oscilloscope were used to record the frequency and time domain signal of received $V(t)$ and are shown in Figure **4-12**. Our signal does show random behavior in the time domain and flat spectrum in the frequency domain. The spectrum is not perfectly flat because the conversion loss of the single sideband up-convector is not exactly the same within 1.2–1.8-GHz band.

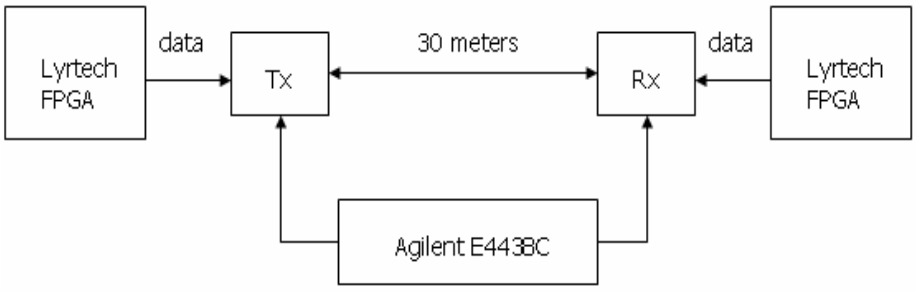

Figure **4-9**: Experiment setup overview.

Figure **4-10**: Experiment setup transmitter view.

Figure **4-11**: Experiment setup receiver view.

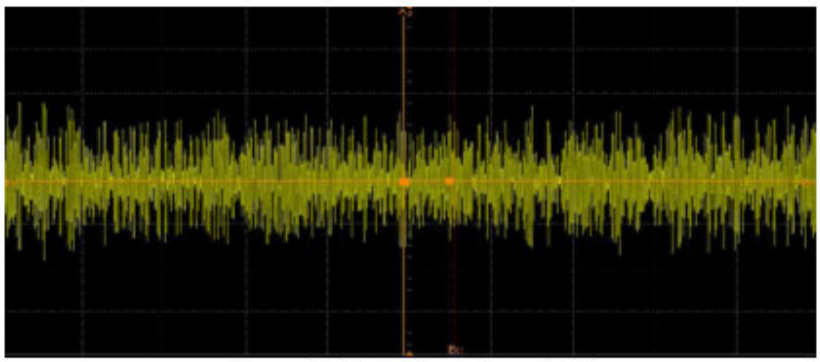

a. Recorded time domain of V(t)

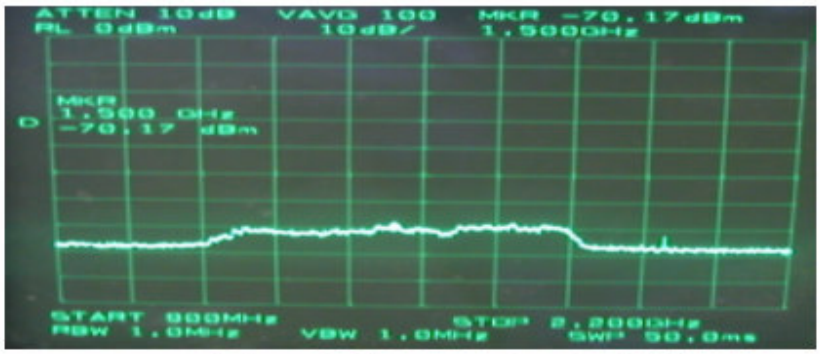

b. Recorded frequency domain of V(t)

Figure **4-12**: Time and frequency domain plots of recorded signal.

In the field test, the audio can be heard with good quality. Due to the unknown and uncertain delay caused by wiring and the propagation channel, it is hard to directly compare the input and the output audio waveform. Thus, we compare the sending and receiving bit stream in this section.

By properly modifying the FPGA design, the system will continuously send header with a bit rate of 110 Kbps. Figure **4-13** shows the transmitted (top plot) and the received bit stream in the ideal channel (second plot). The waveform is recorded by the Agilent DSO-80804B oscilloscope at the output of the low-pass filter and then plotted

using Matlab. We note that the ideal channel amplitude fluctuations, caused by the random $a^2(t)$ term, will not affect the decision for binary modulation. The third and bottom plots in the Figure **4-13** show the same bit stream being received in (a) an additive white Gaussian noise channel, and (b) a channel containing tone interference. The added Gaussian noise covers the entire transmission band 1–2-GHz with $\mathrm{SNR_V} = -4$ dB and $\mathrm{SNR_H} = -5$ dB, respectively. The tone interference in the V channel is located at 1.6 GHz and in the H channel at 1.3 GHz with signal-to-interference ratio (SIR) of −3.5 dB.

The zero crossings show up when the channel is not clean but the message can still be retrieved. Although not shown, when both tone interferences are located within the narrow frequency range $(0.5f_c - B_L < f < 0.5f_c + B_L)$ in the low SIR channel, the bit stream is ruined because of high power tone interference at the output of low-pass filter generated by the sum frequency signal of the tone interference in the V-channel mixed with the tone interference in H-channel. Usually, this problem can be solved by adding a digital filter in the baseband signal processing design.

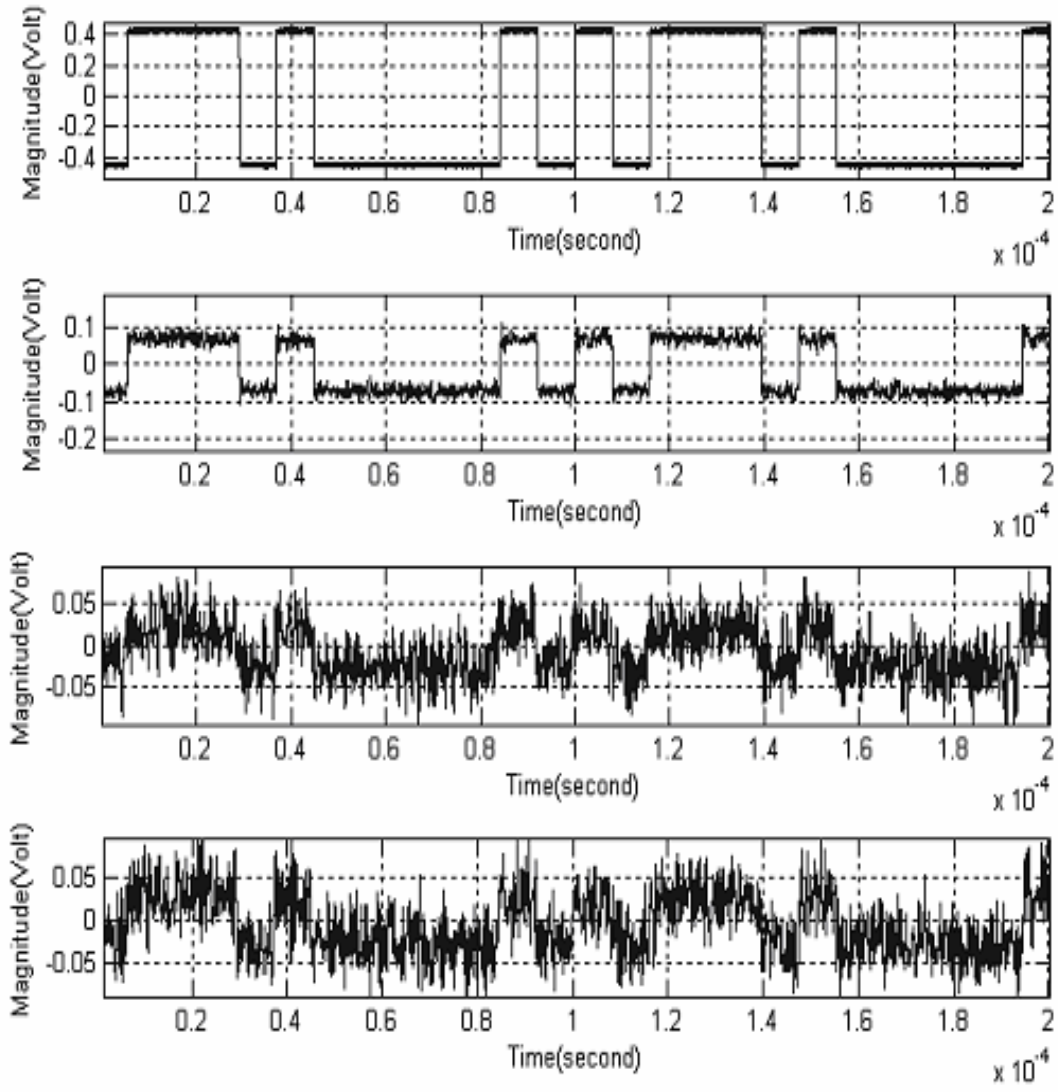

Figure **4-13**: Original transmitted bit stream (Top), Bit stream received in ideal channel (Second from top), Bit stream received in additive white Gaussian noise channel (Third from top), Bit stream received in single-tone interference channel (Bottom).

The system is also tested in the environment when the transmission path contains blockage. In the experiment, the transmission path contains two hardwood trees and one conifer. The periodic bit sequence [1,0,1,0,…] is sent and the distance between transmitter and receiver is 30 meters. The experiment setup is shown in Figure **4-14**. The reason for choosing trees as blockage is because the foliage will generate the multipath and attenuate the power of received signal since the foliage will scatter the transmitted signals.

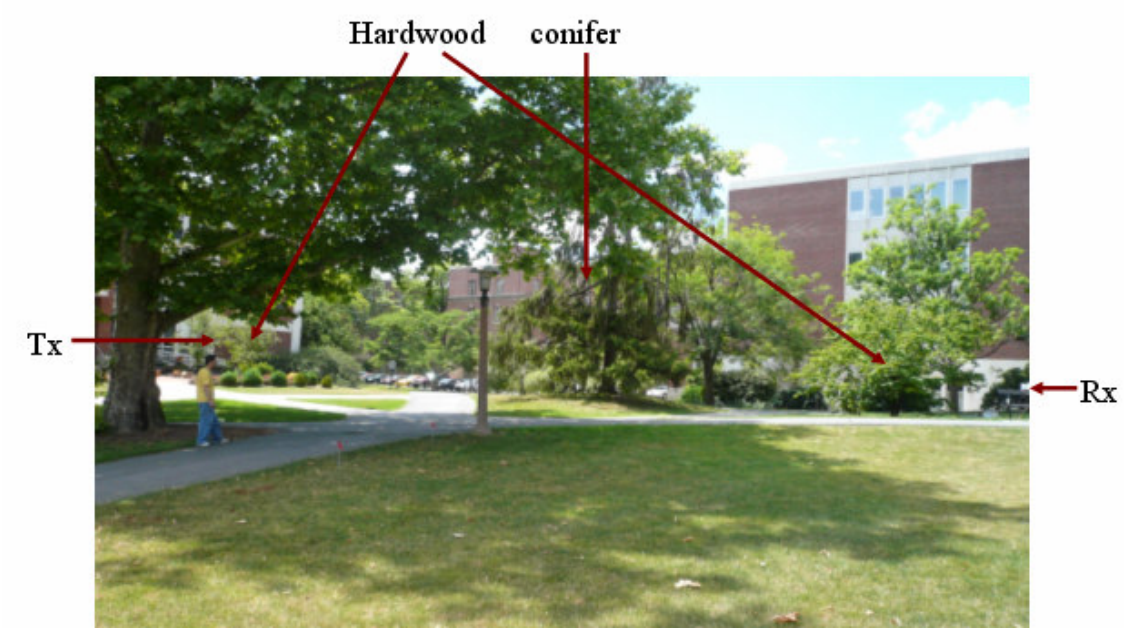

Figure **4-14**: Experiment setup of NMCC system passing trees.

The power spectrum of received $V(t)$ and the received bit stream are shown in Figure **4-15** and Figure **4-16**. From Figure **4-15**, the power level of received $V(t)$ is too low. Thus, our spectrum analyzer cannot recognize it and so does received $H(t)$. The peak located around 1.9-GHz is the cell phone signal. This cell phone interference exists in both channels. The zero crossings show up because the foliage generates the multipath

signals with Doppler shifts. The receiver receives the line of sight signal and those multipath signals simultaneously. Those multipath signals can be considered as interference and increase the noise floor. All the experiments in this chapter are accomplished in the open field. These experimental results not only demonstrate the NMCC system has good immunity to the interference but also verify the system can operate in the real world.

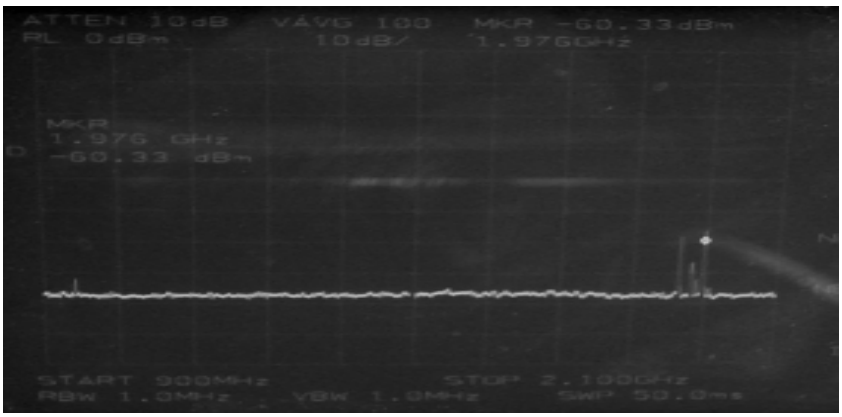

Figure **4-15**: The spectrum of received signal in vertical channel after passing trees.

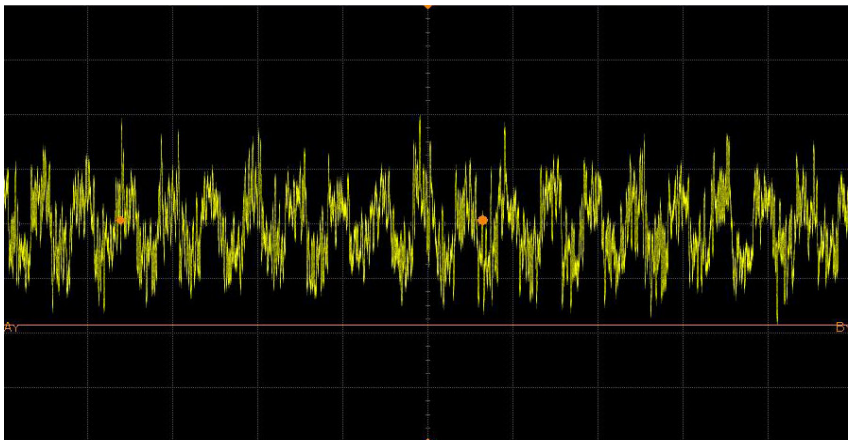

Figure **4-16**: The received baseband signal when the transmission path contains trees.

4.4 Noise cancellation by EMD

In our FPGA design, one sample is taken from each bit to make the bit decision. For this structure, the BER performance is not dependent on the spectrum magnitude of received noise but is dependent on received noise power. Usually, adding a low-pass filter before the decision circuit can reduce the noise power and the BER can be improved. However, it is not adaptive because the bandwidth of low-pass filter is fixed. As channel conditions changes, new filter needs to be implemented. In this section, we will introduce an adaptive noise cancellation method which uses empirical mode decomposition (EMD). The main idea is to subtract the Intrinsic Mode Function (IMF) signals of noise components that are stronger than signal components from received baseband signals.

In 1998, Dr. Norden E. Huang presented novel methods that can decomposition the stationary and non-stationary signal powerfully [24]. This method is called Hilbert Huang Transform (HHT) and the researches demonstrate that this algorithm can be used for the noise cancellation [25]. The HHT is a new adaptive waveform analysis technique based on the EMD. The EMD decomposition represents the data by its IMF signals. In general, the IMF signals should satisfy two conditions [24]:

(1) In the whole data set, the number of local maximum or minimum should equal to the number of zero crossing. This will ensure the maximum is always positive and minimum is always negative.

(2) At any point, the mean value of the envelope defined by the local maximum and the envelope defined by the local minimum the local minima is zero. This is

necessary to ensure the instantaneous frequency will not have the unwanted fluctuation induced by asymmetric waveforms.

The procedure of the EMD decomposition is very simple compared to other non-stationary signal analysis methods. For example, the wavelets analyses needs to find the proper basis for different signals but the EMD is an adaptive process. The procedure for generating IMF signals is shown below. Assume the input signal is $s(t)$ with length T second. The upper envelope $u(t)$ is generated by the maximum of $s(t)$ while the lower envelope $l(t)$ is generated by the minimum of $s(t)$. The mean of upper and lower envelope will be $\left(u(t)+l(t)\right)/2$ and denotes as $m(t)$. The first IMF signal $s_1(t)$ with the highest frequency can be found by

$$s_1(t) = s(t) - m(t) \qquad \textbf{4.1}$$

Theoretically, $s_1(t)$ will be the first IMF signal. In reality, overshoots and undershoots are common, which can also generate new extreme and shift or exaggerate the existing ones. The shifting process can be used to solve this problem. In the shifting process, $s_1(t)$ is treated as data and is used to generate the new first IMF signal. Doing the same procedure that is described above, $m_{1,1}(t)$ is the mean envelope of $s_1(t)$ and the IMF signal corresponds to the first shifting process can shown as

$$s_{1,1}(t) = s_1(t) - m_{1,1}(t) \qquad \textbf{4.2}$$

Assuming $s_{1,k}(t)$ is the IMF signal corresponding to k^{th} shifting process. $s_{1,k}(t)$ can be expressed as

$$s_{1,k}(t) = s_{1,k-1}(t) - m_{1,k-1}(t) \qquad \textbf{4.3}$$

where $m_{1,k-1}(t)$ is the mean envelope of $s_{1,k-1}(t)$.We can declare that $s_{1,k}(t)$ is the first IMF signal when the standard deviation (SD) between $s_{1,k}(t)$ and $s_{1,k-1}(t)$ is smaller than 0.3. The mathematical expression of the SD with parameters $s_{1,k}(t)$ and $s_{1,k-1}(t)$ is shown in Eq. **4.4** [24].

$$SD = \sum_{t=0}^{T} \left[\frac{\left(s_{1,k-1}(t) - s_{1,k}(t) \right)^2}{s_{1,k-1}^2(t)} \right] \qquad \textbf{4.4}$$

By applying the same procedure described above, the second IMF signal can be found from the residue signal $s_2(t)$.

$$s_2(t) = s(t) - I_1(t) \qquad \textbf{4.5}$$

where $I_1(t)$ is the first IMF signal. Repeating above procedure, the remaining IMF signals can be found. The procedure of finding IMF signals will not stop until the k^{th} residue signal is monotonic and no more IMF signals can be extracted. Thus, signal $s(t)$ can be represented by

$$s(t) = \sum_{i=1}^{k} I_i(t) + s_k(t) \qquad \textbf{4.6}$$

The concept of applying the EMD decomposition for noise cancellation is described below. A simplified spectrum plot of received baseband signal in the AWGN channel is shown on Figure **4-17**. The spectrum of noise is flat since the noise is zero mean white Gaussian. From the plot, we can observe that the signal spectrum and noise spectrum have an intercept point at frequency f_0. Defined $SNR(X)$ as the signal to noise

ratio when signal power and noise power are integrated from 0 Hz to X Hz. It is clearly seen that the maximum $SNR(X)$ occurs at $X = f_0$ and $SNR(X)$ starts to decrease when the X is greater than f_0. Clearly, the best way to obtain the maximum SNR is by subtracting the IMF signals which have frequency higher than f_0 from the received baseband signal, and then sending the subtracted signal to the decision circuit.

An experiment was performed to validate that this concept can be used to improve the performance for a sample-based system. In the experiment, the distance between transmitter and receiver is 4 meters and the SNR_V and the SNR_H is -4 dB. The received baseband signal is recorded by "Agilent DSO 80804B" oscillation scope with 25-MHz sample frequency and is shown in Figure **4-18**.

In our FPGA design, the receiver takes one sample from each bit and applies the hard decision rule to make a decision. The zero crossings that show up in Figure **4-18** will cause the error decision if the sample point is just located at the zero crossing regions. The next step is finding the IMF signals of recorded data, and the IMF signals are shown in Figure **4-19**.

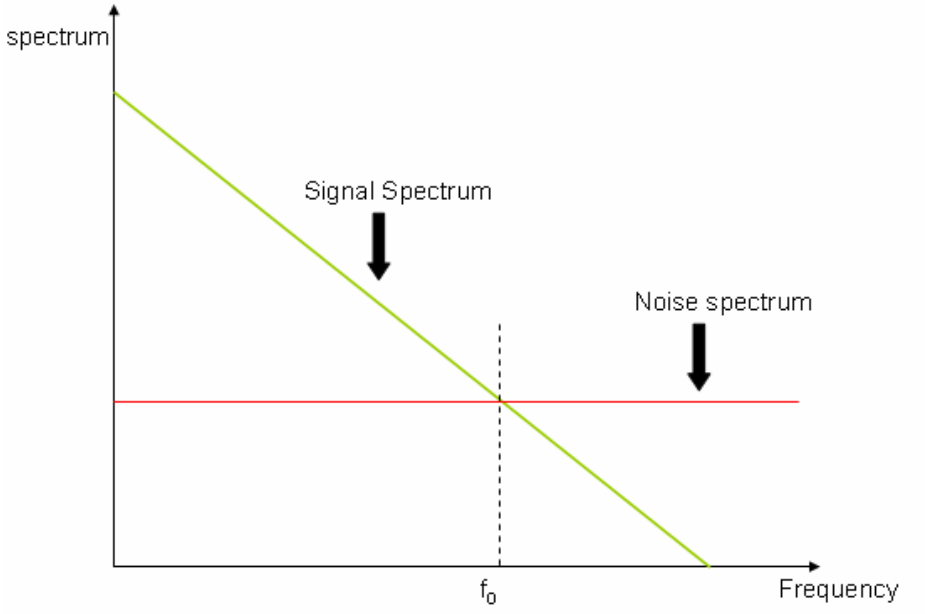

Figure **4-17**: Simplified spectrum plot of received baseband signal.

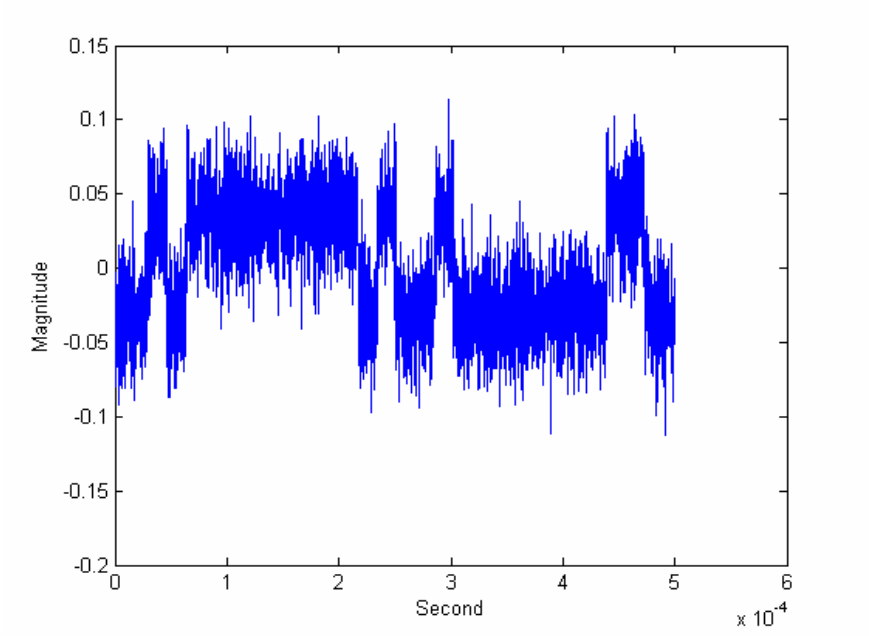

Figure **4-18**: Recorded baseband signal in noisy channel.

.

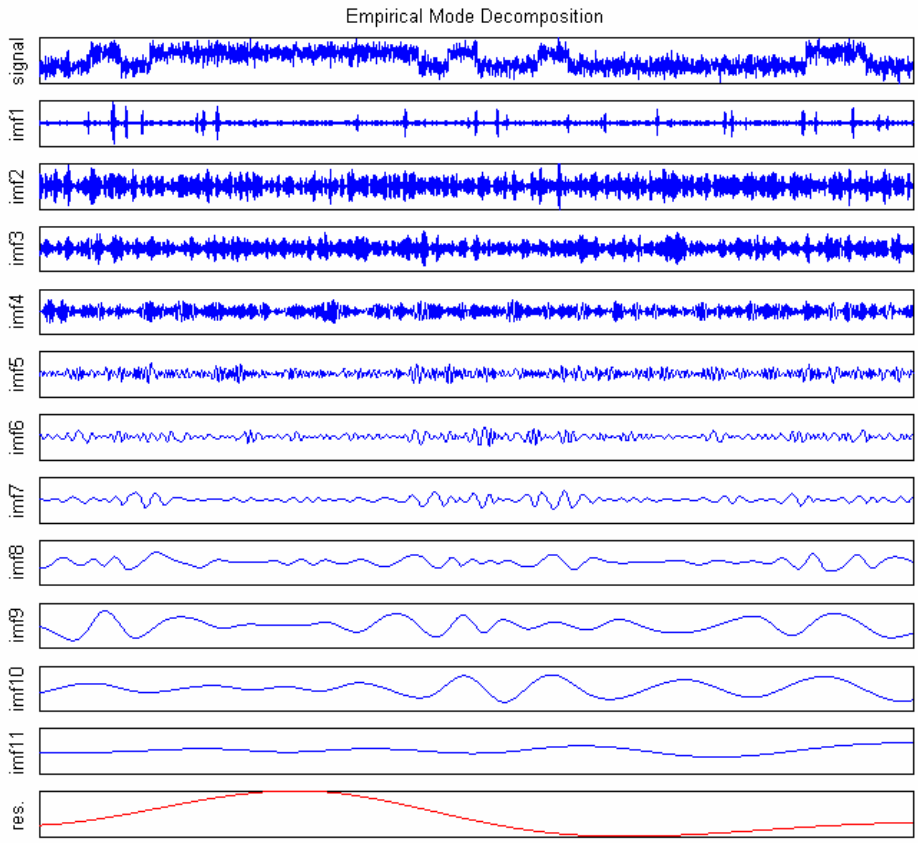

Figure **4-19**: IMF signals of recorded baseband signal.

After finding the IMF signals of the recorded data, the instantaneous frequency of each IMF signal can be obtained by the Hilbert transform. After comparing the instantaneous frequency with the spectrum of received baseband signal, we can observe that the first to fifth IMF signals have frequency always higher than interception point. Thus, we subtract those five IMF signals from recorded data and the result is shown in Figure **4-20**. Comparing the signals after noise cancellation with before noise cancellation, we can observe that all the zero crossings disappear and the decision error will not occur.

These experiment results demonstrate that the EMD is a powerful tool for noise cancellation.

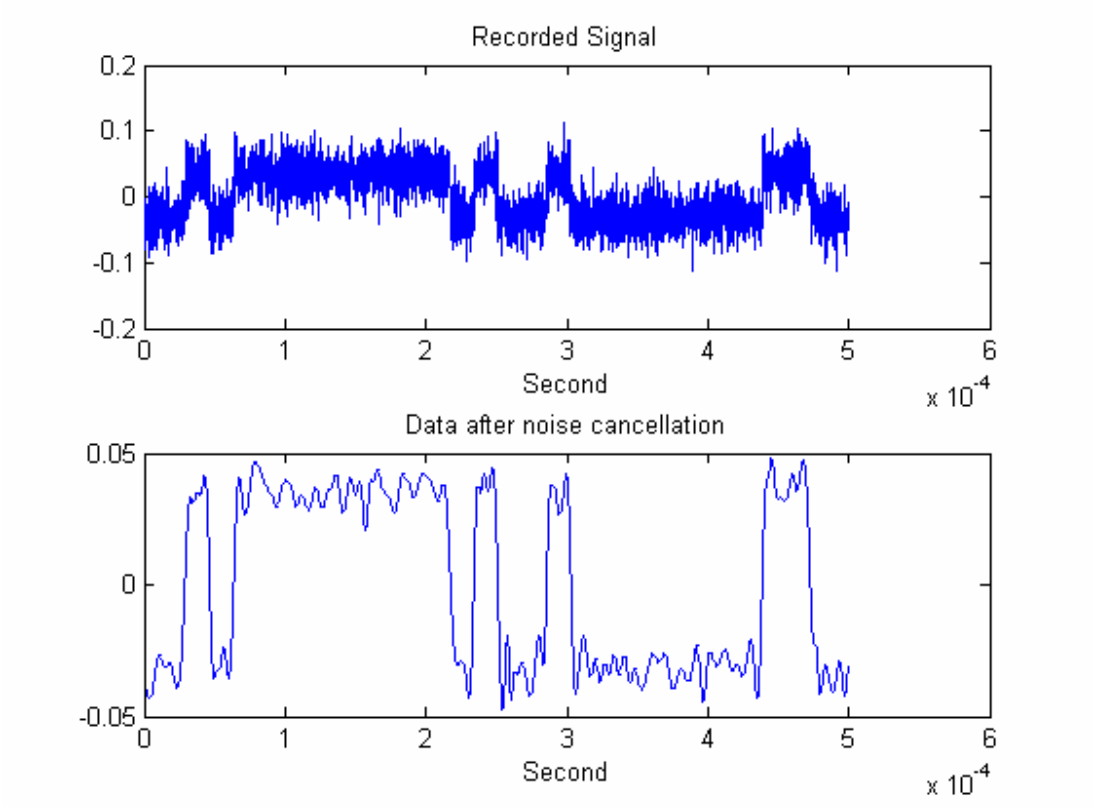

Figure **4-20**: Comparison between the signals before and after noise cancellation.

Chapter 5

Performance of NMCC system subjected to interference

A large processing gain can be achieved because the NMCC system uses a large bandwidth. A drawback in this case is that the system must encounter intentional and non-intentional interference. The first section in this chapter analyzes the system performance in partial-band jamming channels and pulsed noise jamming channels which are commonly used to interfere with spread spectrum or ultra-wideband communication systems [21]. The second section analyzes the system performance in a channel with DS-DS/SS interference which is commonly generated by satellite or other covert communication systems. In the last section, the system in multipath environment, usually generated by ionosphere reflection, atmosphere refraction, and reflections generated by other objects, is analyzed. Instead of using the RAKE receiver, an alternative method is specially designed for the NMCC system to alleviate performance degradation caused by intersymbol interference (ISI) [16][26].

5.1 Partial-Band and Pulse-Noise jamming environment

In a Partial-Band jamming environment, the jammer transmits high power, band-limited zero mean white Gaussian noise as a jamming signal. The bandwidth of the jamming source may be the same as the spread spectrum signal or smaller than the spread

spectrum signal. Usually, the bandwidth of jamming source is smaller than the signal which the jammer intends to interfere, because it is more effective than full band jamming and is easier to generate. We also assume that the bandwidth of jamming source is larger than the bandwidth of low-pass filter used in the receiver.

The received signals from the vertically polarized antenna $\tilde{V}(t)$ and the horizontally polarized antenna $\tilde{H}(t)$ in the Partial-Band jamming channel can be shown as

$$\tilde{V}(t) = \bar{V}(t) + n_v(t) + J(t) \qquad \textbf{5.1}$$

$$\tilde{H}(t) = \bar{H}(t) + n_H(t) + J(t) \qquad \textbf{5.2}$$

where $\bar{V}(t)$ and $\bar{H}(t)$ are received message and reference in V and H channel whose analytical forms were shown in Eq. **2.7** and Eq. **2.8**. $n_v(t)$ and $n_H(t)$ are uncorrelated zero mean Gaussian channel noise whose analytical forms were shown in Eq. **3.4** and Eq. **3.5**, and $J(t)$ is a zero mean white Gaussian jamming signal with center f_J , bandwidth B_J , and power σ_J^2. It is reasonable to assume that the received jamming source in V and H channels are exactly the same since a common jamming source usually reduces the cost. We also assume that the received signals in V and H channels have the same power σ_S^2 and the received channel noise in V and H channel have the same power σ_n^2 . The bandwidth of received signals ($\bar{V}(t)$ and $\bar{H}(t)$) is B_S and the bandwidth of channel noise ($n_v(t)$ and $n_H(t)$) is B_n . In a real system implementation, the bandwidth of the antenna matches that of the received signal ($B_S \approx B_n$). From the discussion seen in

Chapter-2, $\tilde{V}(t)$ will pass through a delay line with delay t_1 and then mix with $\tilde{H}(t)$. The output of delay line can be shown in Eq. **5.3**.

$$\tilde{V}'(t) = \bar{V}(t-t_1) + n_v(t-t_1) + J'(t) \qquad \textbf{5.3}$$

where $J(t-t_1) = J'(t)$. In a real system implementation, t_1 is in the order of microseconds, and can be assumed to be much larger than B_S^{-1}. Thus, $J(t)$ and $J'(t)$ can be considered to be two uncorrelated Gaussian noise waveforms. The mixed signal will pass through a narrow band band-pass filter of bandwidth $2B_L$ designed to catch the sum frequency signal. The output of band-pass filter contains one signal term and eight interference terms. According to the model introduced in Chapter-3, the signal term has power $0.5\rho\sigma_S^4$ after down conversion and then passes through a low-pass filter with bandwidth B_L . The eight noise terms are: $n_1(t) = \text{BPF}\left(n_V(t-t_1)\bar{H}(t)_{sum}\right)$, $n_2(t) = \text{BPF}\left(n_H(t)\bar{V}(t-t_1)_{sum}\right)$, $n_3(t) = \text{BPF}\left(n_H(t)n_V(t-t_1)_{sum}\right)$, $n_4(t) = \text{BPF}\left(J'(t)J(t)_{sum}\right)$, $n_5(t) = \text{BPF}\left(J'(t)\bar{H}(t)_{sum}\right)$, $n_6(t) = \text{BPF}\left(J'(t)n_H(t)_{sum}\right)$, $n_7(t) = \text{BPF}\left(J(t)\bar{V}(t-t_1)_{sum}\right)$, and $n_8(t) = \text{BPF}\left(J(t)n_v(t-t_1)_{sum}\right)$. All the noise terms are uncorrelated to each other and can be considered as zero mean band-limited Gaussian. Similar to Chapter-3, the summation of these noise terms yields a zero mean Gaussian. The powers of $n_1(t)$, $n_2(t)$, and $n_3(t)$ have been found in Chapter-3 and are $0.5G_1\sigma_S^2\sigma_V^2$, $0.5G_1\sigma_S^2\sigma_H^2$, and $0.5G_2\sigma_V^2\sigma_H^2$ respectively. The power of $n_4(t)$, $n_5(t)$, $n_6(t)$, $n_7(t)$, and $n_8(t)$ can be found by following a similar derivation.

If the power of $n_4(t)$ is denoted as P_4, P_4 can be found by the following equation, because the spectrum of sum frequency signal of $J'(t)J(t)$ has the shape of an isosceles triangle:

$$P_4 = \int_{f_c-B_L}^{f_c+B_L} S_4(f)df = \int_{f_c-B_L}^{f_c+B_L} \frac{-2\sigma_J^4 |f-2f_J|}{(2B_J)^2} + \frac{\sigma_J^4}{2B_J} df \qquad \textbf{5.4}$$

where $S_4(f)$ is the power spectral density function of the sum frequency signal of $J'(t)J(t)$ and is equal to zero when $f \geq 2f_J + B_J$ or $f \leq 2f_J - B_J$. The powers of $n_5(t)$ and $n_7(t)$ should be the same and so are the powers of $n_6(t)$ and $n_8(t)$. We denote the power of $n_5(t)$ and $n_7(t)$ as P_{I1} and the power of $n_6(t)$ and $n_8(t)$ as P_{I2}. To find P_{I1} and P_{I2}, the power spectral density functions of sum frequency signals of $J'(t)\bar{H}(t)$ and $J'(t)n_H(t)$ need to be found first.

The power spectral density function of the sum frequency interference, generated by mixing of two uncorrelated zero mean band-limited white Gaussian noise signals with different bandwidths, has a trapezoidal shape. An example is shown in Figure **5-1**. The bandwidth of these two band-limited noises are B_1 and B_2, and the center frequencies are f_1 and f_2. Based on Figure **5-1**, P_{I1} can be found by

$$P_{I1} = \int_{f_c-B_L}^{f_c+B_L} S_{I1}(f)df \qquad \textbf{5.5}$$

where $S_{I1}(f)$ is shown in Eq. **5.6 ,** and $F = f_n + f_J$, $B = 0.5(B_S - B_J)$.

$$S_{I1}(f)=\begin{cases}\dfrac{0.5\sigma_S^2\sigma_J^2}{B_S}, & F-B\le f\le F+B \\ \dfrac{-0.5\sigma_S^2\sigma_J^2\left|f-(f_n+f_j)\right|}{B_SB_J}+0.5\sigma_S^2\sigma_J^2\left(\dfrac{1}{2B_J}+\dfrac{1}{2B_S}\right) & F-B-B_J\le f<F-B \\ & \quad OR \\ & F+B\le f<F+B+B_J \\ 0 & Otherwise\end{cases} \qquad \textbf{5.6}$$

Using the same method, the P_{I2} can be found by

$$P_{I2}=\int_{f_c-B_L}^{f_c+B_L}S_{I2}(f)df \qquad \textbf{5.7}$$

where $S_{I2}(f)$ is shown in Eq. **5.8**.

$$S_{I2}(f)=\begin{cases}\dfrac{0.5\sigma_n^2\sigma_J^2}{B_S}, & F-B\le f\le F+B \\ \dfrac{-0.5\sigma_n^2\sigma_J^2\left|f-(f_n+f_J)\right|}{B_SB_J}+0.5\sigma_S^2\sigma_J^2\left(\dfrac{1}{2B_J}+\dfrac{1}{2B_S}\right) & F-B-B_J\le f<F-B \\ & \quad OR \\ & F+B\le f<F+B+B_J \\ 0 & Otherwise\end{cases} \qquad \textbf{5.8}$$

Since all the filtered interference terms, uncorrelated to each other, can be approximated as zero mean band-limited white Gaussians, the summation of these noise terms is also zero mean white Gaussian, with power given by

$$P_N=0.5(G_1\sigma_S^2\sigma_V^2+G_1\sigma_S^2\sigma_H^2+G_2\sigma_V^2\sigma_H^2)+P_4+2P_{I1}+2P_{I2} \qquad \textbf{5.9}$$

The filtered noise will down convert to baseband, and then pass through a low-pass filter with bandwidth B_L. The BER equation of NMCC system in the Partial-Band jamming channel with two side spectrum therefore can be modeled as

$$P_e = Q\left(\sqrt{\frac{E_b}{N_0}}\right) = Q\left(\sqrt{\frac{\rho\sigma_S^4 T_b B_L}{0.25 P_N}}\right) \qquad \textbf{5.10}$$

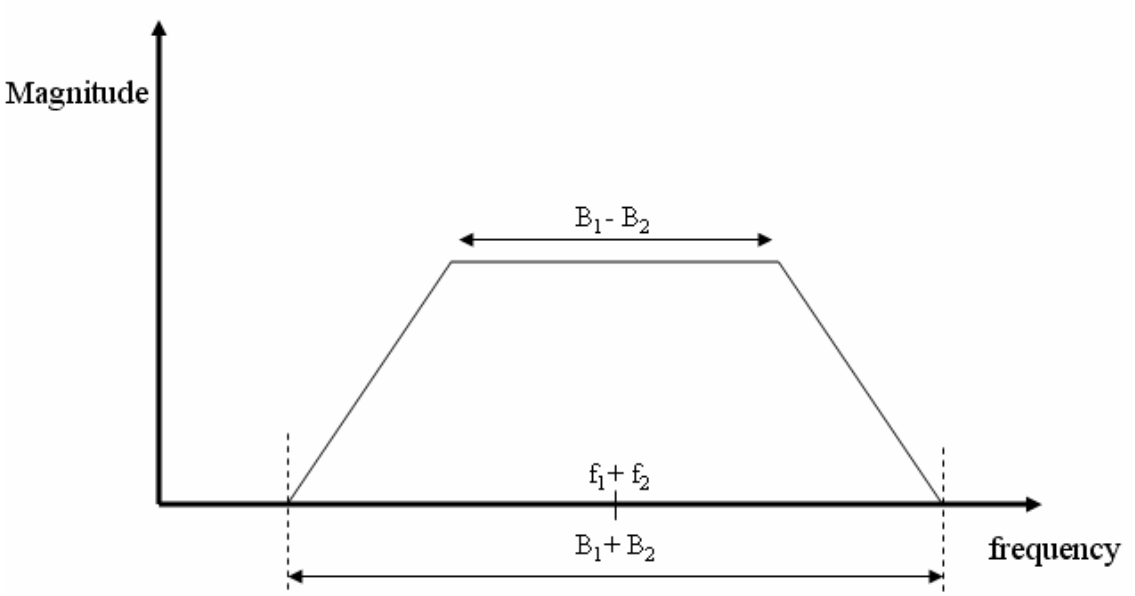

Figure **5-1**: Power spectrum of sum frequency signal which is generated by mixing two band-limited uncorrelated Gaussian random variables.

Simulations were down to verify the model shown in Eq. **5.10**. In the simulation, the bandwidth of signal and antenna were fixed to be at 980 MHz. The bit rate is fixed at 5 Mbps. The bandwidth of the band-pass filter is 100 MHz and the bandwidth of the low-pass filter is 20 MHz. The channel SNR is fixed at -6 dB ($\sigma_n^2/\sigma_S^2 = 3.98$). We simulated two cases: (1)The jammer does not know the center frequency of transmitted signal,

however the jamming signal has the same frequency range and bandwidth as the antenna. Under this assumption, P_4, P_{I1}, and P_{I2} are shown in Eq. **5.11**.

$$P_4 = 0.5\left(1-\left(1-\frac{B_L}{B_S}\right)^2\right)\sigma_J^4$$
$$P_{I1} = 0.5\left(1-\left(1-\frac{B_L}{B_S}\right)^2\right)\sigma_J^2\sigma_S^2 \qquad \textbf{5.11}$$
$$P_{I1} = 0.5\left(1-\left(1-\frac{B_L}{B_S}\right)^2\right)\sigma_J^2\sigma_n^2$$

(2) The jammer knows that the center frequency of the transmitted signal is within some frequency range but does not exactly know where it is. Since the jamming signal must confine itself within the antenna working frequency range and the bandwidth is much smaller than the bandwidth of antenna, the upper parallel edge on the trapezoid shape spectrum always include $2f_n$. Thus, P_{I1} , and P_{I2} can be simply considered to be constants in this jamming environment and they can be shown as

$$P_{I1} = \frac{B_L}{B_S}\sigma_J^2\sigma_S^2$$
$$P_{I2} = \frac{B_L}{B_S}\sigma_J^2\sigma_n^2 \qquad \textbf{5.12}$$

P_4 in this jamming environment will also be obtained from Eq. **5.4**.

In the simulation, the center frequency of jamming signals is the same as our transmitted signal. From Figure **5-2**, we can observe that the BER performance is degraded when the jamming signal concentrates itself around the center frequency (1.5 GHz) of the transmitted signal. The worst case is that when the jammer exactly knows the center frequency of transmitted signal and jammer can directly send a very narrow band

noise around 1.5 GHz with large power. Thus, P_4 will become extremely large and BER will degrade dramatically. In order to solve this problem, a simple solution is to add a narrow band band-stop filter with center located at f_n and stopband bandwidth is $2B_L$, to eliminate any possible narrow band interference around the center. We also simulate the case when the jammer sends the jamming signal into a wrong frequency region and the results are shown in Figure **5-3**. Under our simulation setup (Bandwidth of jamming source is 200 MHz with center at 1.3 GHz), P_4 will be zero. From Figure **5-2** and Figure **5-3**, we can observe that as the jammer gathers more information about the center frequency, the jamming power will be concentrate within a narrow frequency region and the performance will degrade because the value of P_4 will increase. As shown in Chapter-3, the deviation between simulation results and theoretical results also increases when the bandwidth of the jamming signal decreases. That is because the spectrum of filtered noise loses the flatness characteristic and the filtered noise loses the Gaussian characteristics.

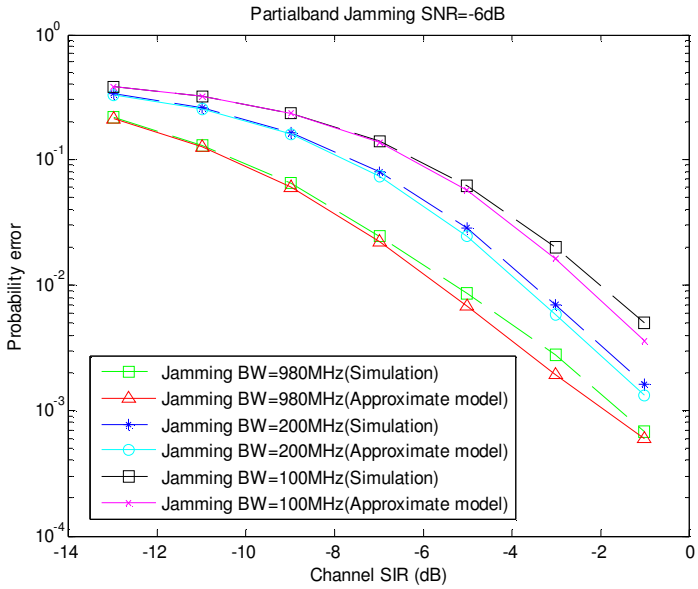

Figure **5-2**: Comparison of SIR and BER characteristics between simulation and approximate model in Partial-Band jamming environment when jamming signal is concentrated around the center frequency (1.5GHz).

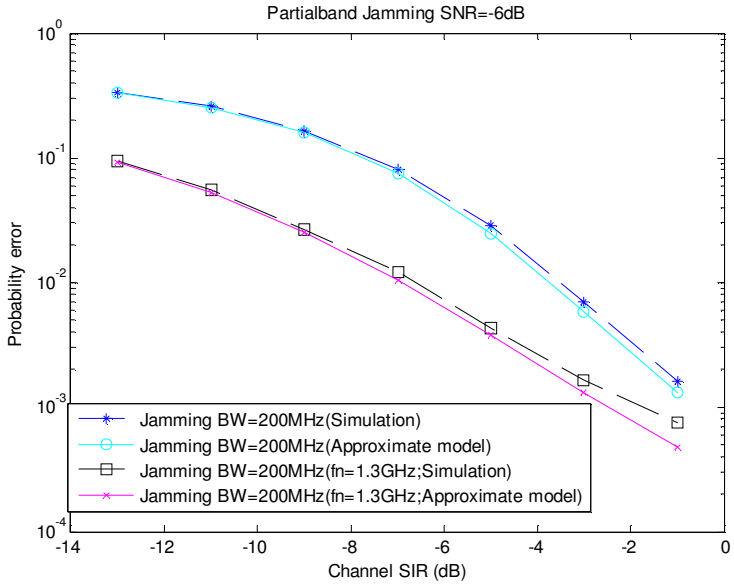

Figure **5-3**: Comparison of SIR and BER characteristics between simulation and approximate model in Partial-Band jamming environment when jamming signal is concentrated at a frequency (1.3GHz) different from the center frequency. For comparison, jamming signal concentrated at center frequency (1.5GHz) is also shown.

The pulsed noise jamming uses similar strategy as the Partial-Band noise jamming. The difference between these two strategies is that the jammer does not continuously send the jamming signal but sends the jamming signal periodically. Usually, we can assume that the pulsed noise repetition frequency is much lower than the bit rate and a quasi-static analysis can used to model the average BER. At the same average SIR, the pulsed noise jammer usually can degrade the system performance more efficiently than the Partial-Band noise jammer. If γ is the probability that the received bit will encounter the jamming signal, the BER model of the NMCC system in pulsed noise jamming environment can be obtained by modifying Eq. **5.10 ,**and is shown as [21].

$$P_e = (1-\gamma)Q\left(\sqrt{\frac{\rho\sigma_S^4 T_b B_L}{0.125(G_1\sigma_S^2\sigma_V^2 + G_1\sigma_S^2\sigma_H^2 + G_2\sigma_V^2\sigma_H^2)}}\right) + \gamma Q\left(\sqrt{\frac{\rho\sigma_S^4 T_b B_L}{0.25\left(0.5(G_1\sigma_S^2\sigma_V^2 + G_1\sigma_S^2\sigma_H^2 + G_2\sigma_V^2\sigma_H^2) + \gamma^{-1}(P_4 + 2P_{I1} + 2P_{I2})\right)}}\right) \quad \textbf{5.13}$$

5.2 Co-channel DS/SS interference

Since the NMCC system uses a large frequency band, it cannot avoid itself being interfered by some non-intentional interference. For example, the Global Positioning System (GPS) signals are operated within 1-2 GHz and will interfere with our system [27]. Because the DS/SS system is widely used in commercial and military communications, we are trying to model the system performance in this section when the

DS-SS interference is present and the interference signal uses BPSK or QPSK modulations.

As seen in the previous section, there exist eight interference terms after the mixing process and passing narrowband filter when there is only one DS/SS interference present in the channel. These interference terms are $n_1(t) = \mathrm{BPF}\left(n_V(t-t_1)\bar{H}(t)_{sum}\right)$, $n_2(t) = \mathrm{BPF}\left(n_H(t)\bar{V}(t-t_1)_{sum}\right)$, $n_3(t) = \mathrm{BPF}\left(n_H(t)n_V(t-t_1)_{sum}\right)$, $n_4(t) = \mathrm{BPF}\left(J'(t)J(t)_{sum}\right)$, $n_5(t) = \mathrm{BPF}\left(J'(t)\bar{H}(t)_{sum}\right)$, $n_6(t) = \mathrm{BPF}\left(J'(t)n_H(t)_{sum}\right)$, $n_7(t) = \mathrm{BPF}\left(J(t)\bar{V}(t-t_1)_{sum}\right)$, and $n_8(t) = \mathrm{BPF}\left(J(t)n_v(t-t_1)_{sum}\right)$. The expression for $J(t)$ and $J'(t)$ are shown in Eq. **5.14**.

$$J(t) = \sqrt{2P}c(t)d(t)\cos(2\pi f_J t)$$
$$J'(t) = \sqrt{2P}c(t-t_1)d(t-t_1)\cos(2\pi f_J t + \theta) \qquad \textbf{5.14}$$

where $c(t)$ is the PN sequence with chip duration T_c, $d(t)$ is the data carrier in this interference with bit duration T_d, P is the power of interference signal ,and $\theta = 2\pi f_J t_1$. Two cases will be discussed here. The first case is that the center frequency of interference signal is outside $f_n - 0.5B_L - 0.5T_c^{-1} \le f \le f_n + 0.5B_L + 0.5T_c^{-1}$. Under this condition, the narrowband interference $n_4(t)$ will not be captured by the low-pass filter after down conversion. As seen in Chapter-3, wideband noise passing through a narrowband filter can be considered as white Gaussians. Thus, the remaining seven filter noise terms can be considered as zero mean white Gaussians, because their corresponding mixed noise are wideband noise. The mean and power for $n_1(t)$, $n_2(t)$ and $n_3(t)$ have already been found and the next step is to find the mean and power of $n_5(t)$, $n_6(t)$, $n_7(t)$, and $n_8(t)$. Clearly, the means of these noise terms are zero because the means of the

transmitted signal and channel noise are zero and are independent of the interference signal. The powers of $n_5(t)$, $n_6(t)$, $n_7(t)$, and $n_8(t)$ can be found by the same concept presented in Chapter-3 and the previous section. For example, the power of sum frequency components signal power of $J'(t)\hat{H}(t)$ is $0.5P\sigma_S^2$. Thus, the power of $n_5(t)$ can be found by

$$P_{I5} = 0.5P\sigma_S^2 \frac{\int_{f_c-B_L}^{f_c+B_L} S_{\bar{H}}(f) \otimes S_J(f) df}{\int_0^{\infty} S_{\bar{H}}(f) \otimes S_J(f) df} \qquad \textbf{5.15}$$

where $S_{\bar{H}}(f)$ is the power spectral density function of $\bar{H}(t)$ and $S_J(f)$ is the power spectral density function of the interference signal, which can be shown as [28] [21]

$$\begin{aligned} S_J(f) &= \int_{-\infty}^{\infty} S_c(f') S_d(f-f') df' \\ &= \int_{-\infty}^{\infty} 0.5PT_dT_c \sin c^2\left[(f-f')T_c\right] \sin c^2\left[(f'-f_J)T_d\right] df' \\ &\quad + \int_{-\infty}^{\infty} 0.5PT_dT_c \sin c^2\left[(f-f')T_c\right] \sin c^2\left[(f'+f_J)T_d\right] df' \\ &\approx 0.5PT_c\left\{\sin c^2\left[(f-f_J)T_c\right] + \sin c^2\left[(f+f_J)T_c\right]\right\} \end{aligned} \qquad \textbf{5.16}$$

$S_c(f)$ is the power spectral density function of $c(t)$ and $S_d(f)$ is the power spectral density function of $\sqrt{2P}d(t)\cos(2\pi f_J t)$. Since the NMCC system is an ultra-wideband communication system, the bandwidth of $S_{\bar{H}}(f)$ is usually much greater than the bandwidth of $S_J(f)$. Thus, the power spectral density function, generated by convolving $S_{\bar{H}}(f)$ and $S_J(f)$, can be considered to be rectangular in shape with bandwidth $B_S + T_c^{-1}$. Eq. **5.15** can then be simplified to

$$P_{I5} \approx 0.5P\sigma_S^2 \frac{2B_L}{B_S + T_c^{-1}} \qquad \textbf{5.17}$$

Using the same concept, the power of $n_7(t)$ is equal to P_{I5} and the power of $n_6(t)$ and $n_8(t)$ can be found as

$$P_{I6} \approx 0.5P\sigma_n^2 \frac{2B_L}{B_S + T_c^{-1}} \qquad \textbf{5.18}$$

Because all the noise terms are zero mean Gaussians, the summation of these seven interference terms is also zero mean Gaussian and denoted as $n(t)$. As shown in the Appendix-1, we prove that the power of $n_5(t) + n_7(t)$ is equal to the summation of their individual powers. Since $n_5(t) + n_7(t)$ and the remaining interference terms are uncorrelated to each other, the power of $n(t)$ is found as

$$P_n = 0.5\left(1 - \left(1 - \frac{B_L}{B_n}\right)^2\right)(2\sigma_S^2\sigma_n^2 + \sigma_n^4) + \frac{2B_L}{B_S + T_c^{-1}}\left(P\sigma_S^2 + P\sigma_n^2\right) \qquad \textbf{5.19}$$

After down conversion, the baseband noise has 25% power of $n(t)$ and approximate BER for the two side spectrum can be modeled as

$$P_e = Q\left(\sqrt{\frac{8\sigma_S^4 \rho T_b B_L}{\left(1 - \left(1 - \frac{B_L}{B_n}\right)^2\right)(2\sigma_S^2\sigma_n^2 + \sigma_n^4) + \frac{2B_L}{B_S + T_c^{-1}}\left(2P(\sigma_S^2 + \sigma_n^2)\right)}}\right) \qquad \textbf{5.20}$$

In our derivation, we assume that the DS/SS interference uses BPSK modulation but Eq. **5.20** can be also applied for the case when the DS/SS interference uses QPSK modulation. The RF QPSK modulated signal can be considered as the summation of two RF BPSK modulated signals with orthogonal carriers (sine and cosine), but at the same carrier frequency [23]. The noise that is generated by mixing this RF QPSK modulated

signal with our transmitted signal or received channel noise is still a zero mean white Gaussian after passing through a narrow band-pass filter. The mixed noise also has the same characteristics as the noise that is generated by mixing RF BPSK modulated signal with our transmitted signal or received channel noise.

A comparison of our simulation results with Eq. **5.20** is shown in Figure **5-4**. The signal bandwidth is fixed at 980 MHz while the bit rate of NMCC system is fixed at 5 Mbps. Two cases are simulated. The first case is when the interference signal is located at 1.2 GHz with chip rate 10 Mbps and uses QPSK modulation. The channel SNR is fixed at -6 dB. The other case is when the interference is located at 1.45 GHz with chip rate 1 Mbps and uses BPSK modulation with Raised-Cosine filter and roll-off factor is 0.25. The channel SNR is fixed at -4 dB. The results demonstrate the system can maintain good BER in low SNR and SIR channels when the interference signal is not located within $f_n - 0.5B_L - 0.5T_c^{-1} \le f \le f_n + 0.5B_L + 0.5T_c^{-1}$.

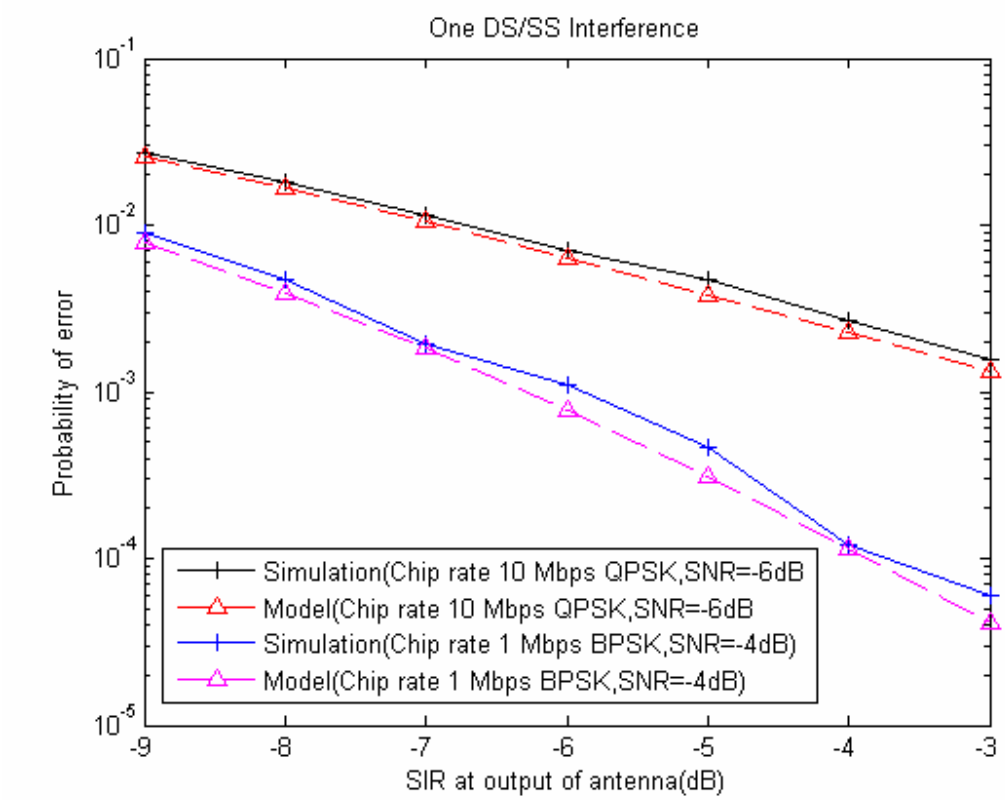

Figure **5-4**: Comparison of SIR and BER characteristics between simulation and approximate model in DS/SS interference environment.

When the center frequency f_J of the DS/SS interference is inside $f_n - 0.5B_L - 0.5T_c^{-1} \le f_J \le f_n + 0.5B_L + 0.5T_c^{-1}$, the band-pass filter (whose bandwidth is twice of the low-pass filter) will capture the full or partial spectrum of $J'(t)J(t)$ and this interference will degrade the BER dramatically. Under this condition, the received baseband signal will contain non-Gaussian interference and can be shown as

$$\begin{aligned} b(t) &= 0.25a^2(t-t_1)m(t-t_1)\otimes h(t) + n'(t) + 0.5Pc(t)c(t-t_1)\cos(2\pi(2f_J - f_c)t + \theta)\otimes h(t) \\ &= m_b(t) + n'(t) + I_J(t) \end{aligned} \quad \textbf{5.21}$$

where $h(t)$ is the impulse response of low-pass filter and $n'(t)$ is the Gaussian noise with power $0.25P_n$ and P_n is shown in Eq. **5.19**. $I_J(t)$ is the high power non-Gaussian interference and $m_b(t)$ is the message desired to be retrieve. For convenience, we assume the $d(t)$ in Eq. **5.14** is always unity to obtain the Eq. **5.21**.

When the receiver starts to demodulate the k^{th} bit from $b(t)$, $I_J(t)$ has a constructive or a deconstructive effect on the k^{th} bit. We can consider $I_J(t)$ at the output of match filter as just a positive or negative value which we denote as I_k [29]. It is difficult to model the BER when received baseband signal contains $I_J(t)$ because the I_k value will depend on chip rate, center frequency of interference signal (f_J), and the statistical characteristic of $c(t)$. Under some conditions, I_k can be considered as a constant but it can be modeled as a random variables under most conditions. For example, when $2f_J$ is equal to f_c and the chip rate of $c(t)$ is much smaller than the bit rate of $m(t)$, then I_k can be considered as a constant based on quasi-static analysis, and the BER is shown in Eq. **5.22**.

$$P_e = 0.5Q\left(\sqrt{\frac{8\sigma_S^4\rho T_b B_L + I_k}{\left(1-\left(1-\frac{B_L}{B_n}\right)^2\right)(2\sigma_S^2\sigma_n^2+\sigma_n^4)+\frac{2B_L}{B_S+T_c^{-1}}\left(2P(\sigma_S^2+\sigma_n^2)\right)}}\right) + 0.5Q\left(\sqrt{\frac{8\sigma_S^4\rho T_b B_L - I_k}{\left(1-\left(1-\frac{B_L}{B_n}\right)^2\right)(2\sigma_S^2\sigma_n^2+\sigma_n^4)+\frac{2B_L}{B_S+T_c^{-1}}\left(2P(\sigma_S^2+\sigma_n^2)\right)}}\right) \quad \textbf{5.22}$$

However, the same equation cannot be used in the case when the chip rate is closer to the bit rate. That is because the k^{th} bit will encounter more than one I_k value during the demodulation. The number of the I_k values will depend on the chip rate of $c(t)$, bit rate of $m(t)$ and center frequency of $J(t)$. Since the power of DS/SS interference is stronger than our transmitted signal ($P > \sigma_S^2$) and $I_J(t)$ is a narrow band non-Gaussian interference, the BER performance will degrade dramatically when the $n_4(t)$ is captured by the low-pass filter after down conversion.

The above discussion suggests that the designer should avoid the center frequency of this noise modulated signal overlapping with other signals. This is not a unique situation for NMCC system but will happen for all the transmitted reference (TR) techniques. A simple solution to solve this problem is directly added a narrow band band–stop filter at the output of receiver's antenna. The center of this band-stop filter should be f_n and the stop band should be $2B_L$. Since $2B_L$ is much smaller than the bandwidth of $V(t)$ and $H(t)$, the received $V(t)$ and $H(t)$ only loses a very small fraction of the transmitted power. Thus, the BER performance will degrade slightly in the AWGN channel but will improve dramatically in the channel containing DS/SS interference. A simulation is done to demonstrate how the band-stop filter affects the BER. From the results shown in Figure **5-5** and Figure **5-6**, adding a band-stop filter does improve the BER when the center of interference signal is inside $f_n - 0.5B_L - 0.5T_c^{-1} \le f_J \le f_n + 0.5B_L + 0.5T_c^{-1}$ while the BER degrades slightly in the AWGN channel.

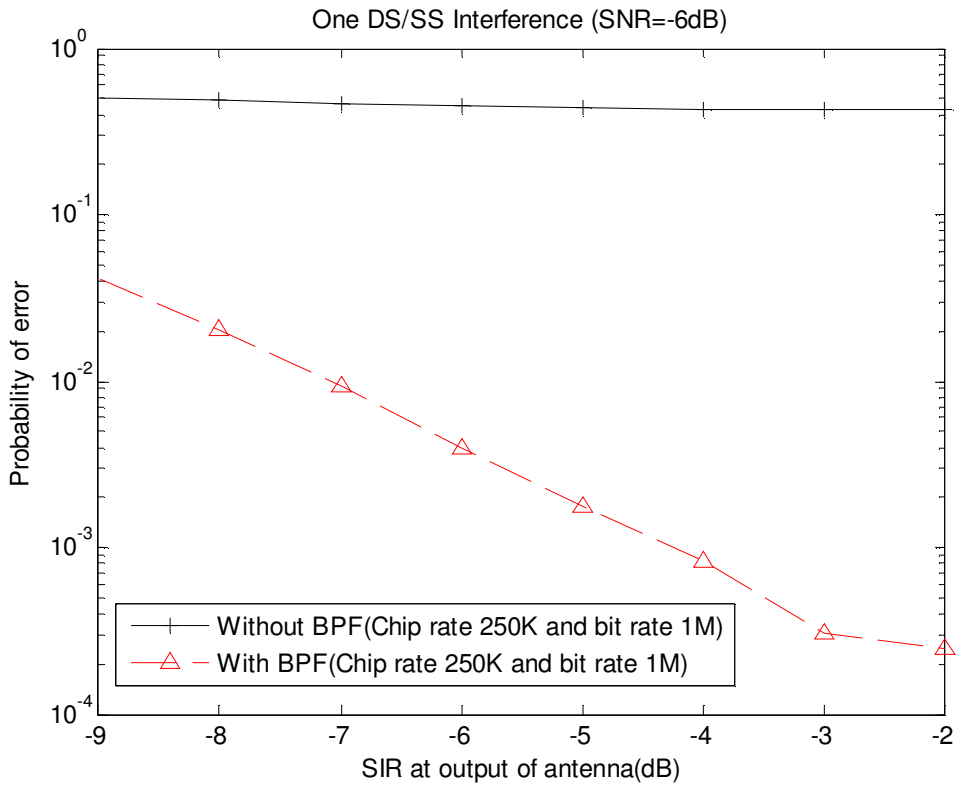

Figure **5-5**: BER comparison before and after adding the band-stop filter when the center frequency of interference is inside $f_n - 0.5B_L - T_c^{-1} \le f_J \le f_n + 0.5B_L + T_c^{-1}$.

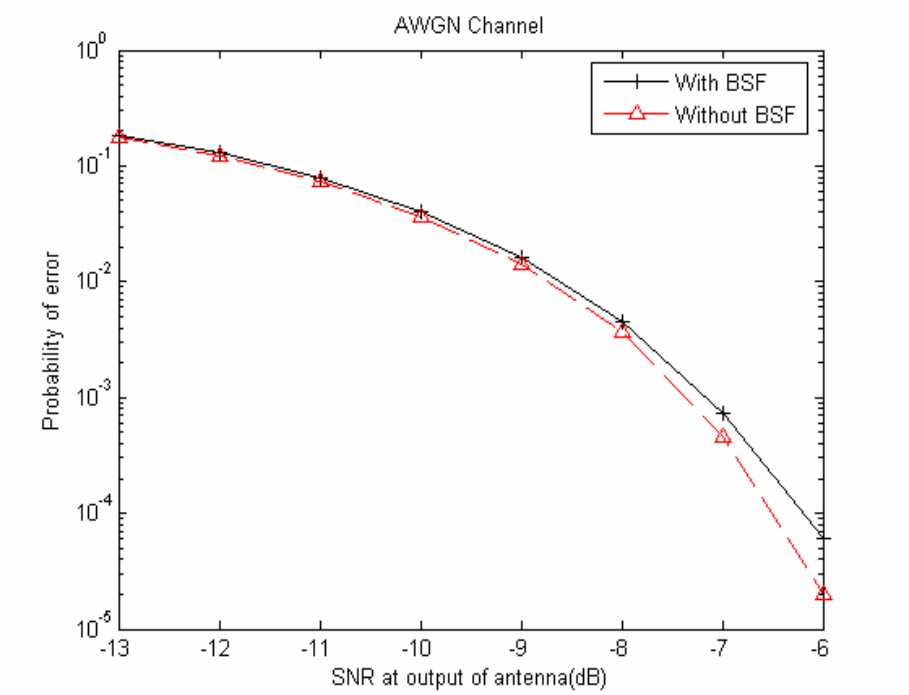

Figure **5-6**: BER comparison before and after adding the band-stop filter in the AWGN channel.

5.3 Multipath environment

5.3.1 Parameters

t_i and t_d: Delay of i^{th} path and the delay of the delay line.

f_i**:** Doppler shift of i^{th} path.

f_n**:** Center frequency of our transmitted signal and antenna (1.5 GHz).

f_c**:** $2f_n$**.**

B_L and B_S **:** Bandwidth of low-pass filter and antenna.

ρ : Power loss factor due to LPF truncate the received baseband signal spectrum

σ_{i-V}^2 and σ_{i-H}^2 **:** Power of i^{th} path in V and H channel.

σ_n^2 : Power of channel noise.

$n_V(t)$ and $n_H(t)$ **:** Received channel noise in V and H channel respectively. (We assume channel noise has the same power but is uncorrelated)

$x(t \mid f)$ **:** Bandlimited signal with center f

$(x(t)y(t) \mid f)$ **:** Sum frequency signal with center f and is generated by $x(t)$ mixing with $y(t)$.

$(V(n), H(m))$ **:** Received n^{th} path in V channel synchronized with received m^{th} path in H channel

(n, m) **:** Received n^{th} path in V channel synchronized with received m^{th} path in H channel plus received n^{th} path in H channel synchronized with received m^{th} path in V channel.

5.3.2 Cross-Multiple to alleviate multipath effect

The NMCC system cannot avoid the performance degradation caused by multipath. Inspired by the RAKE receiver, a new method has been specially designed for the NMCC system, to counteract the multipath affects. Similar to the RAKE receiver, this new structure uses diversity to improve the performance and the theoretical lower bound BER model is obtained. The simulation results demonstrate that this structure does improve the system performance in multipath channel.

To simplify the analysis, the WSSUS (Wide sense stationary uncorrelated scattering) channel with discrete model is used to analyze this new structure in a multipath environment [30]. Since our signal operates within 1-2 GHz, the Doppler shift is usually less than 200 Hz. Under this condition, the received multipath signals have a bandwidth almost equivalent to the original transmitted signal [31]. The center frequency of the received signal will have a slight offset due to Doppler shift and the received signal in V and H channels can be shown as [32]

$$\tilde{V}(t) = \sum_{i=1}^{N} \sigma_{i-V} V(t - t_i \mid f_n + f_i) + n_V(t) \qquad \textbf{5.23}$$

$$\tilde{H}(t) = \sum_{i=1}^{N} \sigma_{i-H} H(t - t_d - t_i \mid f_n + f_i) + n_H(t) \qquad \textbf{5.24}$$

Theoretically, σ_{i-V} and σ_{i-H} will be different since different polarizations are used [33]. The received signal in V channel is sent to a delay line with delay t_d and then is mixed with the received signal in H channel. The mixed signal is shown as

$$S(t) = \sum_{i=1}^{N} \sigma_{i-V}\sigma_{i-H} V(t - t_d - t_i \mid f_n + f_i) H(t - t_d - t_i \mid f_n + f_i) + n(t) \qquad \textbf{5.25}$$

where $n(t)$ can be shown in Eq. **5.26**.

$$\begin{aligned} n(t) = & \sum_{j \neq i} \sum_{i} \sigma_{i-V}\sigma_{j-H} V(t - t_d - t_i \mid f_n + f_i) H(t - t_d - t_j \mid f_n + f_j) \\ & + \sum_{i} n_V(t - t_d)\sigma_{i-H} H(t - t_d - t_i \mid f_n + f_i) + \sum_{i} n_H(t)\sigma_{i-V} V(t - t_d - t_i \mid f_n + f_i) \end{aligned} \qquad \textbf{5.26}$$

In Eq. **5.25**, the term $\sum_{i=2}^{N} \sigma_{i-V}\sigma_{i-H} V(t - t_d - t_i \mid f_n + f_i) H(t - t_d - t_i \mid f_n + f_i)$ acts as the ISI for desired received signal $\sigma_{1-V}\sigma_{1-H} V(t - t_d - t_1 \mid f_n + f_1) H(t - t_d - t_1 \mid f_n + f_1)$ and this narrow band non-Gaussian interference will degrade system performance

dramatically. The idea to alleviate BER degradation is by synchronizing the n^{th} path in the V channel with the m^{th} path in the H channel, but not directly mixing the received signal in V and H channels. We call this a "cross-product". The output sum frequency signal synchronizes the n^{th} path in the H channel with the m^{th} path in the V channel, as is shown in Eq. **5.27**. The block diagram of this structure is shown in Figure **5-7** .

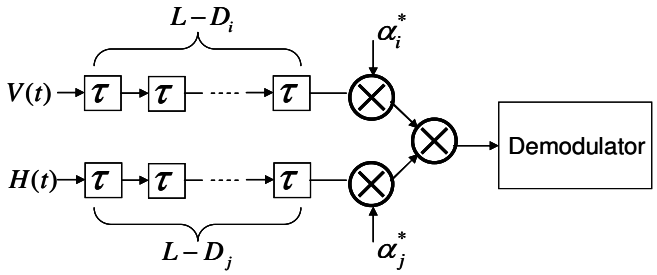

Figure **5-7**: Block diagram of cross-product by using one pair, where L is the maximum delay.

$$
\begin{aligned}
S_{(V(n),H(m))}(t) = {} & \sigma_{n-V}\sigma_{m-H}(V(t-t_d-t_N)H(t-t_d-t_N)\,|\,f_c+f_m+f_n) \\
& + \sum_j\sum_i \sigma_{i-V}\sigma_{j-H}(V(t-t_d-t_i-(t_N-t_n))H(t-t_d-t_j-(t_N-t_m))\,|\,f_c+f_i+f_j) \\
& + \sum_i \sigma_{i-V}(n_H(t-t_d-(t_N-t_m))V(t-t_d-t_i-(t_N-t_n))\,|\,f_c+f_i) \\
& + \sum_i \sigma_{i-H}(n_V(t-t_d-(t_N-t_n))H(t-t_d-t_i-(t_N-t_m))\,|\,f_c+f_i)
\end{aligned}
\qquad \textbf{5.27}
$$

where $(i,j)\neq(n,m)$. By wisely choose the pair (m,n), we can ensure that $t_i-(t_N-t_n)$ and $t_j-(t_N-t_m)$ in the second term in Eq. **5.27**, are always unequal. Thus, no narrow band non-Gaussian interference will exist (no ISI occurs). Unlike the Eq. **5.25**, all the signals in the second term in Eq. **5.27** can be considered as wideband noise with bandwidth $2B_S$ and isosceles triangle shaped spectrum. That is because $H(t-t_d-t_j-(t_N-t_m))V(t-t_d-t_i-(t_N-t_n))$ can be considered as a mix of two

uncorrelated zero mean band-limited Gaussians when $t_i - (t_N - t_n)$ is not equal to $t_j - (t_N - t_m)$.

The third and fourth term in the Eq. **5.27** also act as interference terms. According to the discussion in Chapter-3, they are zero mean uncorrelated Gaussian noise after passing through a narrow band band-pass filter. $S(t)$ will be down-converted by the carrier with frequency $f_c + f_m + f_n$. Thus, each baseband noise is still zero mean Gaussian but the center is not exactly located at 0 Hz. From Chapter-3, it can be noted that the power of received baseband noise is a parameter for calculating the BER. Since the Doppler shift of each path is smaller than 200 Hz, the maximum center offset of received baseband noise should be smaller than 400 Hz , while the bandwidth of low-pass filter is much larger than 400 Hz when we plan to transmit voice and video. Thus, the power deviation between the calculated power by using correct center and that of the received baseband noise assuming the center to be at 0 Hz is small enough to be neglected. For example, when the bandwidth of LPF is 1 MHz and maximum center offset is 400 Hz, the power error of using correct center and using center at f_c is 0.04%. Thus, Eq. **5.27** can be simplified to

$$\begin{aligned} S_{(V(n),H(m))}(t) = {} & \sigma_{n-V}\sigma_{m-H}(V(t-t_N)H(t-t_N) \mid f_c) \\ & + \sum_j \sum_i \sigma_{i-V}\sigma_{j-H}(V(t-t_i-(t_N-t_n))H(t-t_j-(t_N-t_m))V(t-t_i) \mid f_c) \\ & + \sum_i \sigma_{i-V}(n_H(t-(t_N-t_m))V(t-t_i-(t_N-t_n)) \mid f_c) \\ & + \sum_i \sigma_{i-H}(n_V(t-(t_N-t_n))H(t-t_i-(t_N-t_m)) \mid f_c) \end{aligned} \qquad \textbf{5.28}$$

where $(i, j) \neq (n, m)$ For convenience, we assume that t_d is zero since it will not affect the following analysis. The first term in Eq. **5.28** is the signal carrying the bit stream that we want to retrieve while the other three terms are interference terms. All the noise terms will be a zero mean Gaussian with the same center and uncorrelated to each other after passing a narrow band band-pass filter and the summation of them also results in a zero mean Gaussian. Using the same concept for calculating the BER in multiuser environment that are discussed in Chapter-3, the SNR of $S(t)$ after down-conversion can be shown as

$$SNR_{(V(n),H(m))} = \frac{0.5\rho\sigma_{n-V}^2\sigma_{m-H}^2}{0.125G_3\left(\sum_j\sum_i \sigma_{i-V}^2\sigma_{j-H}^2 + \sum_i \sigma_{i-V}^2\sigma_N^2 + \sum_i \sigma_{i-H}^2\sigma_N^2\right)} \quad (i, j) \neq (n, m) \qquad \textbf{5.29}$$

where G_3 is shown in Eq. **3.30**. To have maximum diversity, we are not only using the signal that is generated by synchronizing the n^{th} path in V channel with the m^{th} path in H channel, but will also combine it with the signal that is generated by synchronizing the n^{th} path in H channel with the m^{th} path in V channel and any other pairs that do not contain narrow band non-Gaussian interference after the mixing process. The block diagram of such a combination is shown in Figure **5-8** and the algorithm to choose the best pairs will described further below.

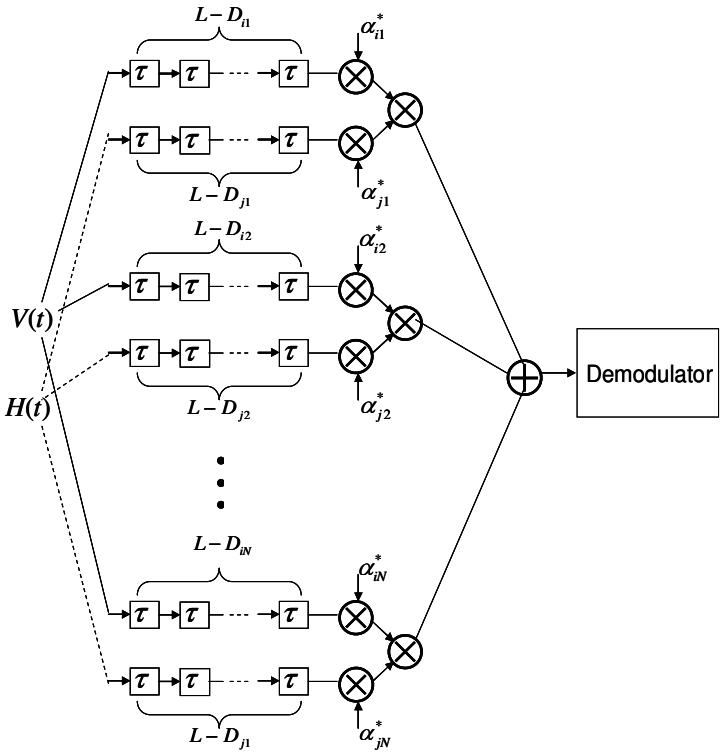

Figure **5-8**: Block diagram of cross-product method by using more than one pair.

Before discussing the algorithm that chooses the best pairs, the baseband SNR of each pair needs to be found first. The signal generated by synchronizing the n^{th} path in the V channel with the m^{th} path in the H channel is shown in Eq. **5.30**.

$$\begin{aligned} S_{(V(m),H(n))}(t) &= \sigma_{n-H}\sigma_{m-V}(V(t-t_N)H(t-t_N)\mid f_c) \\ &+ \sum_j \sum_i \sigma_{i-V}\sigma_{j-H}(V(t-t_i-(t_N-t_m))H(t-t_j-(t_N-t_n))\mid f_c) \\ &+ \sum_i \sigma_{i-H}(n_H(t-(t_N-t_n))V(t-t_i-(t_N-t_m))\mid f_c) \\ &+ \sum_i \sigma_{i-V}(n_V(t-(t_N-t_m))H(t-t_i-(t_N-t_n))\mid f_c) \end{aligned} \qquad \textbf{5.30}$$

As finding $SNR_{(V(n),H(m))}$, this information will be used to find the baseband SNR of $S_{(V(n),H(m))}(t)+S_{(V(m),H(n))}(t)$ and we denote $S_{(V(n),H(m))}(t)+S_{(V(m),H(n))}(t)$ as a pair (n,m).

Using the same concept that is shown above, each noise term can be considered as Gaussian noise after passing through a narrow band band-pass filter, and the summation of these terms will be Gaussian. Thus, the noise of (n,m) after passing through a narrow band band-pass filter can be approximated to be a Gaussian. Knowing that the noise is Gaussian, the next step is to find the power of this noise. From Eq. **5.28** and Eq. **5.30**, we know all the noise terms are uncorrelated to each other except the signals shown in Eq. **5.31**.

$$\begin{aligned}&\sigma_{i-V}\sigma_{j-H}(H(t-t_j-(t_N-t_m))V(t-t_i-(t_N-t_n))\mid f_c) \quad i=1,2,.....N\\&\sigma_{i-H}\sigma_{j-V}(H(t-t_i-(t_N-t_n))V(t-t_j-(t_N-t_m))\mid f_c) \quad j=1,2,.....N\end{aligned} \qquad \textbf{5.31}$$

From Appendix-2, it demonstrates that the power of the summation these two terms is equal to summation their individual powers. Since each pair in Eq. **5.31** is uncorrelated to other pairs with different (i,j) values, and other noise terms belong to (n,m), the baseband noise power of (n,m) can be found by

$$P_{N(m,n)}=0.25G_3\left(\sum_j\sum_i\sigma_{i-V}^2\sigma_{j-H}^2+\sum_i\sigma_{i-V}^2\sigma_N^2+\sum_i\sigma_{i-H}^2\sigma_N^2\right) \quad (i,j)\neq(n,m) \qquad \textbf{5.32}$$

Because the signal terms (first term) in Eq. **5.28** and Eq. **5.30** are coherent, the received baseband SNR of (n,m) pairs can be shown as

$$SNR_{(m,n)}=\frac{P_{S(m,n)}}{P_{N(m,n)}}=\frac{0.5\rho\left(\sigma_{n-V}\sigma_{m-H}+\sigma_{n-H}\sigma_{m-V}\right)^2}{0.25G_3\left(\sum_j\sum_i\sigma_{i-V}^2\sigma_{j-H}^2+\sum_i\sigma_{i-V}^2\sigma_N^2+\sum_i\sigma_{i-H}^2\sigma_N^2\right)} \qquad \textbf{5.33}$$

The same concept can use to calculate baseband SNR of any pair without narrowband non-Gaussian interference, and this information will be used to select the pairs that can

have the best BER after combining. The algorithm to choose the best pairs is shown below.

Step-1: Separate the pairs into two groups. Group-1 is the pairs without other terms synchronized (without narrow band non-Gaussian interference) and Group-2 is the pairs with other terms synchronized (with narrow band non-Gaussian interference). To separate pairs into two groups, it can be simply achieved by doing the autocorrelation of $S_{(V(n),H(m))}(t)$. If the autocorrelation function of $S_{(V(n),H(m))}(t)$ has more than one peak, it means that $S_{(V(n),H(m))}(t)$ contains narrow band non-Gaussian interference. Otherwise, $S_{(V(n),H(m))}(t)$ does not contain narrow band non-Gaussian interference.

Step-2: Sort the pairs in Group-1 from high SNR to low SNR and start combining the pair with the highest SNR with the pair with the second high of SNR. When combining, we assume signal terms belong to different pairs are fully coherent and noise belonging to different pairs are uncorrelated. If the combined SNR ratio is greater than the highest SNR of these two pairs, these pairs can be used and these two pairs will combine with the pair with the third strongest SNR. Otherwise, stop combining and directly use the highest SNR pair. The process will continue until the combined SNR is smaller than the previous combined SNR and the pairs from the highest combined SNR ratio will be selected and used. An example of the combined SNR ratio of combining "g" pairs can be showing as

$$SNR_{com} = \frac{P_{Scom}}{P_{Ncom}} = \frac{\left(\sqrt{P_{S-1}} + \sqrt{P_{S-2}} + \text{.....} + \sqrt{P_{S-g}}\right)^2}{\sum_{i=1}^{g} P_{N-i}} \qquad \textbf{5.34}$$

where P_{S-i} is the received baseband signal power belonging to the i^{th} pair and can be found by the same method as finding $P_{S(m,n)}$ in the Eq. **5.33**. The P_{N-i} is the received baseband noise power belonging to the i^{th} pair and can be found by the same method as finding $P_{N(m,n)}$ in the Eq. **5.32**.

Step-3: Compare the lower bound BER of combined pairs with the pair that has the best BER in the Group-2. If combined pairs have better BER, directly use the combined signals. Otherwise, use the pair with the best BER in Group-2**.** Also the noise terms in Group-1 can be approximate to a zero mean white Gaussian. However, sometimes the pairs in Group-2 can be used even when they contain non-Gaussian interference. For example, in line-of-sight communication, the received line-of-sight signal is much stronger than the received multipath signals. If we synchronize the received line-of-sight signal with the received multipath signal, the BER will worse than the synchronized received line-of-sight signal with received line-of-sight signal because the signal power of multipath signal is too weak compared to the line-of-sight signal. The lower bound BER of combined pairs can be shown in Eq. **5.35**, while the BER of the pair that contains non-Gaussian interference is presented in [34].

$$P_{e\_com} = Q\left(\sqrt{\frac{2P_{Scom}T_bB_L}{P_{Ncom}}}\right) \qquad \textbf{5.35}$$

where P_{Scom} and P_{Ncom} are shown in Eq. **5.34**. The reason that the BER found in Eq. **5.35** is a lower bound is because we assume the noise terms generated by different pairs are uncorrelated to each other. In reality, some terms belong to different pairs are fully

correlated and how many noise terms are correlated depends on the delay response. A simulation is done to compare our method with the RAKE receiver and the channel results are shown in Table **5-1** and Table **5-2**. In the simulation, we assume σ_{i-V} and σ_{i-H} to be equal. This setup ensures that we are always under the worst situation because we cannot synchronize the strongest path in V channel with the strongest path in H channel since their delay times are the same.

Table **5-1**: Channel-1 setup

Path	Delay(μs)	Fractional Power
Path-1	0	0.192
Path-2	0.2	0.394
Path-3	0.5	0.248
Path-4	1.6	0.099
Path-5	2.3	0.067

Table **5-2**: Channel-2 setup

Path	Delay(μs)	Fractional Power
Path-1	0	0.413
Path-2	0.1	0.293
Path-3	0.3	0.145
Path-4	0.5	0.074
Path-5	15	0.067

In the simulation, the bit rate is fixed at 5 Mbps and 100000 bits are sent while the chip rate using for RAKE receiver is 25 Mbps for Channel-1 simulation and is 50 Mbps for Channel-2 simulation. The same Gold sequence with length 2047 chip duration time is used for both simulations. The bandwidth of antenna and the transmitted signal is fixed at 980 MHz. The pairs that are selected from Channel-1 are

$(Path-2, Path-3)$, $(Path-1, Path-2)$, $(Path-1, Path-3)$, $(Path-2, Path-4)$, $(Path-2, Path-5)$, $(Path-3, Path-4)$, $(Path-1, Path-4)$, and $(Path-3, Path-5)$. These pairs are sorted from high SNR to low SNR. The pairs that are selected from Channel-2 are $(Path-1, Path-2)$, $(Path-1, Path-3)$, $(Path-1, Path-4)$, $(Path-1, Path-5)$, $(Path-2, Path-4)$, and $(Path-2, Path-5)$. From the simulation results shown in Figure **5-9** and Figure **5-10**, it is seen that this method does improve system performance in a multipath channel.

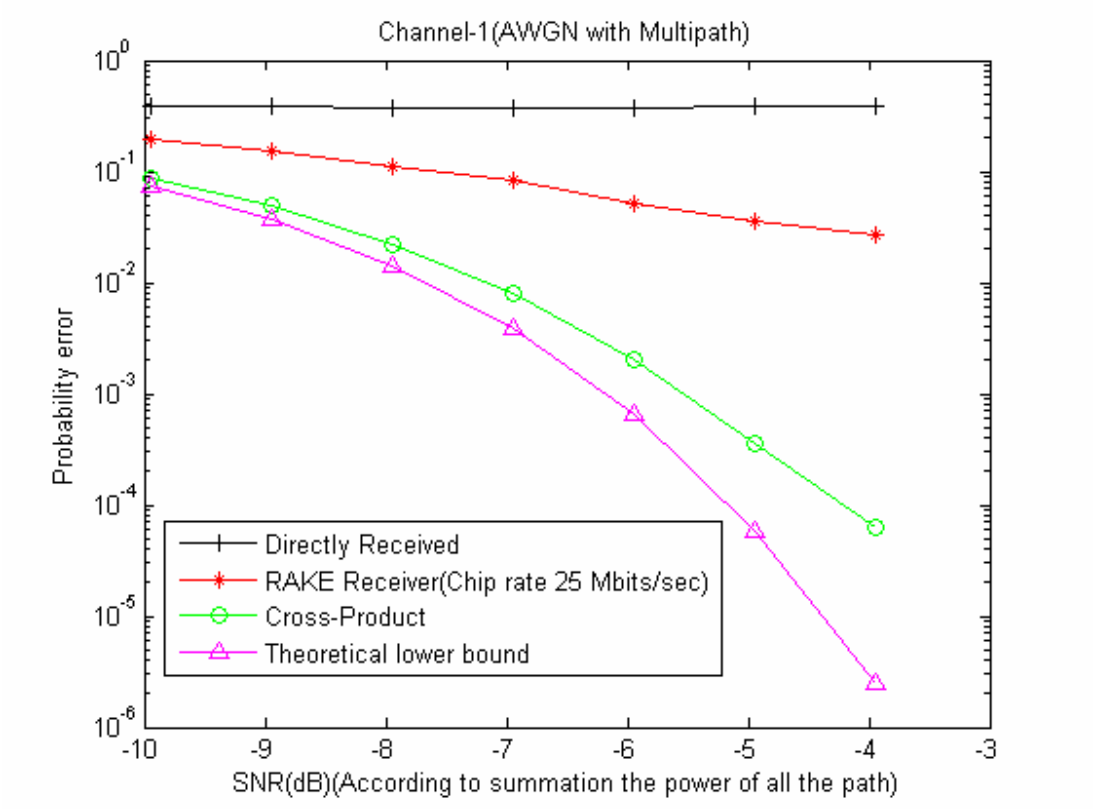

Figure **5-9**: BER comparison in multipath environment.

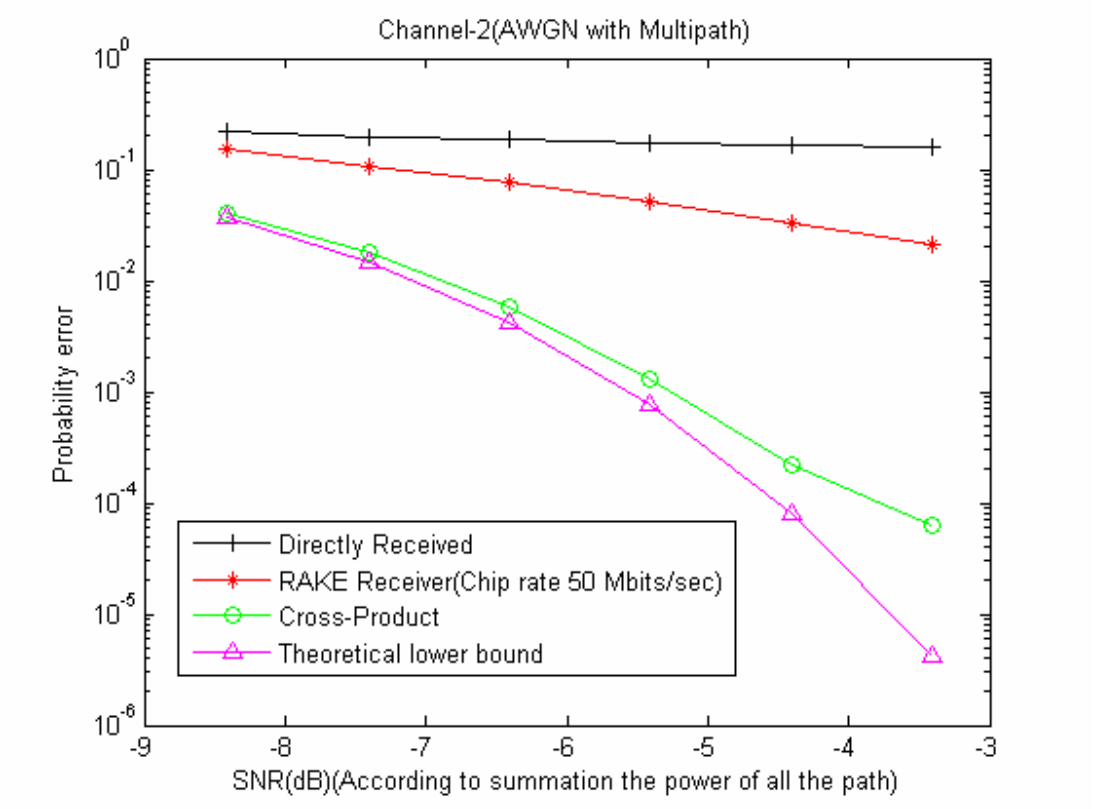

Figure **5-10**: BER comparison in multipath environment.

Chapter 6

Conclusion and future work

6.1 Conclusion

A spread spectrum technique using ultra-wideband noise waveforms has been designed and successfully tested for covert communications. The noise key and the noise-like modulated signal are transmitted over orthogonal polarizations to mimic unpolarized noise. The featureless characteristics of the transmitted waveform ensure the security of communications. It is well-known that the transmitted reference (TR) technique is used to establish communication when there are critical unknown properties of the transmitted signal or channel, and it is easier implemented compared to stored or locally generated reference systems[35][36]. This scheme completely avoids the synchronization problem of stored or locally generated reference systems but performance will worse than them at the same signal-to-noise ratios (SNRs) because the noise-cross-noise term will appear at the output of correlator and more noise terms will be generated. The heterodyne correlation implementation developed in this project alleviates the performance degradation shown by TR systems at low SNR values by collapsing the UWB transmitted signals to a single clean frequency at the receiver. By using a band-limited true Gaussian noise waveform to spread the signal's power into a large bandwidth, an extremely large

processing gain is achieved and the system can operate very well in a noisy and jammed channel.

The performance of this noise-modulated covert communication system in a single user, multiuser, and partial-band jamming environment is properly modeled and compared with simulations. The bandwidth of the transmitted signal controls the BER performance when the bit rate and the SNR at the output of antenna are fixed. The results demonstrate that the system can achieve robust communications in the low SNR or low SIR channels. Since the system operates over a wide frequency range, it cannot avoid the co-channel DS-CDMA interference. The research reveals that the noise modulated system will have good immunity to the DS-CDMA interference by simply adding a narrow band band-stop filter with center the same as our transmitted signal. The cross-product algorithm, specially designed for this system, is an alternative method that can successfully improve the system performance in the multipath environment. Compared to the RAKE receiver, this algorithm has better performance because it uses more diversity. The preliminary field test results successfully validate this concept can operate in low SNR and SIR channel.

All the results demonstrate that the noise-modulated communication system has excellent potential for covert data transmission. However, there are some efforts that need to be done in order to make the system fully functional and achieve “push-to-talk”. The following sections present the future work that need to be accomplished and the possible solutions that can be used to accomplish these works.

6.2 Future work: Channel estimation

The channel impulse responses in the V and H channels need to be obtained when the cross-product algorithm or RAKE receiver needs to be implemented. Inspiring by the noise radar, this section demonstrates that the noise pilot can be used to estimate the delay, Doppler frequency, and fractional power corresponding to each path [37][38]. Since noise pilot is zero mean Gaussian noise, the covertness can be maintained while the system is measuring the channel response. The delay time of each multipath term should be obtained first and this information is used to measure the fractional power and Doppler frequency of each path.

The basic idea is sending a zero mean Gaussian noise as pilot to estimate the channel response. The receiver should know the pilot and have its stored copy. Since the NMCC system uses the dual linear polarization horn antenna, the delay and frequency shift response in V and H channels should be the same but the fractional power corresponding to L^{th} path in V and H channels should be different. If the pilot is denoted as $p(t)$, the same frequency range as our transmitted signals, the received signals in V and H channels in the multipath environment can be expressed as

$$\hat{H}(t) = \sum_{L=1}^{N} a_{H,L} e^{j2\pi f_L t} p(t - t_L) \qquad \textbf{6.1}$$

$$\hat{V}(t) = \sum_{L=1}^{N} a_{V,L} e^{j2\pi f_L t} p(t - t_L) \qquad \textbf{6.2}$$

where f_L, and t_L are the Doppler shift and delay corresponding to the L^{th} path. The $a_{V,L}$ and $a_{H,L}$ are the amplitudes corresponding to the L^{th} path in V and H channels respectively.

At the receiver side, the stored pilot chops into M sections by the window with duration time T. The chopped signal corresponding to the n^{th} section is denoted as $p_n(t)$. T should be properly chosen. In general, T should be much smaller than f_L^{-1} and should be smaller than the delay time between each path [38]. For example, the delay in the suburb on area is between 200-2000 nanoseconds and 1-30 microseconds in the urban areas [30]. The Doppler shift is usually smaller than 1 KHz when the pilot operates within 1-2 GHz.

The block diagram of channel estimator structure using noise pilot is shown in Figure **6-1**. The structure contains "*M*" correlators and "*n-1*" delay lines (DL) are added in front of the n^{th} correlator. Each delay line with delay time is equal to T and the reference signal that is used for the n^{th} correlator is $p_{M+1-n}(t)$.

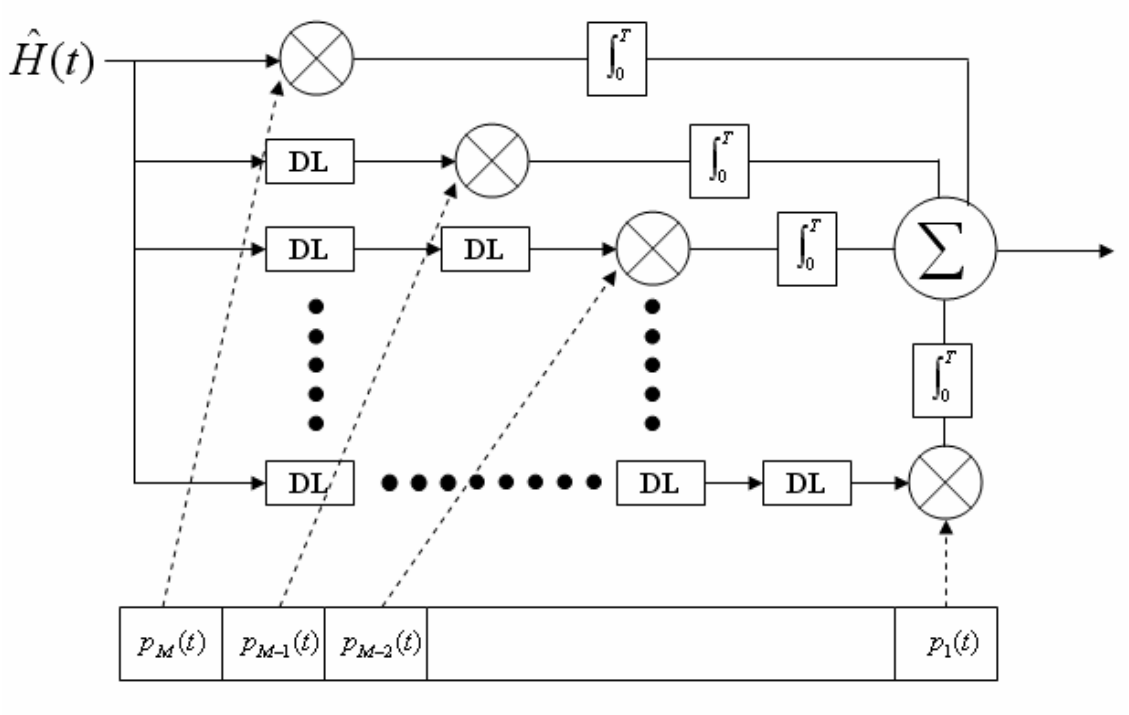

Figure **6-1**: Structure of channel estimator (DL=delay line).

The output of n^{th} correlator at time t is shown in Eq. **6.3** while the incoming signal $\hat{H}(t)$ is introduced in Eq. **6.1**.

$$P_n(t) = \int_0^T p_n(\tau)\hat{H}(t-(n-1)T+\tau)d\tau \qquad \textbf{6.3}$$

From Eq. **6.3** and Eq. **6.1**, it is clearly to show that there will have N significant correlation peaks at the output of summation circuit when t is equal to $MT + t_L$ ($L = 1, 2, 3.....N$). Thus, the delay time information of each path can be obtained according to the time that peaks will appear. A simulation is done and the results are shown in Figure **6-2**. In the simulation, the pilot is band-limited zero mean white Gaussian with frequency range 100-200 MHz. The sample frequency is 600 MHz and each window contains 80 samples. There are three multipath terms in the channel. The

first path has 1.16-μs delay, 1.2-KHz frequency shift, and 50% fractional power. The second path has 2.16-μs delay, 1.8-KHz frequency shift, and 20% fractional power .The third path has 3.33-μs delay, 4.8-KHz frequency shift, and 30% fractional power. From results shown in Figure **6-2**, the delay time of each path is successfully obtained.

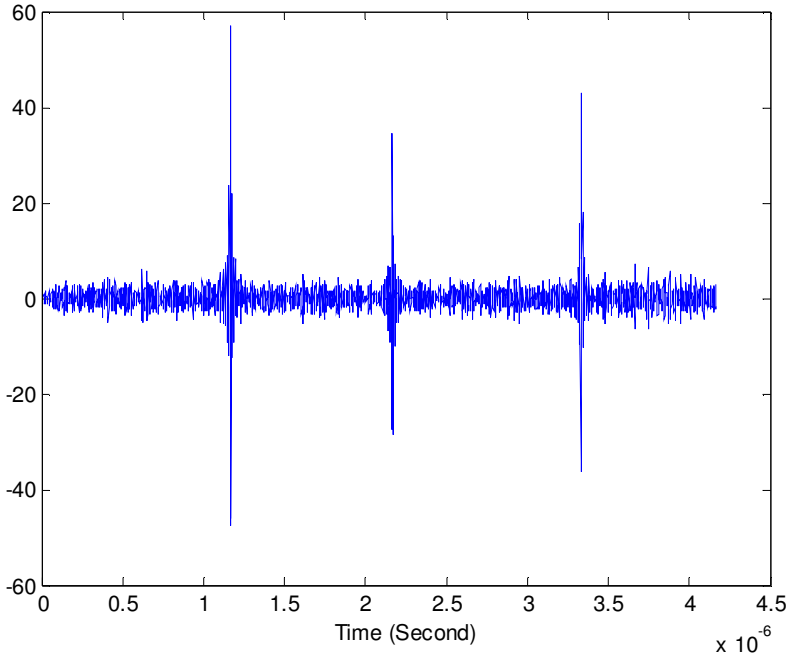

Figure **6-2**: Simulation results of delay time estimation.

The frequency shift corresponding to L^{th} path can be found by the vector V_L and is shown as

$$V_L = \left[P_1(MT + t_L), P_2(MT + t_L) \ldots\ldots P_{M-1}(MT + t_L), P_M(MT + t_L)\right] \qquad \textbf{6.4}$$

where $P_n(\,)$ can be calculated by Eq. **6.3**. By plotting vector V_L with down sample factor T / f_S^{-1}, we can observe that the V_L forms a sinusoid wave with period f_L^{-1}. That is because the T is much smaller than f_L^{-1} and $e^{j2\pi f_L(t+\tau)}$ in the Eq. **6.3** can be considered

as constant when $0 \le \tau \le M$ [31]. The fractional power belonging to the L^{th} path can be found by

$$R_L = \frac{Pow(V_L)}{\sum_{L=1}^{N} Pow(V_L)} \qquad \textbf{6.5}$$

where the $Pow(V_L)$ can be shown as

$$Pow(V_L) = \sum_{i=1}^{M} \frac{P_i^2 (MT + t_L)}{M} \qquad \textbf{6.6}$$

The Figure **6-3** shows the time domain plot of the V_L and the Figure **6-4** shows the frequency domain plot of the V_L. The frequency shift of each path can be exactly obtained. Table **6-1** also presents the measured fractional power. We can observe that the error is less than 5%. The simulation results demonstrate that the noise pilot has great potential for channel estimation. More research need to be done for evaluating the computation time which is an important factor of any algorithm planned to be used for real- time processing.

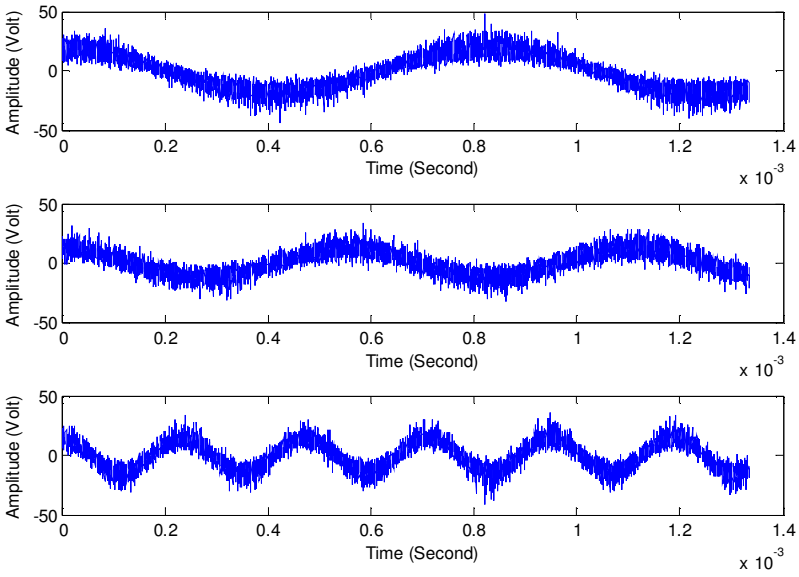

Figure **6-3**: The time domain plots of V_L (L=1,2,3).

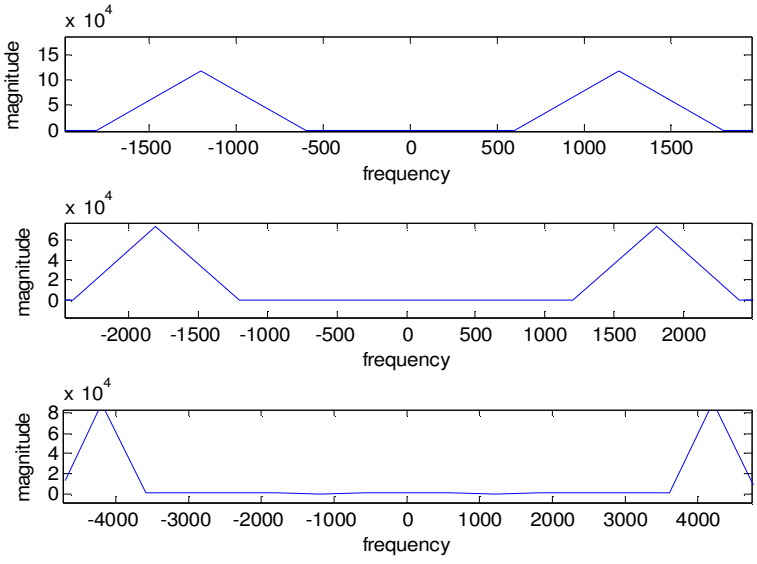

Figure **6-4**: Frequency domain plots of V_L (L=1,2,3).

Table **6-1**: Measured fractional power

	1st Path	2nd Path	3rd Path
Actual fractional power	0.5	0.2	0.3
Measured fractional power	0.513	0.19	0.297
Error (%)	2.6	5	1

6.3 Future work: Carrier synchronization

In wireless communications, the center frequency of received signal will change with the time due to the Doppler shift generated by the channel or random frequency drifting causing by the crystal oscillator. In order to perform down-conversion properly, the phase locked loop (PLL) needs to be implemented into the system. The well-known square loop or Costas loop are widely used to solve this problem [39]. Because the commercially available phase locked loop (PLL) circuit only accepts the input signals with frequency less than 100 MHz, the frequency doubler and frequency divider should be added before the carrier synchronization circuit. The block diagram of square loop which has been implemented into the NMCC system at receiver side is shown in Figure **6-5**.

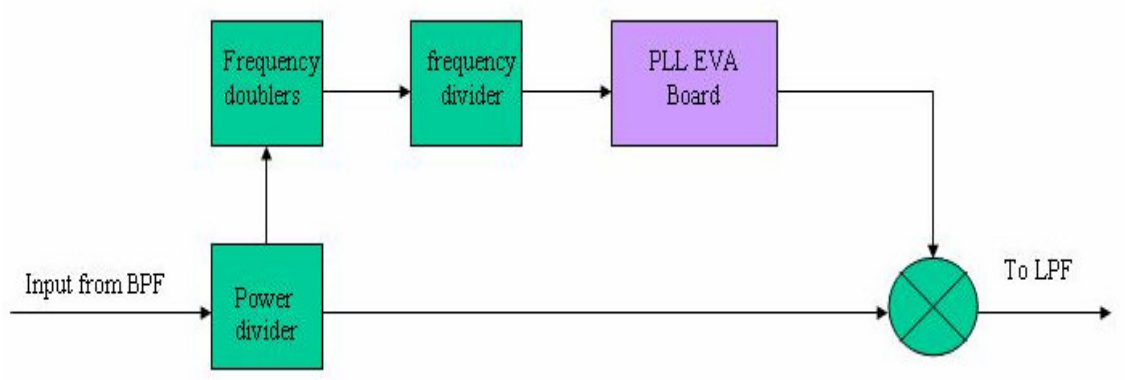

Figure **6-5**: Square loop that is implemented in the NMCC system.

From our experiment, the $a^2(t)$ terms in the Eq. **2.9** generates extra frequency components. The extra oscillation prevents the analog type frequency doubler and frequency divider from exactly catching the center frequency of the input signal. Thus, the PLL cannot lock to the carrier frequency of the received signal. Adding a narrow-band band-pass filter before the frequency doubler seems to be a solution. Unfortunately, the experiment results show this method will not work because the waveform has been distorted by this narrow-band filter.

An alternative method is direct down-conversion of the received signal into baseband, and implementing digital square loop in the FPGA design to avoid the problems that are generated by analog type components. The computation time determines whether this idea can be used for carrier synchronization or not. We believe that the NMCC system can achieve “push-to-talk” when the carrier synchronization and channel estimation can be accomplished and implemented into the system.

6.4 Future work: Exact PDF of received noise

Because the NMCC system is an ultra-wideband communication system, the ratio between the bandwidth of transmitted signal and the bandwidth of low-pass filter is very large. Thus, we assume that the filtered noise is zero mean white Gaussian. However, there is restriction of bandwidth in some applications and the ultra-wideband signal is not allowed. Thus, the ratio between the bandwidth of transmitted signal and the bandwidth of low-pass filter becomes small, and the deviation between simulation results and the BER model shown in Chapter-3 and Chapter-5 will increase, because the filtered noise loses white noise characteristics.

Finding the exact pdf of the filtered noise allows us to derive the BER equation that can be used for all the situations with small deviation. The pdf of sum frequency noise may be obtained by the concept that is presented by Andrews [40]. The task is finding the pdf of filtered noise because the pdf of sum frequency noise usually has a very complex mathematical expression.

Bibliography

1. J.K. Daher, J.M. Harris, and M.L. Wheeler, "An evaluation of the radio frequency susceptibility of commercial GPS receive", *IEEE Aerospace and Electronic Systems Magazine*, Vol. 9, pp. 21-25, Oct. 1994

2. www.sss-mag.com/shistory.html

3. C.E. Cook and H.S. Marsh, "An introduction to spread spectrum", *IEEE Communications Magazine*, vol. 21, no. 2, pp. 8-16, March 1983

4. R.A. Scholtz, "The origins of spread-spectrum communications", *IEEE Transactions on Communications*, vol. 30, no. 5, pt. 2, pp. 822-854, May 1982.

5. Roger L, Peterson, Rodger E. Ziemer, and David E. Borth,*"Introduction to spread spectrum communications Ch-2"*, Pretice-Hall Inc, 1995

6. R.B.Ward," Acquisition of Pseudonoise Signals by Sequential Estimation", *IEEE Trans on Communication Technology*, Vol. COM-32,pp.550-560,May 1984

7. W.K.Alem and C.L.Weber," Acquisition techniques for PN sequence", *Natl.Telecommun.Conf.Rec*,Dec 1977

8. P.C.J. Hill, E.R. Adams, and V.E. Comley, "Techniques for detecting and characterising covert communication signals", *Proc. IEEE Military Communications Conference (MILCOM '97), Monterey*, CA, pp. 1361-1365, November 1997

9. M. Gouda, E.R. Adams, and P.C.J. Hill, "Detection & discrimination of covert DS/SS signals using triple correlation", *Proc. Fifteenth National Radio Science Conference (NRSC '98)*, Cairo, Egypt, pp. C35/1-C35/6, February 1998

10. G. Burel, "Detection of spread spectrum transmissions using fluctuations of correlation estimators", *Proc. IEEE International Symposium on Intelligent Signal Processing and Communication Systems (ISPACS'00)*, Hawaii, HI, November 2000

11. N. C. Beaulieu, W. L. Hopkins, and P. J. McLane, "Interception of frequency-hopped spread-spectrum signals", *IEEE Journal on Selected Areas in Communications*, vol., 8, no. 5, pp. 853-870, June 1990

12. Kevin M.Cuomo, Alan V. Oppenheim, and Steven H. Strogatz," Synchronization of Lorenz-Based Chaotic Circuits with Applications to Communication", *IEEE Trans on Circuits and System-2* ,Vol 40,No. 10, Oct 1993

13. George R. Cooper, Lisa Heald Cooper," Covert communication with a purely random spreading function", *IEEE, MILCOM* no.2.4, 1982

14. Haartsen, J.C., Meijerink, A., Bekkaoui, A., Taban, A. and Tauritz, J.L.: "Novel wireless modulation technique based on noise", *Proc. 10th Annual IEEE Symp. on Communications and Vehicular Technology in the Benelux (SCVT 2004)*, Ghent, Belgium, Nov. 2004

15. Haartsen, J.C., Shang, X., Balkema, J.W., Meijerink, A. and Tauritz, J.L.: "A new wireless modulation scheme based on frequency-offset", *Proc. 12th Annual IEEE Symp. on Communications and Vehicular Technology in the Benelux (SCVT 2005)*, Enschede, Netherlands, Nov. 2005

16. M. Dawood and R.M. Narayanan, "Receiver operating characteristics for the coherent UWB random noise radar," *IEEE Transactions on Aerospace and Electronic Systems*, vol. 37, no. 2, pp. 586-594, April 2001

17. Wipro Technologies,"*Software-defined radio white paper a technology overview"*

18. Matthew Won DeMay *,"Spread Spectrum Communication Using UWB Random Noise Signals: Complete System Simulation and Implementation"* ,Master Thesis 2006

19. Athanasios Papoulis, S. Unnilrishna Pillai," *Probability, Random Variables and Stochastic Processes CH-9* ",4-th edition,2002

20. Sablatash, M.; Lodge, J.L.; Moreland, K.W," Theory and methods for design of pulse shapes for broadcast teletext", *IEEE Trans on Broadcasting* Vol 35, No 1, March 1989 Page(s):40 – 55

21. Roger L. Peterson, Rodger E.Ziemer, David E. Borth," *Introduction to Spread Spectrum Communications Ch-2,Ch-6"* , Prentice Hall 1995

22. Lyrtech "*SignalWAVe user's guide"* , Nov 2005

23. Theodore S. Rappaport,"*Wireless Communications Principles and Practice 2nd edition Ch-4,Ch-6.8.4*", Hall PTR 2002

24. N.E. Hung "The empirical mode decomposition and the Hilbert spectrum for nonlinear and non-stationary time series analysis", *Pro.R.Soc London*. A, Vol.454,pp903-995

25. Zhou-Fu Liu,Zhen-Peng Liao,En-Fang Sang", Speech Enhancement Based on Hilbert-Hung Transform" *IEEE 2005 Machine Learning and Cybernetics*,pp4098-4512

26. Gordon L. Stuber,*" Principles of Mobile Communication 2nd edition"* , Kluwer Academic Publishers Group 2001

27. Iyidir, B.; Ozkazanc, Y.," Jamming of GPS receivers" *IEEE 12th Signal Processing and Communication Applications Conference*, 2004.

28. R.C. Titsworth and L. R. Welch, "*Power Spectra of Signals Modulated by Random and Pseudorandom Sequences*", Tech Rep.32-140, Jet Propulsion Laboratory, Pasadena, Calif, October 1961

29. Sergio Verdu,*" Multiuser Detection Ch-2,Ch-3"*Cambridge 1998

30. Andrea Goldsmith,"*Wireless Communications*", 2005 Cambridge University

31. Axelsson, S.R.J.," Noise radar using random phase and frequency modulation", *IEEE Tran on Geosciences and remote sensing*, Volume 42, No. 11, Nov. 2004 Page(s):2370 – 2384

32. Ram M. Narayanan and Muhammad Dawood,"Doppler Estimation Using a Coherent Ultrawide-Band Random Noise Radar", *IEEE Tran on Antennas and propagation,*Vol. 48,No. 6, June 2000

33. C.A Balanis," *Advance engineering electromagnetic Ch-4,Ch-5*" 1989 Wiley

34. O.Fonseca and I.N. Psaromilgkos,"BER performance of BPSK transmissions over multipath channels," *Electronics Letters,* Vol. 42, No.20 ,Sep 2006

35. C.K. Rushforth, "Transmitted-reference techniques for random or unknown channels," *IEEE Transactions on Information Theory*, vol. 10, no 1, pp. 39-42, January 1964.

36. R.M. Gagliardi, "A geometrical study of transmitted reference communication systems," *IEEE Transactions on Communication Technology*, vol. 12, no. 4, pp. 118-123, December 1964

37. S.R.J.Axelsson,"On the theory of noise Doppler radar", *Proc. IGARSS, Honolulu,HI*,pp.856-860, July 24-28,2000

38. Syne R.J.Axelsson,"Noise Radar For Range/Doppler Processing and Digital Beamforming Using Low-Bit ADC", *IEEE Tran on Geosciences and remote sensing*,Vol. 41 No. 12 Dec 2003

39. L.E.Franks,"Carrier and bit synchronization in data communication-a tutorial review", *IEEE Trans, on Comm. Vol.Com-28,pp1107-1121,August 1980*

40. Larry C. Andrews," The Probability Density Function for the Output of a Cross-Correlator With Bandpass Inputs", *IEEE Tran on Information Theory*, vol 19,no 1, Jan 1973

Appendix A

Power of interference terms in jamming channel

The $\hat{V}(t)$ and $\hat{H}(t)$ can be represented as

$$\begin{aligned}\hat{H}(t) &= x(t-t_1)\cos(2\pi f_n(t-t_1)) - y(t-t_1)\sin(2\pi f_n(t-t_1)) \\ \hat{V}(t) &= m(t)\left[x(t)\cos(2\pi f_n t) + y(t)\sin(2\pi f_n t)\right]\end{aligned} \quad \textbf{A.1}$$

,where $f_c = 2f_n$. The $x(t)$ and $y(t)$ are Gaussian random variable independent to each other and the $m(t)$ is the data that transmitted by NMCC system. Applying Eq. **A.1**, the sum frequency signals of $J(t)\hat{V}(t-t_1)$ and $J(t-t_1)\hat{H}(t)$ can be expressed as (For convenience, we assume the delay of the delay line is zero ($t_1 = 0$) since it will not affect the derivation. Eq. **A.2**

$$\begin{aligned}(J(t)\hat{V}(t))_{sum} &= I_V(t) = 0.5\sqrt{2P}m(t)m_d(t)c(t)\left[x(t)\cos(2\pi(f_n+f_J)t) + y(t)\sin(2\pi(f_n+f_J)t)\right] \\ (J(t)\hat{H}(t))_{sum} &= I_H(t) = 0.5\sqrt{2P}m_d(t)c(t)\left[x(t)\cos(2\pi(f_n+f_J)t) - y(t)\sin(2\pi(f_n+f_J)t)\right]\end{aligned} \quad \textbf{A.2}$$

,where $c(t)$ is the PN sequence that used by non-intentional DS-SS interference and the $m_d(t)$ is the data that carries by this interference. The P is the power of this interference. The power of filtered summation $I_V(t)$ and $I_H(t)$ can be found in Eq. **A.3** since ideal filter can be considered as linear component.

$$\begin{aligned}E\left[\left(BPF\left(I_V(t)+I_H(t)\right)\right)^2\right] &= E\left[\left(BPF(I_V(t)\right)^2\right] + E\left[\left(BPF(I_H(t)\right)^2\right] + 2E\left[BPF(I_H(t)I_V(t))\right] \\ &= P_{I5} + P_{I7} + 2BPF\left(E\left[I_H(t)I_V(t)\right]\right)\end{aligned} \quad \textbf{A.3}$$

The P_{I5} and P_{I7} are the power of filtered $I_V(t)$ and $I_H(t)$ respectively. They can be found by Eq. **5.17** and are $P\sigma_S^2 B_L \Big/ \left(B_S + T_c^{-1}\right)$. The $2E\left[I_V(t)I_H(t)\right]$ terms in Eq. **A.3** can be found as

$$\begin{aligned}
2E\left[I_V(t)I_H(t)\right] &= 2E[(m(t)m_d^2(t)c^2(t)\left(x(t)\cos(2\pi(f_n+f_J)t)+y(t)\sin(2\pi(f_n+f_J)t)\right) \\
&\quad \times(x(t)\cos(2\pi(f_n+f_J)t)-y(t)\sin c(2\pi(f_n+f_J)t))] \\
&= 2R_{m_d,m_d}(0)R_{c,c}(0)m(t)\left(E\left[x^2(t)\cos^2(2\pi(f_n+f_J)t)\right]-E\left[y^2(t)\sin^2(2\pi(f_n+f_J)t)\right]\right) \\
&= R_{m_d,m_d}(0)R_{c,c}(0)E[m(t)]\left(E\left[x^2(t)\right]-E\left[y^2(t)\right]\right) \\
&= R_{m_d,m_d}(0)R_{c,c}(0)E[m(t)]\times 0 \\
&= 0
\end{aligned} \qquad \textbf{A.4}$$

Since the $2E\left[I_V(t)I_H(t)\right]$ is zero, the $2BPF\left(E\left[I_H(t)I_V(t)\right]\right)$ is also zero. The power of $BPF\left(I_V(t)+I_H(t)\right)$ is equal to sum their individual power after passing the filter. Thus, the power of $\text{BPF}\left(J'(t)\hat{H}(t)_{sum}\right)$ plus $\text{BPF}\left(J(t)\hat{V}(t-t_1)_{sum}\right)$ is equal to sum their individual power.

Appendix B

Power of interference terms in multipath channel

The mean of sum frequency components signals of $\sigma_{i-V}\sigma_{j-H}H(t-t_j-(t_N-t_m))V(t-t_i-(t_N-t_n))$ and $\sigma_{i-H}\sigma_{j-V}H(t-t_i-(t_N-t_n))V(t-t_j-(t_N-t_m)$ are zero. The power of summation these twp sum frequency components signals can be found by Eq. **B.1**

$$
\begin{aligned}
P=&E[(\sigma_{i-V}\sigma_{j-H}a(t-t_j-T_m)a(t-t_i-T_n)\cos(2\pi f_cT+\theta(t-t_j-T_m)-\theta(t-t_i-T_n)+\alpha)\\
&+\sigma_{i-H}\sigma_{j-V}a(t-t_j-T_n)a(t-t_i-T_m)\cos(2\pi f_cT+\theta(t-t_j-T_n)-\theta(t-t_i-T_m)+\alpha))^2]\\
=&E[(\sigma_{i-V}\sigma_{j-H}a(t-t_j-T_m)a(t-t_i-T_n)\cos(2\pi f_cT+\theta(t-t_j-T_m)-\theta(t-t_i-T_n)+\alpha))^2]\\
&+E[(\sigma_{i-H}\sigma_{j-V}a(t-t_j-T_n)a(t-t_i-T_m)\cos(2\pi f_cT+\theta(t-t_j-T_n)-\theta(t-t_i-T_m)+\alpha))^2]\\
&+2\sigma_{i-H}\sigma_{j-V}\sigma_{i-V}\sigma_{j-H}E[a^2(t-t_j-T_m)a^2(t-t_i-T_n)\cos(2\pi f_cT+\theta(t-t_j-T_m)-\theta(t-t_i-T_n)+\alpha)\\
&\times\cos(2\pi f_cT+\theta(t-t_j-T_n)-\theta(t-t_i-T_m)+\alpha)]\\
=&P_1+P_2+2E\left[\sigma_{i-H}\sigma_{j-V}\sigma_{i-V}\sigma_{j-H}a^2(t-t_j-T_m)a^2(t-t_i-T_n)\cos\left(4\pi f_ct+2\alpha\right)\right]\\
&+2E\left[\sigma_{i-H}\sigma_{j-V}\sigma_{i-V}\sigma_{j-H}a^2(t-t_j-T_m)a^2(t-t_i-T_n)\cos\left(2\theta(t-t_j-T_n)-2\theta(t-t_i-T_m)\right)\right]
\end{aligned}
\qquad \textbf{B.1}
$$

where P_1 and P_2 are power of sum frequency components signals of $\sigma_{i-V}\sigma_{j-H}H(t-t_j-(t_N-t_m))V(t-t_i-(t_N-t_n))$ and $\sigma_{i-H}\sigma_{j-V}H(t-t_i-(t_N-t_n))V(t-t_j-(t_N-t_m)$. The $T_n=t_N-t_n$, $T_m=t_N-t_m$, and $\alpha=2\pi f_n((t_m+t_n)-t_i-t_j-2t_N)$. The $E\left[\sigma_{i-H}\sigma_{j-V}\sigma_{i-V}\sigma_{j-H}a^2(t-t_j-T_m)a^2(t-t_i-T_n)\cos\left(4\pi f_ct+2\alpha\right)\right]$ in the Eq. **B.1** is zero.

Since the $\theta(t-t_j-T_n)$ and $\theta(t-t_i-T_m)$ are uniform random variable within $[\pi,-\pi]$. The $2\theta(t-t_j-T_n)$ and $-2\theta(t-t_i-T_m)$ are also uniform random variable within $[\pi,-\pi]$. If delay time between each path is large enough, the $2\theta(t-t_j-T_n)$ and

$-2\theta(t-t_i-T_m)$ can be considered as two independent random variable. Thus, the PDF of $2\theta(t-t_j-T_n)-2\theta(t-t_i-T_m)$ has isosceles triangle shape with center at located at zero and the range is between $[2\pi,-2\pi]$. Since the pdf is symmetry to the zero, the $E\left[\sigma_{i-H}\sigma_{j-V}\sigma_{i-V}\sigma_{j-H}a^2(t-t_j-T_m)a^2(t-t_i-T_n)\cos\left(2\theta(t-t_j-T_n)-2\theta(t-t_i-T_m)\right)\right]$ is equal to zero and the Eq. **B.1** can be reduced to Eq. **B.2**

$$P = P_1 + P_2 \qquad \textbf{B.2}$$

Thus, the power of summation of $\sigma_{i-V}\sigma_{j-H}H(t-t_j-(t_N-t_m))V(t-t_i-(t_N-t_n))$ and $\sigma_{i-H}\sigma_{j-V}H(t-t_i-(t_N-t_n))V(t-t_j-(t_N-t_m)$ is summation their individual power.

Appendix C

Stage by stage measurement

The time domain signal is recorded by Agilent DSO80804B oscillation scope and frequency domain signal is measured by HP 8562E spectrum analyzer. The place with red arrow in Figure **C-1** is the place that did the measurement. The sequential order of measured results present in this section is correspond to the number in the Figure **C-1**.

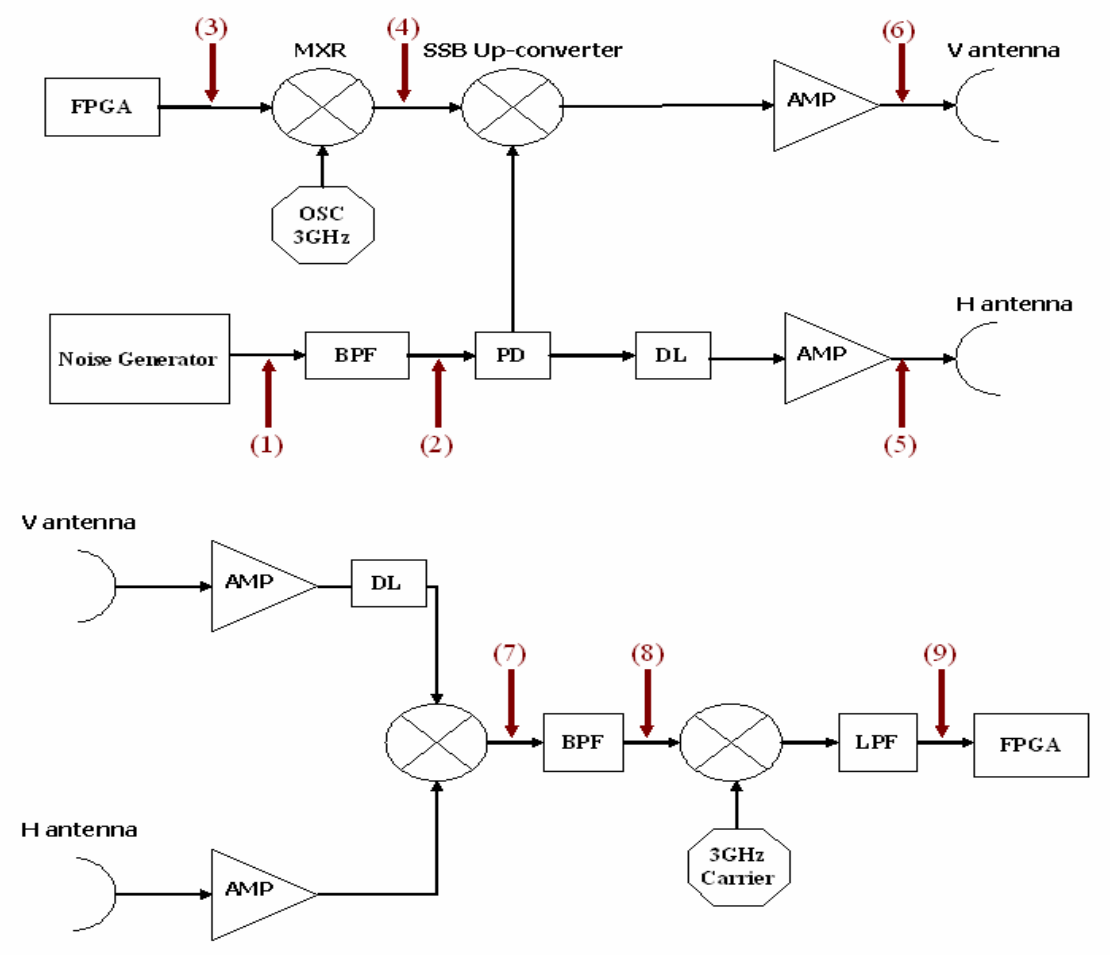

Figure **C-1**: Transmitter block diagram (top) and receiver block diagram (bottom).

(1) Signal at output of noise generator (Transmitter):

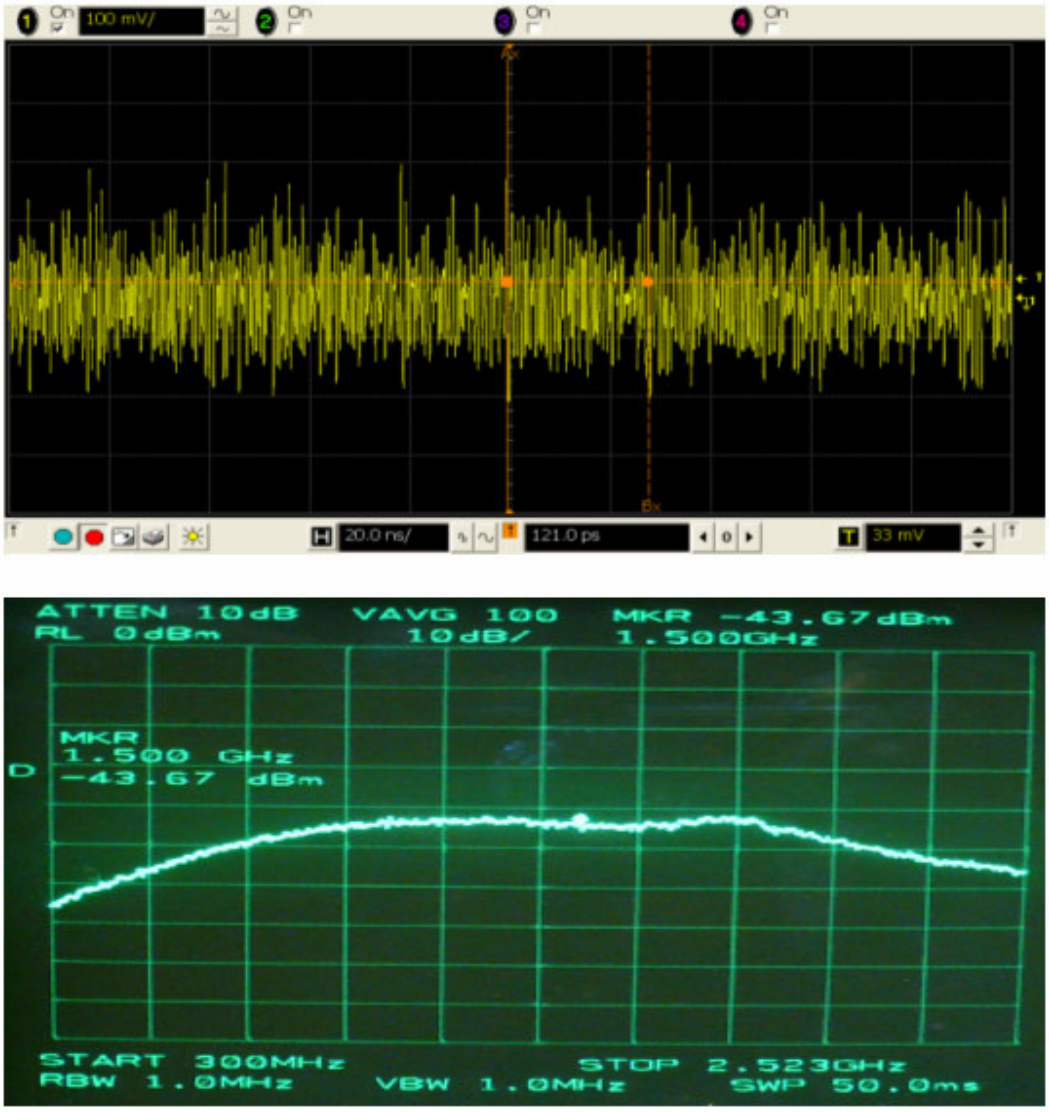

Figure **C-2**: Recorded time (top) and frequency (bottom) plot at output of noise generator in the transmitter side.

(2) Signal at output of band-pass filter (Transmitter):

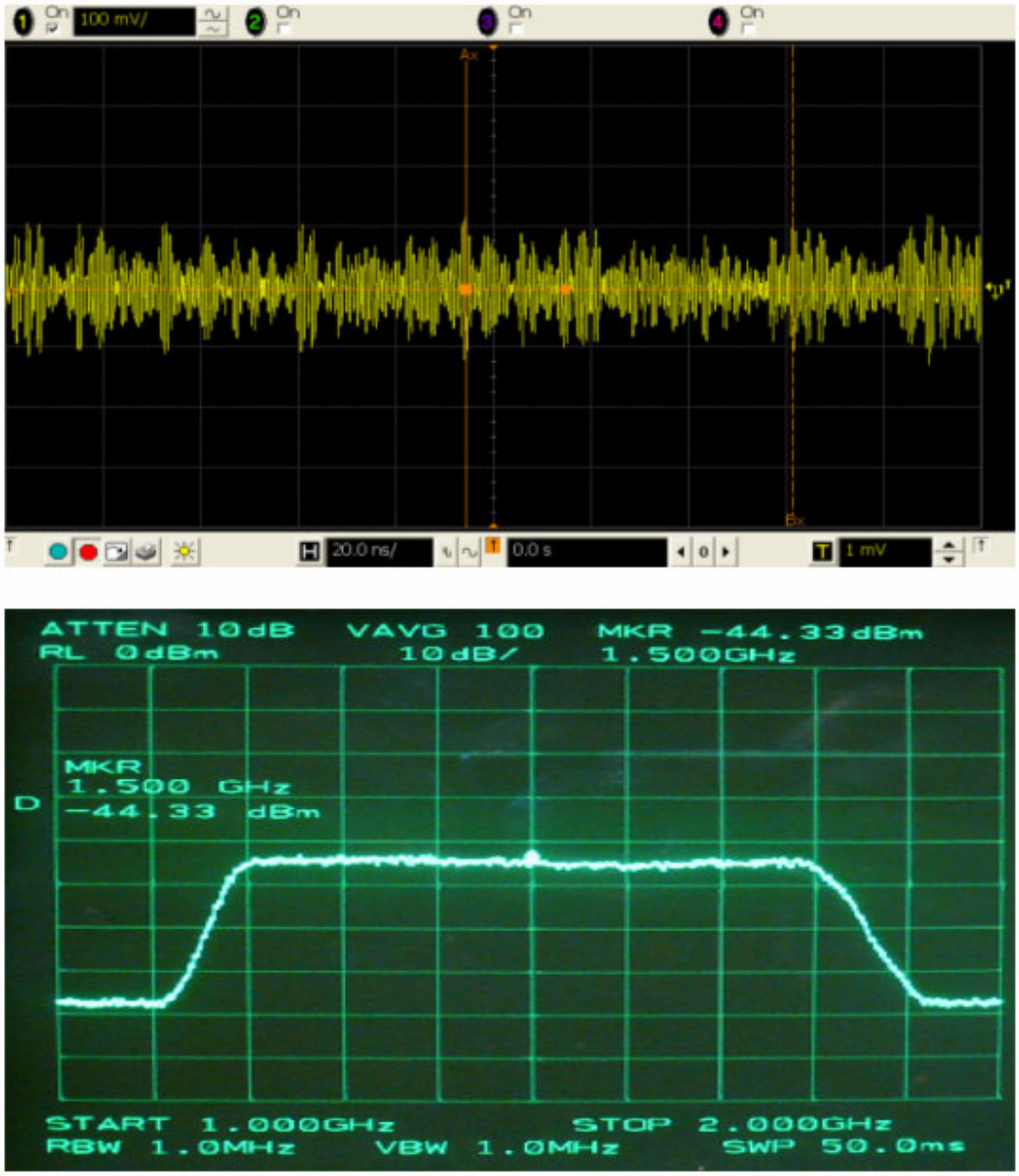

Figure **C-3**: Recorded time (top) and frequency (bottom) plot at output of band-pass filter in the transmitter side.

(3) Signal at output of FPGA board (Transmitter):

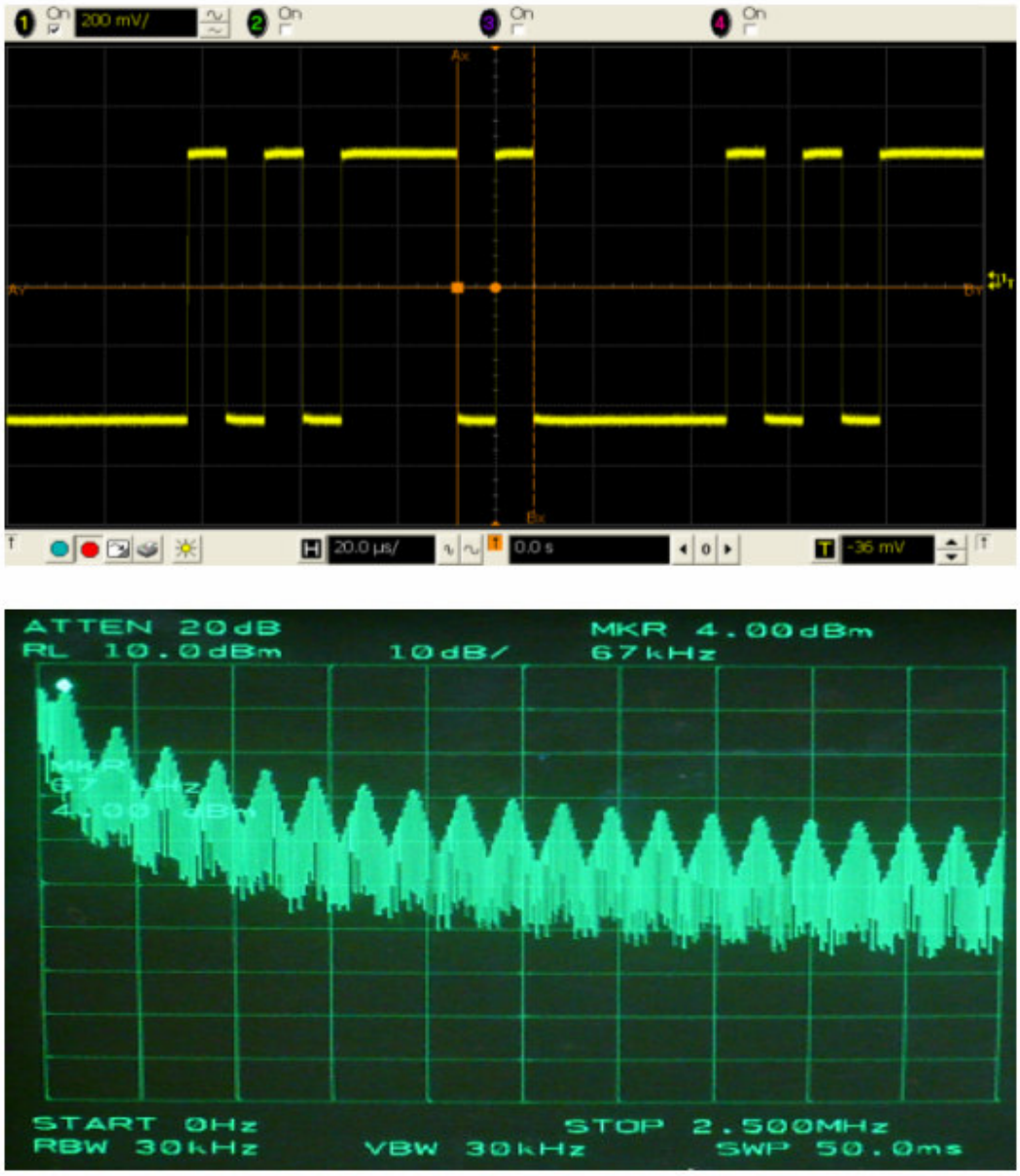

Figure **C-4**: Recorded time (top) and frequency (bottom) plot at output of FPGA board in the transmitter side.

(4) Signal at output of mixer (Transmitter):

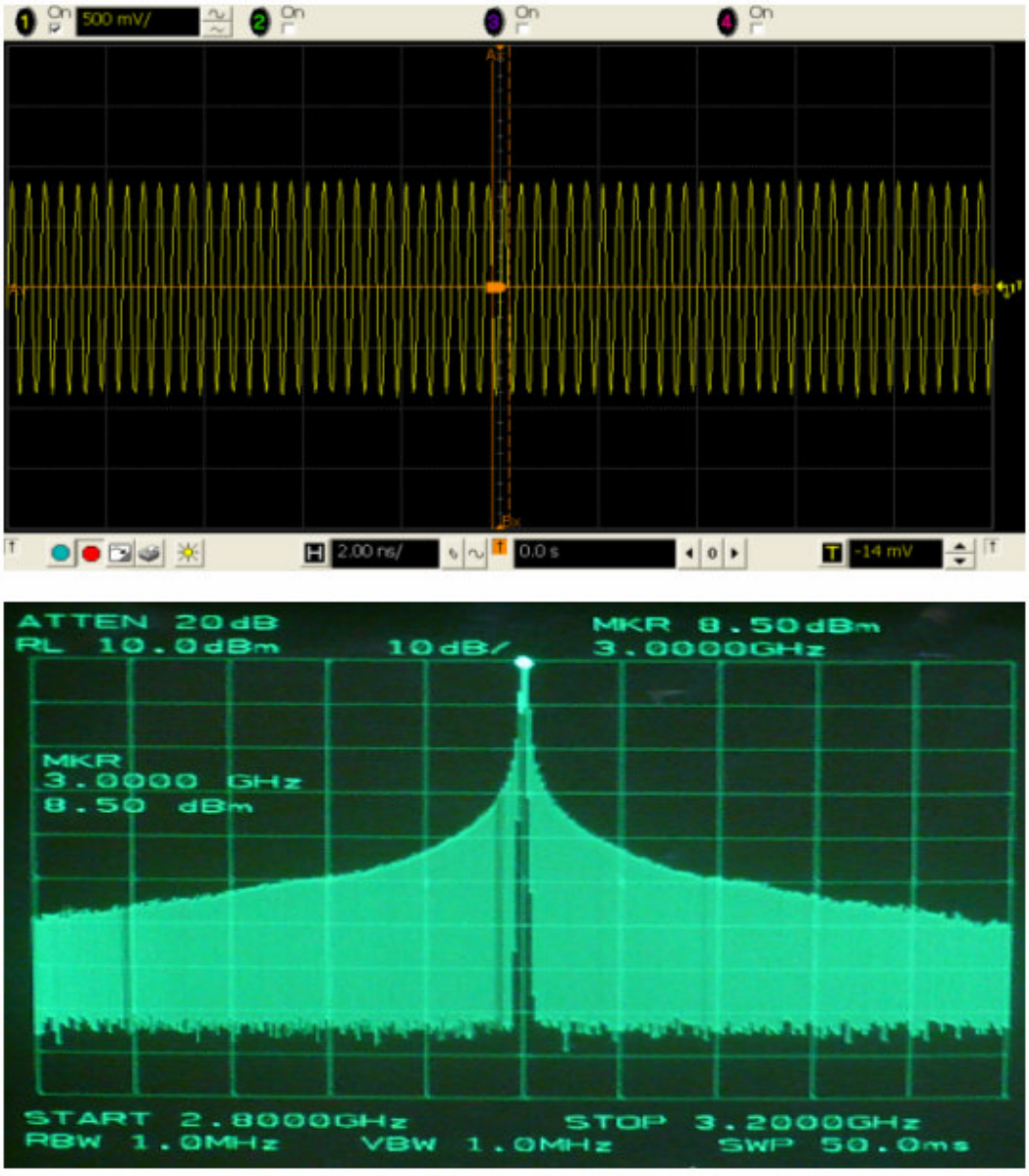

Figure **C-5**: Recorded time (top) and frequency (bottom) plot at output of mixer in the transmitter side.

(5) Signal sends to horizontal polarization antenna (Transmitter):

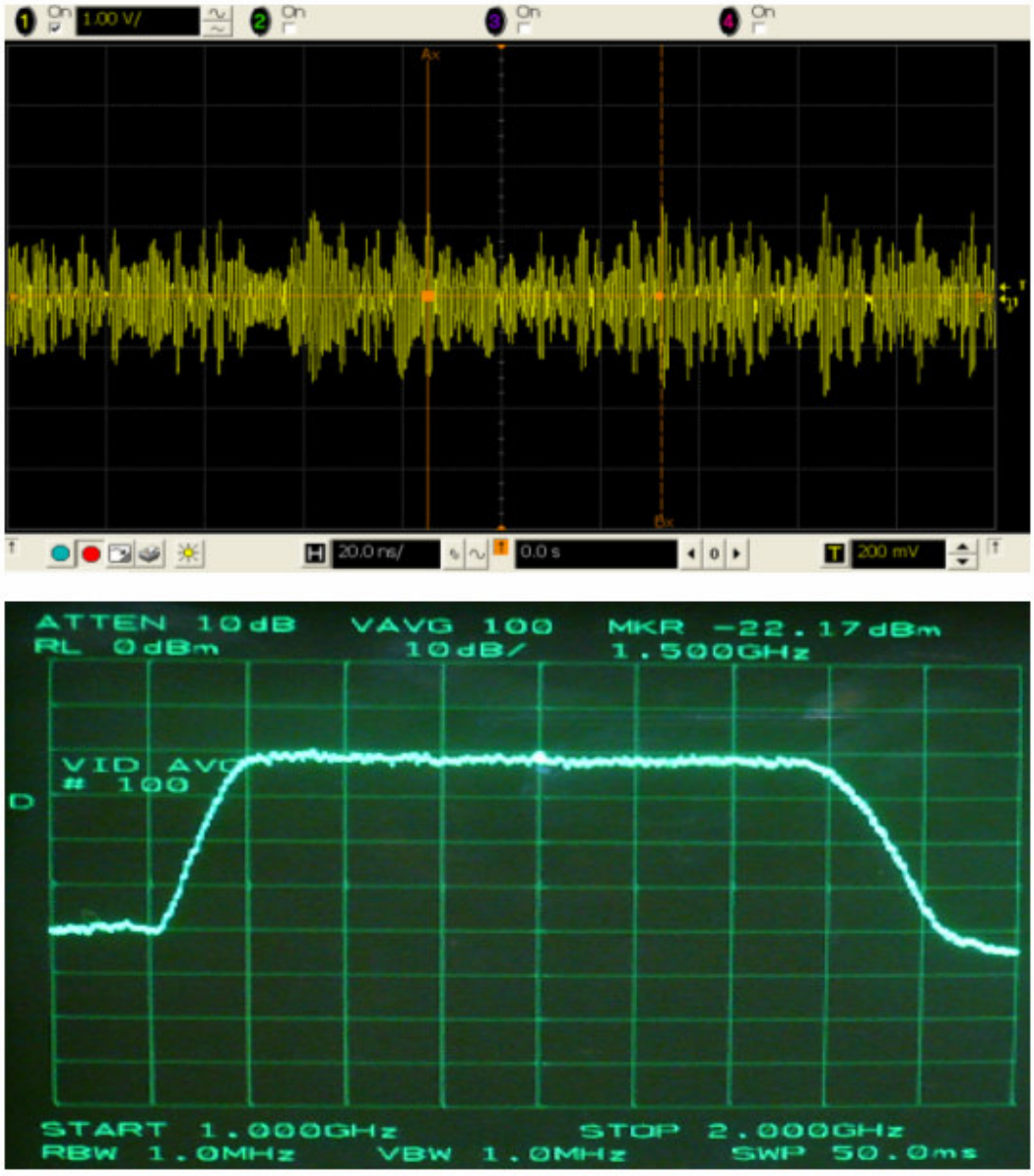

Figure **C-6**: Recorded time (top) and frequency (bottom) plot for the signal that will send to horizontal polarization antenna.

(6) Signal sends to vertical polarization antenna (Transmitter):

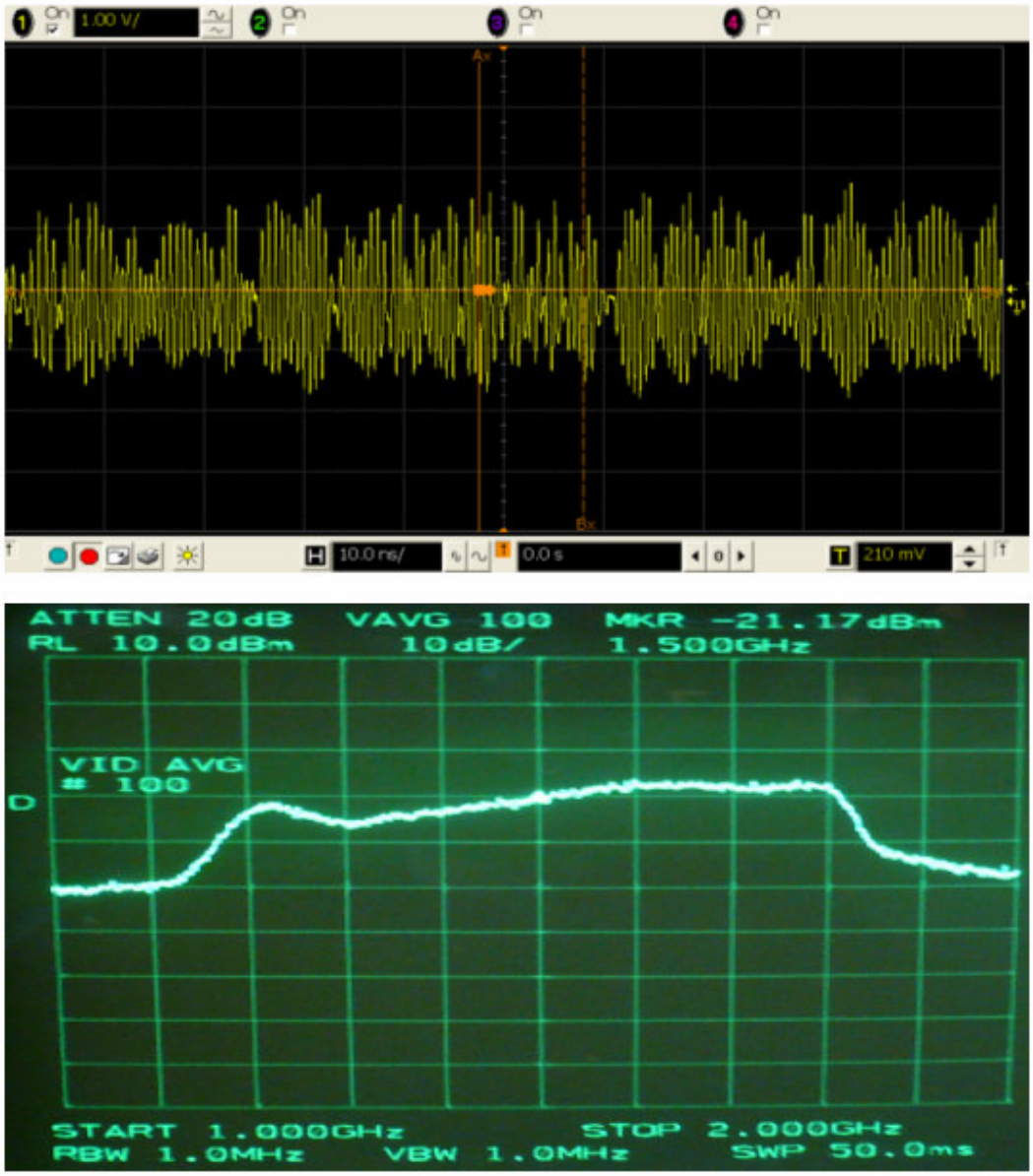

Figure **C-7**: Recorded time (top) and frequency (bottom) plot for the signal that will send to vertical polarization antenna.

(7) Signal at output of first mixer (Receiver):

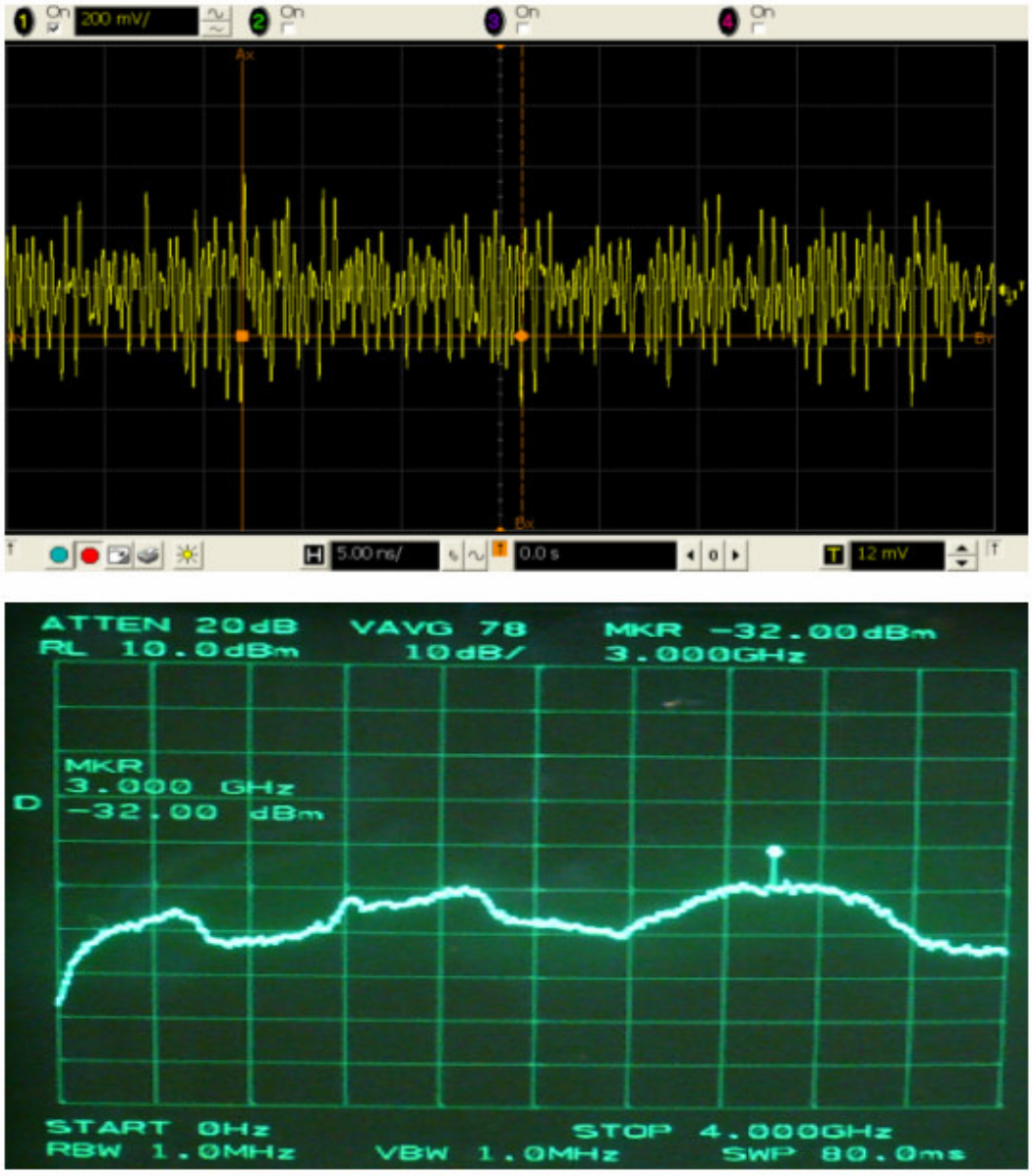

Figure **C-8**: Recorded time (top) and frequency (bottom) plot at output of the first mixer in the receiver side.

(8) Signal at output of band-pass filter (Receiver):

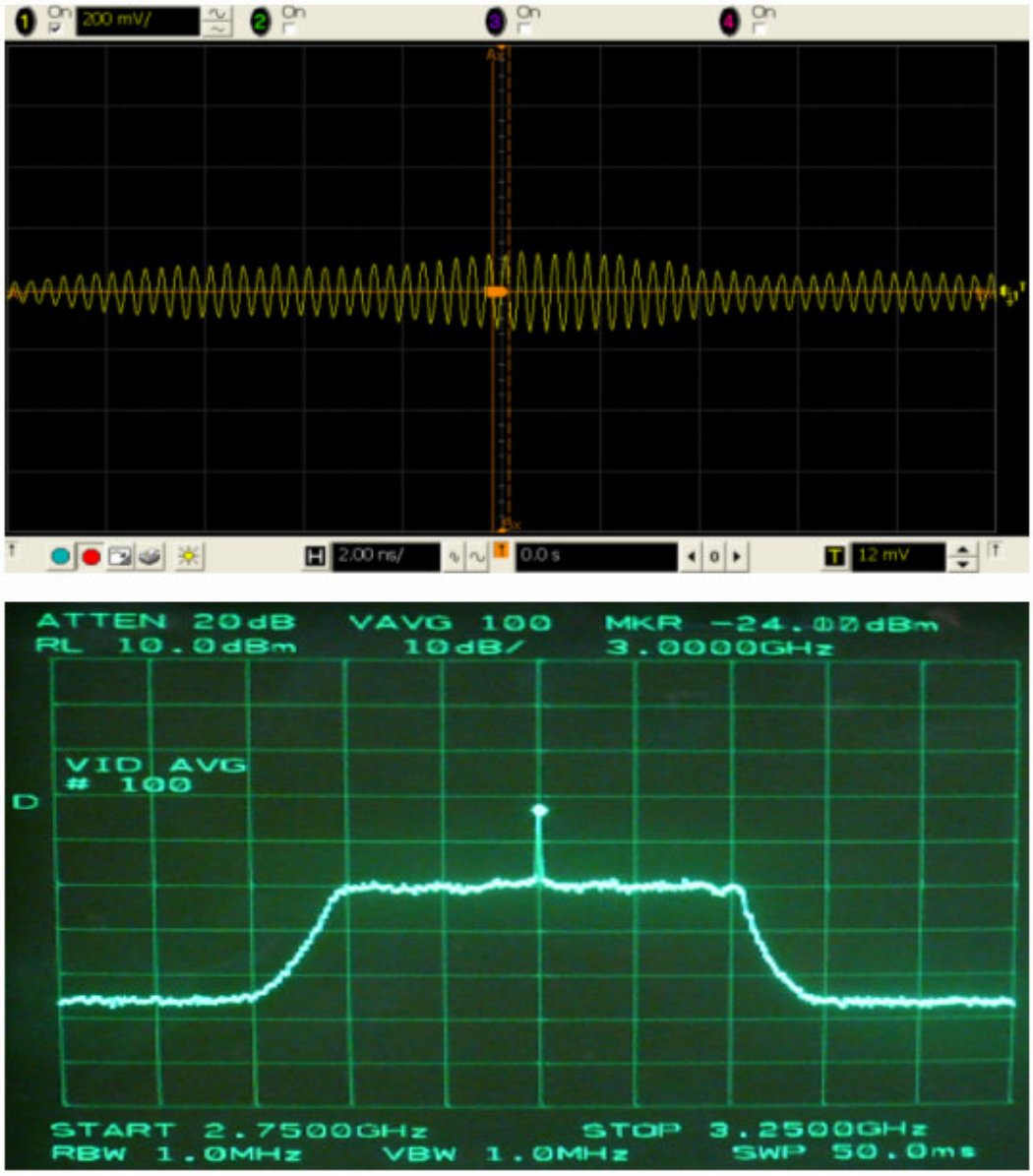

Figure **C-9**: Recorded time (top) and frequency (bottom) plot at output of the band-pass filter in the receiver side.

(9) Signal at output of low-pass filter (Receiver):

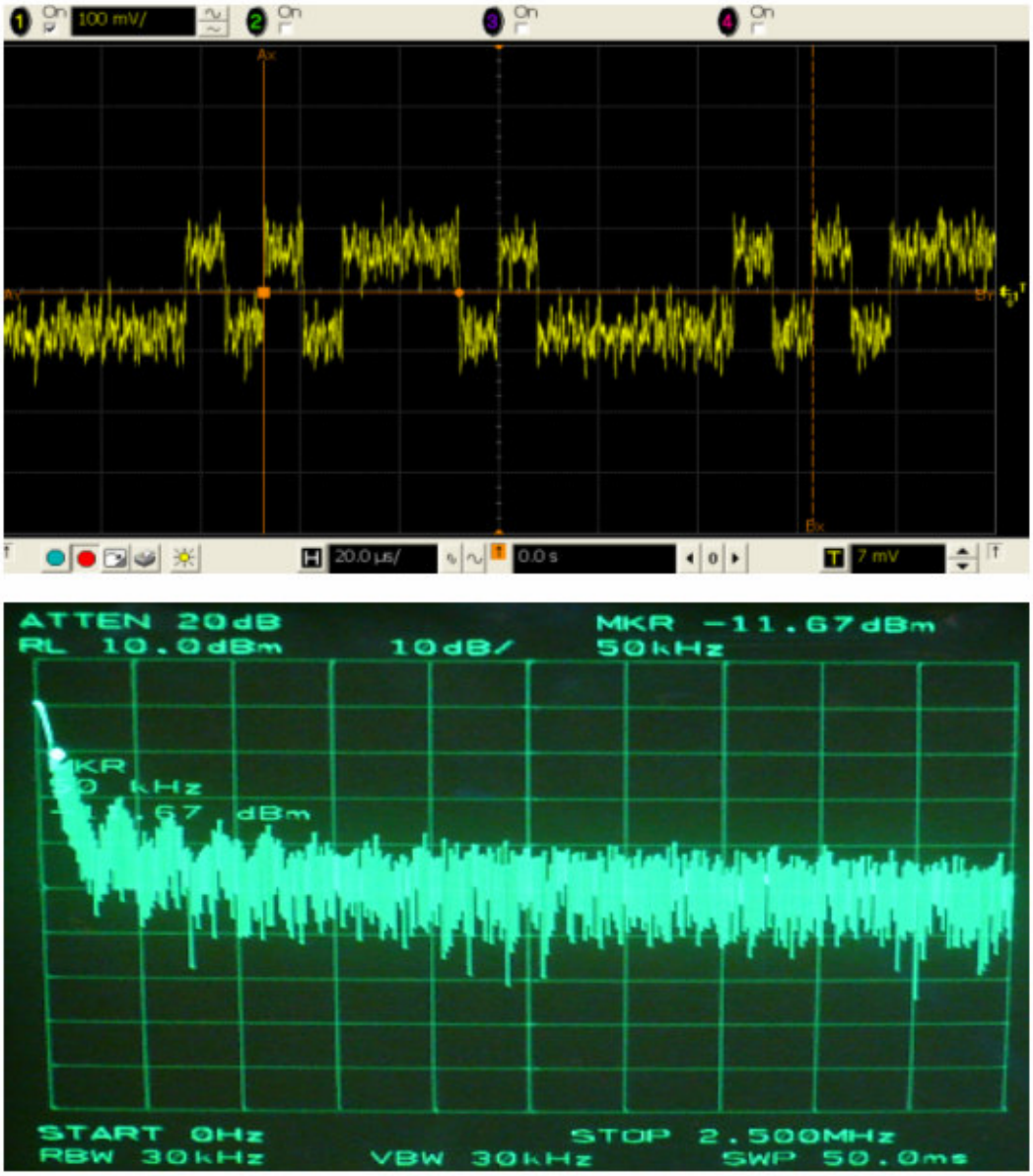

Figure **C-10**: Recorded time (top) and frequency (bottom) plot at output of the low-pass filter in the receiver side.

Appendix D

Matlab Code

1. AWGN Channel (Single-User):

```
clc;
format long;
clear All;

%Parameter setup==================
SNRchannel=-14:1:-6;
samplefre=36*10^9;
Ts=1/samplefre;
datarate=5*10^6;%Data is running 5Mbps
t=0:1/samplefre:(100/datarate)-(1/samplefre);
BW=980*10^6;
BERtotal=zeros(1,9);
%==============================

for g=1:1:9
for m=1:1:1000
input=randint(1,100);

%=========================================
%BPSK modulation
BPSK=dmodce(input,datarate,samplefre,'ask',2);
allsize=length(BPSK);
%put signal on carrier
carrier3G=cos(2*pi*3*10^9*t);
passband=carrier3G.*BPSK;
%=====================================

%Generating H signal===============
noise1=wgn(1,allsize,0);
loBW=1.5*10^9-0.5*BW;
upBW=1.5*10^9+0.5*BW;
Hsignal=BPF (loBW,upBW,noise1,samplefre);
% ==========================


%Generating V signal=================
transmitt=passband.*Hsignal;
loBW2=1.5*10^9-0.5*BW-datarate;
upBW2=1.5*10^9+0.5*BW+datarate;
```

```
Vsignal=antenna(loBW2,upBW2,transmitt,samplefre);
%================ ==============


%Power amplifier make sure that Vertical and Horizontal signal has the same
%power
V1=Vsignal*sqrt(pow(Vsignal)/pow(Vsignal));
H1=Hsignal*sqrt(pow(Vsignal)/pow(Hsignal));
 % ==========================

%Add channel noise=============================================
wgnH = wgn(1,allsize,0);
wgnV = wgn(1,allsize,0);
recnV=antenna(loBW2,upBW2,wgnV,samplefre); %channel noise
recnH=antenna(loBW2,upBW2,wgnH,samplefre); %channel noise

%Make sure the recived noise and signal at the same SNR
 recVPower=pow(V1);%received signal power
recNVPower=recVPower/(10^(SNRchannel(g)/10));%find received noise power
NVcoeffe=sqrt(recNVPower/pow(recnV));%coeffieient adjust power
recnV=NVcoeffe*recnV;%rec V noise with proper SNRchannel


recHPower=pow(H1);%received signal power
recNHPower=recHPower/(10^(SNRchannel(g)/10));%find received noise power
NHcoeffe=sqrt(recNHPower/pow(recnH));%coeffieient adjust power
recnH=NHcoeffe*recnH;%rec H noise with proper SNRchannel
%============================================================

%Received Signal ==========================
Vrec=V1+recnV;
Hrec=H1+recnH;
rec=Vrec.*Hrec;
%First BPF between 2.95GHz~3.05GHz
spassband=BPF2950Mto3050M(rec,samplefre);
%Mix with carrier and send to low pass filter 0~20MHz
sbase=spassband.*carrier3G;
%LPF=20M
s20baseband=LPF20M(sbase,samplefre);
%Demodulation and calculate the error
output=ddemodce(s20baseband,datarate,samplefre,'ask',2);
errNum=biterr(output,input);
counter(m)=errNum;
end
BERtotal(g)=sum(counter)/(10^5);
end
```

2. Loss-Factor calculation:

```
%Derive the loss factor================================
rec=V1.*H1; %V1 and H1 is in AWGN single user environment
spassband=BPF(2*10^9,4*10^9,rec,samplefre);
```

```
sbase=spassband.*carrier3G;
s20baseband=LPF20M(sbase,samplefre);
s1Gbaseband=LPF1G(sbase,smplefre);
lossfactor=pow(s20baseband)/pow(s1Gbaseband);
```

3. Time and frequency domain plot:

```
plotspec(V1,1/samplefre); %Plot transmitted V signal
plotspec(H1,1/samplefre); %Plot transmitted H signal
```

4. AWGN Channel (Multi-User):

```
%Simulation BER performance with different Gain for MTT paper
%Multi-User Environment N=3 and N=5
clc;
clear;
format long;
SNRchannel=-11:1:-4;
samplefre=12*10^9;
Ts=1/samplefre;
datarate=5*10^6;%Data is running 5MHz
t=0:1/samplefre:(100/datarate)-(1/samplefre);
 BERtotal3=zeros(1,8);
BERtotal5=zeros(1,8);
for g=1:1:8
counter1=ones(1,1200);
counter2=ones(1,1200);
for m=1:1:1200
input1=randint(1,100);
input2=randint(1,100);
input3=randint(1,100);
input4=randint(1,100);
input5=randint(1,100);
MaxPower=1; %in Watt
AntennaImp=50;
SNR=0;
%=========================================
%BPSK modulation
BPSK1=dmodce(input1,datarate,samplefre,'ask',2);
BPSK2=dmodce(input2,datarate,samplefre,'ask',2);
BPSK3=dmodce(input3,datarate,samplefre,'ask',2);
BPSK4=dmodce(input4,datarate,samplefre,'ask',2);
BPSK5=dmodce(input5,datarate,samplefre,'ask',2);
allsize=length(BPSK1);

%put signal on carrier
carrier3G=cos(2*pi*3*10^9*t);
P1=carrier3G.*BPSK1;
P2=carrier3G.*BPSK2;
P3=carrier3G.*BPSK3;
P4=carrier3G.*BPSK4;
P5=carrier3G.*BPSK5;
%====================================
```

```
%Generate H signal 1.015GHz to 1.985GHz
noise1=wgn(1,allsize,0);
noise2=wgn(1,allsize,0);
noise3=wgn(1,allsize,0);
noise4=wgn(1,allsize,0);
noise5=wgn(1,allsize,0);
Hsignal1=BPF(1015*10^6,1985*10^6,noise1,samplefre);
Hsignal2=BPF (1015*10^6,1985*10^6,noise2,samplefre);
Hsignal3=BPF (1015*10^6,1985*10^6,noise3,samplefre);
Hsignal4=BPF (1015*10^6,1985*10^6,noise4,samplefre);
Hsignal5=BPF (1015*10^6,1985*10^6,noise5,samplefre);
%Go to Sigle sideband downconverter 1.01GHz to 1.99GHz=========================
%Generate V signal
transmit1=P1.*Hsignal1;
transmit2=P2.*Hsignal2;
transmit3=P3.*Hsignal3;
transmit4=P4.*Hsignal4;
transmit5=P5.*Hsignal5;

Vsignal1=antenna(101*10^6,199*10^6,transmit1,samplefre);
Vsignal2=antenna(101*10^6,199*10^6,transmit2,samplefre);
Vsignal3=antenna(101*10^6,199*10^6,transmit3,samplefre);
Vsignal4=antenna(101*10^6,199*10^6,transmit4,samplefre);
Vsignal5=antenna(101*10^6,199*10^6,transmit5,samplefre);

%Power amplifier make sure that Vertical and Horizontal signal has the same
%power
V1=Vsignal1*sqrt(pow(Vsignal1)/pow(Vsignal1));
V2=Vsignal2*sqrt(pow(Vsignal1)/pow(Vsignal2));
V3=Vsignal3*sqrt(pow(Vsignal1)/pow(Vsignal3));
V4=Vsignal4*sqrt(pow(Vsignal1)/pow(Vsignal4));
V5=Vsignal5*sqrt(pow(Vsignal1)/pow(Vsignal5));

H1=Hsignal1*sqrt(pow(Vsignal1)/pow(Hsignal1));
H2=Hsignal2*sqrt(pow(Vsignal1)/pow(Hsignal2));
H3=Hsignal3*sqrt(pow(Vsignal1)/pow(Hsignal3));
H4=Hsignal4*sqrt(pow(Vsignal1)/pow(Hsignal4));
H5=Hsignal5*sqrt(pow(Vsignal1)/pow(Hsignal5));

%Adding delay time=========================
V2len=(allsize/100)*1.5;%Add delay time
V3len=(allsize/100)*3;%Add delay time
V4len=(allsize/100)*4.2;%Add delay time
V5len=(allsize/100)*5.6;%Add delay time
HH2=[zeros(1,V2len),H2(1:(allsize-V2len))];
HH3=[zeros(1,V3len),H3(1:(allsize-V3len))];
HH4=[zeros(1,V4len),H4(1:(allsize-V4len))];
HH5=[zeros(1,V5len),H5(1:(allsize-V5len))];
%==========================================

%Add channel noise============================================
wgnH = wgn(1,allsize,0);
```

```
wgnV = wgn(1,allsize,0);
recnV=antenna(101*10^6,199*10^6,wgnV,samplefre); %channel noise
recnH=antenna(101*10^6,199*10^6,wgnH,samplefre); %channel noise
%Make sure the recived noise and signal at the same SNR

%Add channel noise=============================================
recVPower=pow(V1);%received signal power
recNVPower=recVPower/(10^(SNRchannel(g)/10));%find received noise power
NVcoeffe=sqrt(recNVPower/pow(recnV));%coeffieient adjust power
recnV=NVcoeffe*recnV;%rec V noise with proper SNRchannel
recHPower=pow(H1);%received signal power
recNHPower=recHPower/(10^(SNRchannel(g)/10));%find received noise power
NHcoeffe=sqrt(recNHPower/pow(recnH));%coeffieient adjust power
recnH=NHcoeffe*recnH;%rec H noise with proper SNRchannel
%=============================================================

Vrec3=V1+V2+V3+recnV;
Hrec3=H1+HH2+HH3+recnH;
rec3=Vrec3.*Hrec3;

Vrec5=V1+V2+V3+V4+V5+recnV;
Hrec5=H1+HH2+HH3+HH4+HH5+recnH;
rec5=Vrec5.*Hrec5;
%First BPF between 2.9GHz~3.1GHz
spassband3=BPF2900Mto3100M(rec3,samplefre);
spassband5=BPF2900Mto3100M(rec5,samplefre);
%Mix with carrier and send to low pass filter 0~20MHz
sbase3=spassband3.*carrier3G;
sbase5=spassband5.*carrier3G;
%LPF=20M
s20baseband3=LPF20M(sbase3,samplefre);
s20baseband5=LPF20M(sbase5,samplefre);
%Demodulation and calculate the error
output3=ddemodce(s20baseband3,datarate,samplefre,'ask',2);
output5=ddemodce(s20baseband5,datarate,samplefre,'ask',2);
errNum3=biterr(output3(11:90),input1(11:90));
counter3(m)=errNum3;
errNum5=biterr(output5(11:90),input1(11:90));
counter5(m)=errNum5;
 end
BERtotal3(g)=sum(counter3)/(96000);
BERtotal5(g)=sum(counter5)/(96000);
end
```

5. Sub-Function:

(a)pow( )

```
function y=pow(x)
% y=pow(x) calculates the power in the input sequence x
y=sum(x.^2)/length(x);
```

(b)LPF20M( )

```
function LPFout=LPF20M(recbase,samplefre);
allsize=length(recbase);
```

```
freb=fft(recbase,allsize);
Pbb=freb.*conj(freb)/allsize;
Pbby=zeros(1,allsize);
freb2=zeros(1,allsize);
for i=1:1:allsize
    if  (0/samplefre)*allsize<=i & i<=((20*10^6)/samplefre)*allsize;
       Pbby(i)=Pbb(i);
       freb2(i)=freb(i);
    elseif  (1-((20*10^6)/samplefre))*allsize<=i & i<=(1-(0/samplefre))*allsize;
        Pbby(i)=Pbb(i);
        freb2(i)=freb(i);
    else
       Pbby(i)=Pbb(i)*0.000000000001;
       freb2(i)=freb(i)*.000000000001;
    end
end
LPFout=real(ifft(freb2,allsize));
```

(c)BPF2950Mto3050M( )

```
function recpassband=BPF2950Mto3050M(rec,samplefre);
allsize=length(rec);
frer=fft(rec,allsize);
Prr=frer.*conj(frer)/allsize;
Prry=zeros(1,allsize);
frer2=zeros(1,allsize);
for i=1:1:allsize
    if  ((2.95*10^9)/samplefre)*allsize<=i & i<=((3.05*10^9)/samplefre)*allsize
       Prry(i)=Prr(i);
       frer2(i)=frer(i);
    elseif  (1-((3.05*10^9)/samplefre))*allsize<=i & i<=(1-((2.95*10^9)/samplefre))*allsize
        Prry(i)=Prr(i);
        frer2(i)=frer(i);
    else
       Prry(i)=Prr(i)*0.000000000001;
       frer2(i)=frer(i)*.000000000001;
    end
end
recpassband=real(ifft(frer2,allsize));
```

(d)BPF( )

```
function recpassband=BPF (low,up,rec,samplefre);
allsize=length(rec);
frer=fft(rec,allsize);
Prr=frer.*conj(frer)/allsize;
Prry=zeros(1,allsize);
frer2=zeros(1,allsize);
for i=1:1:allsize
    if  ((low)/samplefre)*allsize<=i & i<=((up)/samplefre)*allsize
       Prry(i)=Prr(i);
       frer2(i)=frer(i);
    elseif  (1-((up)/samplefre))*allsize<=i & i<=(1-((low)/samplefre))*allsize
```

```
        Prry(i)=Prr(i);
        frer2(i)=frer(i);
    else
       Prry(i)=Prr(i)*0.000000000001;
       frer2(i)=frer(i)*.000000000001;
    end
end
recpassband=real(ifft(frer2,allsize));
```

(e)antenna( )

```
function recpassband=antenna (low,up,rec,samplefre);
allsize=length(rec);
frer=fft(rec,allsize);
Prr=frer.*conj(frer)/allsize;
Prry=zeros(1,allsize);
frer2=zeros(1,allsize);
for i=1:1:allsize
    if  ((low)/samplefre)*allsize<=i & i<=((up)/samplefre)*allsize
       Prry(i)=Prr(i);
       frer2(i)=frer(i);
    elseif  (1-((up)/samplefre))*allsize<=i & i<=(1-((low)/samplefre))*allsize
        Prry(i)=Prr(i);
        frer2(i)=frer(i);
    else
       Prry(i)=Prr(i)*0.000000000001;
       frer2(i)=frer(i)*.000000000001;
    end
end
recpassband=real(ifft(frer2,allsize));
```

(f) plotspec( )

```
% plotspec(x,Ts) plots the spectrum of the signal x
% Ts = time (in seconds) between adjacent samples in x

function plotspec(x,Ts)
 N=length(x);                        % length of the signal x
t=Ts*(1:N);                          % define a time vector
ssf=(-N/2:N/2-1)/(Ts*N);                % frequency vector
fx=fft(x(1:N));                      % do DFT/FFT
fxs=fftshift(fx);                    % shift it for plotting
subplot(2,1,1), plot(t,x)               % plot the waveform
xlabel('seconds'); ylabel('amplitude')    % label the axes
subplot(2,1,2), plot(ssf,abs(fxs))        % plot magnitude spectrum
xlabel('frequency'); ylabel('magnitude')   % label the axes
```

VITA

JACK CHUANG

710 S.Atherton St. Apt406, State College, PA 16801, Phone: (814) 883-0277,jxc591@psu.edu

EDUCATION

Pennsylvania State University, Ph.D. in Electrical Engineering, Aug 2008, GPA 3.52
The New Jersey Institute of Technology, M.S. in EE, May 2004, GPA 3.8
National Sun Yat-Sen University (NSYSU), Taiwan, B.S. in EE, June 2001, GPA 3.2

AREA OF INTEREST

Covert communication system design, UWB radar system design, Signal processing

SKILL

RF and Baseband Equipment: Network Analyzer, Spectrum Analyzer, Communication Test Set, Dynamic Signal Analyzer,CW Signal generator and FPGA
RF and EM Software: HFSS
Programming: MATLAB, C++
RF IC Design: HSPICE, PSPICE

RESEARCH EXPERIENCE

- Designed and built the prototype UWB covert communication system by using random noise waveform.
- Designed baseband signal processing on Lyrtech FPGA board for real time field experiment.
- Analyzed the system performance in AWGN, jamming, and multipath channel. Developed method to reduce bit error rate (BER) in the multipath channel. The BER is reduced comparing with using RAKE receiver.
- Applied Hilbert-Huang Transform (HHT) on baseband signal processing and successfully increased the signal to noise ratio (SNR) and signal to interference ratio (SIR).

PUBLICATIONS

1. R. M. Narayanan and J.Chuang," Covert communications using heterodyne correlation random noise signals" IET Electronics Letters ,Vol 43, No 22, Oct 2007
2. Jack Chuang, Matthew W. DeMay, and R. M. Narayanan, "Secure Spread Spectrum Communication Using Ultrawideband Random Noise Signals"2006 IEEE MILCOM ,D.C, U.S.A
3. Jack Chuang and R. M. Narayanan, "Covert communications using random noise signals: overall system simulation and modulation analysis" 2005 SPIE, Orlando,U.S.A